Reply to the comments by Referee #2

To Associate Editor and Referee #2,

We appreciate you reading our paper carefully and giving valuable comments and suggestions again. We have considered your recommendations for revisions and made the necessary changes. The major points that we deal with in the revised manuscript are as follows:

1. We have changed "V1.0" to "V1" throughout the text. The GOSAT project has released V01.00, V01.01, and V01.20 produces, but the CO_2 products of all the three versions are exactly the same data.
2. We have eliminated Figure 2 of the original manuscript not to defocus the scope of this paper that discusses UTLS CO_2 data. We have described that the simultaneous retrieval of surface parameters did not affect retrieved CO_2 concentrations in the UTLS regions, but could increase the number of normally retrieved CO_2 data.
3. Following the recommendations of the two Referees, we have investigated the effect of considering TIR CO_2 averaging kernel functions on CO_2 concentrations in the UTLS regions. For this purpose, we have done the two types of analysis.
   3-1. We have compared TIR and CONTRAIL CME CO_2 data with and without TIR CO_2 averaging kernel functions over each of the nine airports, and showed the comparison results in Figure 4 of the revised manuscript. Here, we have created CO_2 vertical profiles using CME ascending/descending CO_2 data below the tropopause and stratospheric CO_2 concentrations taken from the Nonhydrostatic Icosahedral Atmospheric Model (NICAM)–Transport Model (TM) (Niwa et al., 2011) that introduced CONTRAIL CO_2 data to the inverse model (Niwa et al., 2012), and then applied TIR CO_2 averaging kernel functions to the created profiles.
   3-2. Keeping the detailed evaluation of 2-1 in mind, we assumed a CO_2 vertical profile on the basis of the combination of CONTRAIL CME level flight CO_2 data ("CONTRAIL (raw)") and CarbonTracker CT2013B monthly-mean CO_2 profiles (Peters et al., 2007) at each of the CME level flight measurement locations, applied TIR CO_2 averaging kernel functions to the assumed profiles, and then compared the CO_2 data with averaging kernels ("CONTRAIL (AK)") with TIR CO_2 data in the UTLS regions. In Figure 5, 6, and 7 of the revised manuscript, we showed the comparison results of both the CONTRAIL (raw) and CONTRAIL (AK) data.

   We have explained the methods of the comparisons in Section 5, and showed the comparison results in Section 6 in the revised manuscript.
4. We have eliminated Figure 5 of the original manuscript. This is because we have evaluated the effect of considering TIR CO_2 averaging kernel functions on TIR and CONTRAIL CME CO_2 comparisons quantitatively in the revised manuscript.
5. Following the suggestion of Referee #1, we have showed the comparison results for each latitude band, instead of showing the comparison results for each airline route, in Figure 7 of the revised manuscript. We have also modified Table 2 to show the bias values of TIR CO_2 data against CONTRAIL (AK) CO_2 data.
6. We have eliminated Figure 10 of the original manuscript to avoid speculative discussion.

Individual responses to the two Referees' comments are listed below.

Reply to Referee #2

General comments:

Authors compare GOSAT TIR CO_2 retrievals to carbon dioxide observations by CONTRAIL flights, both to vertical profiles and to level flight data. The comparison study is an important step towards improving the TIR CO_2 retrieval product and should present a valuable source of information to potential users of CO_2 product. However, current version of the manuscript requires revisions that are likely to alter the results and conclusion before the paper can be considered fully suitable for publication.

The reported results include TIR CO_2 comparison with vertical profiles around Narita airport and with

level flight data observed around the world. Comparisons for Narita profiles are made with averaging kernel (AK) smoothing applied and reveal low bias (Fig. 2) with respect to CONTRAIL data in mid troposphere along with a significant random error at the range of several ppm. This part of comparison looks valid. In the following sections the TIR CO_2 retrievals are compared to the level flight data, but it is done without applying corrections with averaging kernel (as presented in Eq. 5). Comparison without applying correction is, however, of a limited value for this type of remote sensing product. As authors state in multiple occasions the TIR retrieval does show strong dependence on the retrieval prior, indicating large weight of the prior in the retrieval. Potential users of the product for inverse modeling applications have to apply corrections themselves according to established practice, otherwise they would end up using mostly prior model simulation instead of observations by GOSAT TIR. Which is not what they intend. For the same reason there are few or no known published attempts to compare similar TIR product to level flight data that do not resolve vertical concentration profile. Accordingly, revision of the level flight part is strongly recommended. As the manuscript title suggests the comparison at UTLS level making a major contribution to the study results, a major revision is required.

Reply:

We appreciate your comments. We have seriously taken your comments, and made comparisons between TIR and CONTRAIL CME level flight CO_2 data with considering TIR CO_2 averaging kernel functions in the revised manuscript. As described above, we have used CarbonTracker CT2013B monthly-mean CO_2 profiles (Peters et al., 2007) to assume a CO_2 vertical profile at each of the CME level flight measurement locations. Then, we applied TIR CO_2 averaging kernel functions to the assumed profiles to smooth them to the vertical resolution of TANSO-FTS TIR observations, and defined them as "CONTRAIL (AK)." Then, we extracted CONTRAIL (AK) data that corresponded to the TIR retrieval layers where TIR CO_2 data were compared with original CONTRAIL CME data ("CONTRAIL (raw)"), and compared their averages with the TIR CO_2 averages in the several layers. In Figure 5, 6, and 7 of the revised manuscript, we showed the comparison results of both the CONTRAIL (raw) and CONTRAIL (AK) CO_2 data.

Specific comments:

1. On Page 13006, Line 19 authors state they did not apply "TIR CO_2 averaging kernels to CONTRAIL CME CO_2", and in the following discussion provide mostly verbal argument that skipping the correction is justified. Instead the reader would expect to see results of numerical tests supporting authors' position. For products like GOSAT SWIR XCO_2 comparison with uncorrected values produce essentially same result, but in TIR case the value of averaging kernel is well below 1 (Fig. 9) which implies large weight of the prior in the product. As follows from Eq 5, application of the said correction with relatively small values of averaging kernel (in the order of 0.2 or less as shown on Fig 9) may attract the corrected value strongly to prior concentration, reducing difference between CONTRAIL and prior, from what is shown on Figs 6 and 7 by several times and compromising much of discussion in Section 6. From the reviewer's standpoint, revision and improvement of comparison with CONTRAIL level flight data is essential, which could be most easily done by extending the level flight data vertically using modeled or climatological profiles, and applying the averaging kernel afterwards. Importance of the correction given by Eq. 5 is emphasized by its use as a regular practice in the inverse modeling applications, where the model vs observation difference is estimated using same equation. Use of the Eq. 5 by modelers in calculating model to observation misfit effectively implies replacing the retrieval prior by model simulated profile. Comparison with uncorrected data, such as shown on Fig 7, may divert potential users from understanding strong and weak points of TIR L2 data.

Reply:

We appreciate your comments. In the revised manuscript, we have quantitatively discussed the effect of considering TIR CO_2 averaging kernel functions on CO_2 concentrations in the UTLS regions. Over the nine airports, we have created CO_2 vertical profiles using CONTRAIL CME ascending/descending CO_2 data below the tropopause and stratospheric CO_2 concentrations taken from the Nonhydrostatic Icosahedral Atmospheric Model (NICAM)–Transport Model (TM) (Niwa et al., 2011), and applied TIR CO_2 averaging kernel functions to the created profiles. Then, we have compared TIR and CONTRAIL CME CO_2 data with and without TIR CO_2 averaging kernel functions over each of the nine airports, and showed the comparison results in Figure 4 of the revised manuscript. The NICAM-TM CO_2 data used in this evaluation were calculated on the basis of surface flux data that were estimated in the inverse model that introduced CONTRAIL

CO_2 data in addition to surface CO_2 data; therefore, we think they are appropriate datasets to evaluate the impact of considering TIR CO_2 averaging kernel functions on the CONTRAIL CME UTLS CO_2 data. Furthermore, we have assumed a CO_2 vertical profile on the basis of the combination of CONTRAIL CME level flight CO_2 data and CarbonTracker CT2013B monthly-mean CO_2 profiles (Peters et al., 2007) at each of the CME level flight measurement locations, applied TIR CO_2 averaging kernel functions to the assumed profiles, and then compared the CO_2 data with averaging kernels with TIR CO_2 data in the UTLS regions. The CarbonTracker CT2013B CO_2 data are available to the public, so that readers can refer to the dataset that we used as a CO_2 climatological dataset. We have also modified Table 2 to show the latitudinal dependence of the bias of TIR CO_2 data against CONTRAIL CO_2 data with averaging kernels, so that it should be useful for users to correct the TIR CO_2 data.

2. In the abstract (P12994 L24) and other locations authors mention the retrieval prior CO_2 they use have several biases. Another source of retrieval biases is spectral bias. It is not clear how large is relative contribution of these two. Comparison of the TIR product made with another prior or bias corrected prior appears desirable, given contamination of the product with prior biases. Also, from the absence of the prior contributors in the coauthors list and acknowledgements one can suspect that there wasn't enough contact between prior developers and retrieval team.

Reply: Following your suggestions, we have evaluated the effect of L1B spectral bias on retrieved CO_2 concentrations in the UTLS regions by the equation of $\mathbf{d_{CO2}} = \mathbf{G_{CO2}}\,\mathbf{d_{spec}}$. $\mathbf{G_{CO2}}$ is a gain matrix for CO_2 retrieval, $\mathbf{d_{spec}}$ is a spectral bias vector that was created assuming that the V161.160 spectra had the same bias as V130.130 L1B spectra reported in Kataoka et al. (2014), and $\mathbf{d_{CO2}}$ is a vector of bias errors in retrieved CO_2 concentrations attributable to the spectral bias. In order to evaluate the effect of a priori uncertainty on retrieved CO_2 concentrations, we arbitrarily decreased a priori concentration by 1% in test TIR CO_2 retrieval, and then compared the retrieved CO_2 concentrations with those retrieved using the original a priori data. Please see the second and third paragraphs of Section 7 of the revised manuscript for further details. We had reported a negative bias seen in the a priori UTLS CO_2 data with Dr. Saeki and Dr. Maksyutov who are responsible to create the a priori data for the TANSO-FTS retrieval processing, and discussed this problem with them. As you suggested, we should have acknowledged them in this paper. They have a plan to recreate a priori data for the future reprocessing of both TANSO-FTS SWIR and TIR L2 data.

Technical corrections:

P12994 L2. The first sentence better to rewrite to avoid using construct as "thermal infrared (TIR) band . . . has been observing carbon dioxide . . .". Clearer phrase could sound as "TANSO-FTS has been observing carbon dioxide in thermal infrared (TIR) band". Similar wording appears later as well. Authors write on P12996 L10 ". . . (TES) has retrieved CO_2 concentrations . . .". One may argue that TES can measure or observe radiances, but retrieval would be done on the ground. The paper should be checked again to correct places with somewhat tentative language.

Reply: We have rewritten the text following your suggestions. We greatly appreciate your suggestions.

Validation of GOSAT/TANSO-FTS TIR UTLS CO_2 data (Version 1~~.0~~) using CONTRAIL measurements

N. Saitoh[1], S. Kimoto[1], R. Sugimura[1], R. Imasu[2], S. Kawakami[3], K. Shiomi[3], A. Kuze[3], T. Machida[4], Y. Sawa[5], and H. Matsueda[5]

[1]{Center for Environmental Remote Sensing, Chiba University, Chiba, Japan}

[2]{Atmosphere and Ocean Research Institute, University of Tokyo, Kashiwa, Japan}

[3]{Japan Aerospace Exploration Agency, Tsukuba, Japan}

[4]{National Institute for Environmental Studies, Tsukuba, Japan}

[5]{Meteorological Research Institute, Tsukuba, Japan}

Correspondence to: N. Saitoh (nsaitoh@faculty.chiba-u.jp)

Abstract

~~The thermal infrared (TIR) band of the~~ Thermal and Near Infrared Sensor for Carbon Observation (TANSO)–Fourier Transform Spectrometer (FTS) on board the Greenhouse Gases Observing Satellite (GOSAT) has been observing carbon dioxide (CO_2) concentrations in several atmospheric layers in the thermal infrared (TIR) band since its launch. This study compared TANSO-FTS TIR ~~V1.0~~V1 CO_2 data and CO_2 data obtained in the Comprehensive Observation Network for TRace gases by AIrLiner (CONTRAIL) project in the upper troposphere and lower stratosphere (UTLS), where the TIR band of TANSO-FTS is most sensitive to CO_2 concentrations, to validate the quality of the TIR ~~V1.0~~V1 UTLS CO_2 data from 287 to 162 hPa. We first evaluated the impact of considering TIR CO_2 averaging kernel functions on CO_2 concentrations using CO_2 profile data obtained by the CONTRAIL Continuous CO_2 Measuring Equipment (CME), and found that the impact at around the CME level flight altitudes (~11 km) was on average less than 0.5 ppm in low latitudes and less than 1 ppm in middle and high latitudes. From a comparison made during flights between Tokyo and Sydney, the averages of the TIR upper atmospheric CO_2 data were within 0.1% of the averages of the CONTRAIL CME CO_2 data with and without TIR CO_2 averaging kernels for all seasons in the Southern Hemisphere~~agreed well with the averages of the data obtained by~~

~~the CONTRAIL Continuous CO_2 Measuring Experiment (CME) within 0.1% for all of the seasons in the Southern Hemisphere~~. The results of ~~a~~ comparisons for all of the eight airline routes showed that the agreements of TIR and CME CO_2 data were worse in spring and summer than in fall and winter in the Northern Hemisphere in the upper troposphere. While the differences between TIR and CME CO_2 data were on average within 1 ppm in fall and winter, TIR CO_2 data had a negative bias up to 2.4 ppm against CME CO_2 data with TIR CO_2 averaging kernels in the northern low and middle latitudes in spring and summer.~~the agreement between the TIR and CONTRAIL CO_2 data was within 0.5% on average in the Northern Hemisphere, which was better than the agreement between a priori and CONTRAIL CO_2 data. The quality of TIR lower stratospheric CO_2 data depends largely on the information content, and therefore has a seasonal dependence. In high latitudes, TIR V1.0 lower stratospheric CO_2 data are only valid in the summer. The magnitude of bias in the TIR upper atmospheric CO_2 data did not have a clear longitudinal dependence. The comparison results for flights in northern low and middle latitudes showed that the agreement between TIR and CONTRAIL CO_2 data in the upper troposphere was worse in the spring and summer than in the fall and winter. This could be attributed to a larger negative bias in the upper atmospheric a priori CO_2 data in the spring and summer and a seasonal dependence of spectral bias in TANSO-FTS TIR Level 1B (L1B) radiance data.~~ The negative bias in the northern middle latitudes resulted in ~~made~~ the maximum of TIR CO_2 concentrations being lower than that of CME~~ONTRAIL~~ CO_2 concentrations, which le~~dads~~ to an underestimate of the amplitude of CO_2 seasonal variation.

1 Introduction

Carbon dioxide (CO_2) in the atmosphere is a well-known strong greenhouse gas (IPCC, 2013, and references therein), with concentrations that have been observed both *in situ* and by satellite sensors. Its long-term observation began in Mauna Loa, Hawaii, and the South Pole in the late 1950s (Keeling et al., 1976a, 1976b, 1996). Since then, comprehensive CO_2 observations in the atmosphere have been conducted worldwide in several observatories and tall towers (Bakwin et al., 1998), by aircraft flask sampling (e.g., Crevoisier et al., 2010), and via the AirCore sampling system (Karion et al., 2010) in the framework of researches by the National Oceanic and Atmospheric Administration (NOAA). Atmospheric CO_2 concentrations have gradually increased at a globally averaged annual rate of 1.7±0.5 ppm

from 1998 to 2011, although its growth rate has relatively large interannual variation (IPCC, 2013). Upper atmospheric CO_2 observations have been made in many areas by several projects using commercial airliners, such as the Comprehensive Observation Network for TRace gases by AIrLiner (CONTRAIL) project (Machida et al., 2008) and the Civil Aircraft for the Regular Investigation of the atmosphere Based on an Instrument Container (CARIBIC) project (Brenninkmeijer et a., 2007). Continuous long-term measurements of CO_2 made by several airplanes of Japan Airlines (JAL) in the CONTRAIL project have revealed details of its seasonal variation and interhemispheric transport in the upper atmosphere (Sawa et al., 2012) and interannual and long-term trends of its latitudinal gradients (Matsueda et al., 2015).

Atmospheric CO_2 observations by satellite sensors are categorized into two types: those utilizing CO_2 absorption bands in the shortwave infrared (SWIR) regions at around 1.6 and 2.0 μm, and those in the thermal infrared (TIR) regions at around 4.6, 10, and 15 μm. The Scanning Imaging Absorption Spectrometer for Atmospheric Chartography (SCIAMACHY) on the Environmental Satellite (ENVISAT) first observed CO_2 column-averaged dry-air mole fractions (XCO_2) from spectra at 1.57 μm (Buchwitz et al., 2005; Barkley et al., 2006). The Thermal and Near Infrared Sensor for Carbon Observation (TANSO)–Fourier Transform Spectrometer (FTS) on board the Greenhouse Gases Observing Satellite (GOSAT), which was launched in 2009 (Yokota et al., 2009), has observed XCO_2 with high precision by utilizing the 1.6 and/or 2.0 μm CO_2 absorption bands (Yoshida et al., 2011, 2013; O'Dell et al., 2012; Butz et al., 2011; Cogan et al., 2012). The Orbiting Carbon Observatory 2 (OCO-2) was successfully launched in 2014, and started regular observations of XCO_2 with high spatial resolution. Satellite CO_2 observations at TIR absorption bands have a longer history beginning with the High-Resolution Infrared Sounder (HIRS) (Chédin et al., 2002, 2003, 2005). The Atmospheric Infrared Sounder (AIRS) has achieved more accurate observations of middle and upper tropospheric CO_2 concentrations (Crevoisier et al., 2004; Chahine et al., 2005; Maddy et al., 2008; Strow and Hannon, 2008). The Tropospheric Emission Spectrometer (TES) has observed~~retrieved~~ CO_2 concentrations in several vertical layers with high accuracy by taking advantage of its high wavelength resolution (Kulawik et al., 2010, 2013). The Infrared Atmospheric Sounding Interferometer (IASI) has observed~~derived~~ upper atmospheric CO_2 amounts from~~from~~ its TIR spectra (Crevoisier et al., 2009). TANSO-FTS also has a TIR band in addition to its three SWIR bands, and obtains vertical information of CO_2 concentrations in addition to XCO_2 in the same field of view (Saitoh et al., 2009).

Rayner and O'Brien (2001) and Pak and Prather (2001) showed the utility of global CO_2 data obtained by satellite sensors for estimating its source and sink strength, and many studies of CO_2 inversion have been conducted using a huge amount of satellite data since the 2000s. Chevallier et al. (2005) first used satellite CO_2 data, observed with the Operational Vertical Sounder (TOVS), to estimate CO_2 surface fluxes. They reported that a regional bias in satellite CO_2 data hampers the outcomes. Nassar et al. (2011) demonstrated that the wide spatial coverage of satellite CO_2 data is beneficial to CO_2 surface flux inversion through the combined use of TES and surface flask CO_2 data, particularly in regions where surface measurements are sparse. In addition to CO_2 surface inversion results using TIR observations, global XCO_2 data observed with the SWIR bands of TANSO-FTS have been actively used for estimating CO_2 source and sink strength (Maksyutov et al., 2013; Saeki et al., 2013; Chevallier et al., 2014; Basu et al., 2013, 2014; Takagi et al., 2014). One of the important things to consider when incorporating satellite data in CO_2 inversion is the accuracy of the data, as suggested by Basu et al. (2013). Uncertainties in satellite CO_2 data should be assessed seasonally and regionally to determine the seasonal and regional characteristics of the satellite CO_2 bias.

The importance of upper atmospheric CO_2 data in the inversion analysis of CO_2 surface fluxes was discussed in Niwa et al. (2012). They used CONTRAIL CO_2 data in conjunction with surface CO_2 data to estimate surface flux, and demonstrated that adding middle and upper tropospheric data observed by the aircraft could greatly reduce the posteriori flux errors, particularly in tropical Asian regions. Middle and upper tropospheric and lower stratospheric CO_2 concentrations and column amounts of CO_2 can be simultaneously observed in the same field of view with TANSO-FTS on board GOSAT. Provided that the quality of upper atmospheric CO_2 data simultaneously obtained with TANSO-FTS is proven to be comparable to that of TANSO-FTS XCO_2 data (Yoshida et al., 2013; Inoue et al., 2013), the combined use of upper atmospheric CO_2 and XCO_2 data observed with TANSO-FTS could be a useful tool for estimating CO_2 surface flux.

GOSAT, which is the first satellite to be dedicated to greenhouse gas monitoring, was launched on January 23, 2009. As described above, ~~the TIR band of~~ TANSO-FTS on board GOSAT has been observing CO_2 concentrations in several vertical layers in the TIR band. In this study, we focused on CO_2 concentrations in the upper troposphere and lower stratosphere (UTLS), where the TIR band of TANSO-FTS is most sensitive. We validated these data by

comparison with upper atmospheric CO_2 data obtained in a wide spatial coverage in the CONTRAIL project. Sections 2 and 3 explain the GOSAT and CONTRAIL measurements, respectively. Section 4 details the retrieval algorithm used in the latest version 1~~.0~~ (V1~~.0~~) CO_2 level 2 (L2) product of the TIR band of TANSO-FTS. Section 5 describes the methods of comparing TANSO-FTS TIR V1 L2 and CONTRAIL CO_2 data. Sections 6~~5~~ and 7~~6~~ show and discuss the results of the~~a~~ comparisons between ~~between TANSO-FTS~~ TIR ~~V1.0 L2~~ and CONTRAIL CO_2 data. Section 8~~7~~ summarizes this study.

2 GOSAT observations

GOSAT is a joint satellite project of the National Institute for Environmental Studies (NIES), Ministry of the Environment (MOE), and Japan Aerospace Exploration Agency (JAXA) for the purpose of making global observations of greenhouse gases such as CO_2 and CH_4 (Hamazaki et al., 2005; Yokota et al., 2009). It was launched on January 23, 2009, from the Tanegashima Space Center, and has continued its observations for more than six years. GOSAT is equipped with the TANSO-FTS for greenhouse gas monitoring and the TANSO-Cloud and Aerosol Imager (CAI) to detect clouds and aerosols in the TANSO-FTS field of view (Kuze et al., 2009). TANSO-FTS consists of three bands in the SWIR region and one band in the TIR region. ~~The SWIR bands observe~~ C~~c~~olumn amounts of greenhouse gases are observed in the SWIR bands and ~~the TIR band observes~~ vertical information of gas concentrations are obtained in the TIR band (Yoshida et al., 2011, 2013; Saitoh et al., 2009, 2012; Ohyama et al., 2012, 2013).

Kuze et al. (2012) provided a detailed description of the methods used for the processing and calibration of level 1B (L1B) spectral data from TANSO-FTS. They explained the algorithm for the version 150.151 (V150.151) L1B spectral data. The TIR ~~V1.0~~V1 L2 CO_2 product we focused on in this study was created from a later version, V161.160, of L1B spectral data. The following modifications were made to the algorithm from V150.151 to V161.160: improving the TIR radiometric calibration through the improvement of calibration parameters, turning off the sampling interval non-uniformity correction, modifying the spike noise criteria of the quality flag, and reevaluating the misalignment between the GOSAT satellite and TANSO-FTS sensor. Kataoka et al. (2014) reported that the biase~~accuracie~~s of TANSO-FTS TIR V130.130 L1B radiance spectra based on comparisons with the Scanning High-resolution Interferometer Sounder (S-HIS) spectra for warm scenes were 0.5 K at 800–900 cm^{-1} and

700–750 cm^{-1}, 0.1 K at 980–1080 cm^{-1}, and more than 2 K at 650–700 cm^{-1}. Although the magnitude of the spectral bias evaluated on the basis of V130.130 L1B data would change in V161.160 L1B data, the issue of L1B spectral bias still remains. The spectral bias inherent in TIR L1B spectra would be mainly because of uncertainty of polarization correction. Another possible cause was discussed in Imasu et al. (2010). When retrieving CO_2 concentrations from the TIR band of TANSO-FTS, the spectral bias that is predominant in CO_2 absorption bands should be considered (Ohyama et al., 2013).

3 CONTRAIL Continuous Measurement Equipment (CME) observations

We used CO_2 data obtained in the CONTRAIL project to validate the quality of TANSO-FTS TIR ~~V1.0~~V1 L2 CO_2 data. CONTRAIL is a project to observe atmospheric trace gases such as CO_2 and CH_4 using instruments installed on commercial aircraft operated by JAL. Observations of trace gases in this project began in 2005. Two types of measurement instruments, the Automatic Air Sampling Equipment (ASE) and the Continuous CO_2 Measuring Equipment (CME), have been installed on several JAL aircraft to measure trace gases over a wide area (Machida et al., 2008).

This study used CO_2 data obtained with CME on several airline routes from Narita Airport, Japan. CO_2 observations with CME use a LI-COR LI-840 instrument that utilizes a nondispersive infrared absorption (NDIR) method (Machida et al., 2008). In the observations, two different standard gases, with CO_2 concentration of 340 ppm and 390 ppm based on NIES09 scale, are regularly introduced into the NDIR for calibration. The accuracy of CME CO_2 measurements is 0.2 ppm. See Machida et al. (2008), Matsueda et al. (2008), and Machida et al. (2011) for details of the CME CO_2 observations and their accuracy and precision.

4 Retrieval algorithm of TANSO-FTS TIR ~~V1.0~~V1 CO_2 data

4.1 Basic retrieval settings

Saitoh et al. (2009) provided an algorithm for retrieving CO_2 concentrations from the TIR band of TANSO-FTS. The first version, V00.01, of the L2 CO_2 product of the TIR band of TANSO-FTS was basically processed by the algorithm described in Saitoh et al. (2009). The

~~V1.0~~V1 L2 CO_2 product that we focused on in this study also adopted a non-linear maximum a posteriori (MAP) method with linear mapping, as was the case for the V00.01 product. We utilized the following expressions in TIR CO_2 retrieval:

$$\hat{\mathbf{z}}_{i+1} = \mathbf{W}^* \mathbf{x}_a + \mathbf{G}[\mathbf{y} - \mathbf{F}(\hat{\mathbf{x}}_i) + \mathbf{K}_i \mathbf{W}(\mathbf{W}^* \hat{\mathbf{x}}_i - \mathbf{W}^* \mathbf{x}_a)]$$
$$\mathbf{G} = [\mathbf{W}^T \mathbf{K}_i{}^T \mathbf{S}_\varepsilon{}^{-1} \mathbf{K}_i \mathbf{W} + (\mathbf{W}^* \mathbf{S}_a \mathbf{W}^{*T})^{-1}]^{-1} \mathbf{W}^T \mathbf{K}_i{}^T \mathbf{S}_\varepsilon{}^{-1} \quad (1)$$

where $\mathbf{x_a}$ is an a priori vector, $\mathbf{S_a}$ is a covariance matrix of the a priori vector, $\mathbf{S_\varepsilon}$ is a covariance matrix of measurement noise, $\mathbf{K_i}$ is a CO_2 Jacobian matrix calculated using the i^{th} retrieval vector $\hat{\mathbf{x}}_\mathbf{i}$ on full grids, $\mathbf{F}(\hat{\mathbf{x}}_\mathbf{i})$ is a forward spectrum vector based on $\hat{\mathbf{x}}_\mathbf{i}$, $\mathbf{y}$ is a measurement spectrum vector, and $\hat{\mathbf{z}}_{\mathbf{i+1}}$ is the $i+1^{th}$ retrieval vector defined on retrieval grids. $\mathbf{W}$ is a matrix that interpolates from retrieval grids onto full grids. $\mathbf{W}^*$ is the generalized inverse matrix of $\mathbf{W}$.

The full grids are vertical layer grids for radiative transfer calculation, and the retrieval grids are defined as a subset of the full grids. In the ~~V1.0~~V1 L2 CO_2 retrieval algorithm, linear mapping between retrieval grids and full grids was also applied, but the number of full grid levels was 78 instead of 110 in the V00.01 algorithm. The determination of retrieval grids in the ~~V1.0~~V1 algorithm basically followed the method of the V00.01 algorithm. It was based on the areas of a CO_2 averaging kernel matrix in the tropics, but the retrieval grid levels were fixed for all of the retrieval processing, as presented in Table 1. Averaging kernel matrix $\mathbf{A}$ is defined (Rodgers, 2000) as

$$\mathbf{A} = \mathbf{GKW} . \quad (2)$$

~~(2)~~

Figure 1 shows typical averaging kernel functions of TIR ~~V1.0~~V1 L2 CO_2 retrieval ~~in middle latitudes in summer~~. The degrees of freedom (DF) in th~~e~~is case~~s~~ (trace of the matrix $\mathbf{A}$) were~~was~~ (a) 2.22, (b) 1.81, and (c) 1.36, respectively~~2.09~~. The seasonally averaged DF values of TIR ~~V1.0~~V1 CO_2 data ranged from 1.12 to 2.35. In the low and middle latitudes between 35°N and 35°S, ~~almost all~~ the CO_2 DF values were around~~exceeded~~ 2.0 or more; this means that observations by the TIR band of TANSO-FTS can provide information on CO_2 concentrations in more than two vertical layers, one of which we focused on in this study.

A priori and initial values for CO_2 concentrations were taken from the outputs of the NIES transport model (NIES-TM05) (Saeki et al., 2013). A priori and initial values for temperature and water vapor were obtained from Japan Meteorological Agency (JMA) Grid Point Value (GPV) data. Basically, the retrieval processing of TANSO-FTS was only conducted under clear-sky conditions, which was judged based on a cloud flag from TANSO-CAI in the daytime (Ishida and Nakajima, 2009; Ishida et al., 2011) and on a TANSO-FTS TIR spectrum in the nighttime.

4.2 Improvements in the~~of~~ TIR ~~V1.0~~V1 CO_2 algorithm

The following conditions are the improvements made in the TANSO-FTS TIR ~~V1.0~~V1 L2 CO_2 algorithm from the V00.01 algorithm. The ~~V1.0~~V1 algorithm used the CO_2 10 μm absorption band in addition to the CO_2 absorption band at around 15 μm band; the wavelength regions of 690–750 cm^{-1}, 790–795 cm^{-1}, 930–990 cm^{-1}, and 1040–1090 cm^{-1} were used in the CO_2 retrieval. We did not apply any channel selection. In these wavelength regions, temperature, water vapor, and ozone concentrations were retrieved simultaneously with CO_2 concentration. Moreover, surface temperature and surface emissivity were simultaneously derived as a correction parameter of the spectral bias inherent in TANSO-FTS TIR V161.160 L1B spectra at the above-mentioned CO_2 absorption bands. We assumed that the spectral bias could be divided into two components: a wavelength-dependent bias whose amount varied depending on wavelength and a wavelength-independent bias whose amount was uniform in a certain wavelength region. We tried to correct such a wavelength-independent component of the spectral bias by adjusting the value of surface temperature. Similarly, a wavelength-dependent component of the spectral bias was corrected by adjusting the value of surface emissivity in each wavelength channel. Therefore the matrices of $\mathbf{K}$ and $\mathbf{S_a}$ of expression (1) are as follows:

$$\mathbf{K} = (\mathbf{K}_{CO2}\ \mathbf{K}_{H2O}\ \mathbf{K}_{O3}\ \mathbf{K}_{T}\ \mathbf{k}_{sT\_1}\ \mathbf{k}_{sT\_2}\ \mathbf{k}_{sT\_3}\ \mathbf{k}_{sT\_4}\ \mathbf{k}_{sT\_5}\ \mathbf{k}_{sE\_1}\ \mathbf{k}_{sE\_2}\ \mathbf{k}_{sE\_3}\ \mathbf{k}_{sE\_4}\ \mathbf{k}_{sE\_5}), \quad (3)$$

$$\mathbf{S_a} = \begin{vmatrix} \mathbf{S_{CO2}} & & & & & & & & & & \\ & \mathbf{S_{H2O}} & & & & & & & & & \\ & & \mathbf{S_{O3}} & & & & & & & & \\ & & & \mathbf{S_T} & & & & & & & \\ & & & & S_{sT\_1} & & & & & & \\ & & & & & S_{sT\_2} & & & \mathbf{0} & & \\ & & & & & & S_{sT\_3} & & & & \\ & & & & \mathbf{0} & & & S_{sT\_4} & & & \\ & & & & & & & & S_{sT\_5} & & \\ & & & & & & & & & S_{sE\_1} & \\ & & & & & & & & & & S_{sE\_2} \\ & & & & & & & & & & & S_{sE\_3} \\ & & & & & & & & & & & & S_{sE\_4} \\ & & & & & & & & & & & & & S_{sE\_5} \end{vmatrix}, \quad (4)$$

where $\mathbf{K_{CO2}}$, $\mathbf{K_{H2O}}$, $\mathbf{K_{O3}}$, and $\mathbf{K_T}$ are Jacobian matrices of CO_2, water vapor, ozone, and temperature on full grids, respectively, and $\mathbf{S_{CO2}}$, $\mathbf{S_{H2O}}$, $\mathbf{S_{O3}}$, and $\mathbf{S_T}$ are a priori covariance matrices of CO_2, water vapor, ozone, and temperature on full grids, respectively. The vectors $\mathbf{k_{sT\_1}}$, $\mathbf{k_{sT\_2}}$, $\mathbf{k_{sT\_3}}$, $\mathbf{k_{sT\_4}}$, and $\mathbf{k_{sT\_5}}$ are the Jacobian vectors of surface temperature in the wavelength regions of 690–715 cm^{-1}, 715–750 cm^{-1}, 790–795 cm^{-1}, 930–990 cm^{-1}, and 1040–1090 cm^{-1}, respectively. The vectors $\mathbf{k_{sE\_1}}$, $\mathbf{k_{sE\_2}}$, $\mathbf{k_{sE\_3}}$, $\mathbf{k_{sE\_4}}$, and $\mathbf{k_{sE\_5}}$ are the Jacobian vectors of surface emissivity in each of the five wavelength regions, respectively. The elements of the Jacobian vectors of surface parameters that were defined for each of the five wavelength regions were set to be zero in the other wavelength regions. The values S_{sT_1}, S_{sT_2}, S_{sT_3}, S_{sT_4}, and S_{sT_5} and S_{sE_1}, S_{sE_2}, S_{sE_3}, S_{sE_4}, and S_{sE_5} are a priori variances of surface temperature and surface emissivity in each of the five wavelength regions, respectively. Simultaneous retrieval of the surface parameters in the ~~V1.0~~V1 algorithm was conducted just for the purpose of correcting the TIR V161.160 L1B spectral bias; it had no physical meaning. We estimated the surface parameters separately in each of the five wavelength regions to consider differences in the amount of spectral bias in each wavelength region. The matrices $\mathbf{S_a}$ for CO_2, temperature, water vapor, and ozone were diagonal matrices with vertically fixed diagonal elements with a standard deviation of 2.5%, 3 K, 20%, and 30%, respectively. Here, a priori and initial values for ozone were obtained from the climatological data for each latitude bin for each month given by MacPeters et al. (2007). We assumed rather

large values as a priori variances of the surface parameters (a standard deviation of 10 K for surface temperature), which could allow more flexibility in the L1B spectral bias correction by the surface parameters. The a priori and initial values for surface emissivity were calculated by linear regression analysis using the Advanced Space-borne Thermal Emission Reflection Radiometer (ASTER) Spectral Library (Baldridge et al., 2009) using ~~on the basis of~~ land-cover classification, vegetation, and wind speed information. The a priori and initial values for surface temperature were estimated using radiance data in several channels around 900 cm^{-1} of the TIR V161.160 L1B spectra.

~~4.3 Effects of spectral bias on CO_2 retrieval~~

In the TIR ~~V1.0~~V1 L2 algorithm, we estimated surface temperature and surface emissivity to correct the spectral bias inherent in the TANSO-FTS TIR L1B spectra (Kataoka et al., 2014). The existence of a relatively large spectral bias around the CO_2 15 μm absorption band in TANSO-FTS TIR L1B spectra (Kataoka et al., 2014) resulted in a decrease in the number of normally retrieved CO_2 profiles. This is probably because the TIR L1B spectral bias in the CO_2 15 μm absorption band was sometimes too large for the L2 retrieval calculation to converse in a limited iteration. The correction of the TIR L1B spectral bias through the simultaneous retrieval of the surface parameters did not affect retrieved CO_2 concentrations in the UTLS regions, which was the focus of this study, but it altered the number of normally retrieved CO_2 profiles.~~Here, we evaluated the impact of the correction of the TIR L1B spectral bias through the simultaneous retrieval of the surface parameters on the TIR L2 CO_2 retrieval. Figure 2 shows comparisons between several types of TIR CO_2 profiles retrieved by changing the treatment of the surface parameters in the retrieval and coincident CONTRAIL CME CO_2 profiles over Narita airport. Criteria for the coincident pairs of a 100 km distance from Narita airport, a time difference in 2 hours, and a day difference within ±1 day yielded a total of 141 coincident profile pairs in 2010. In the comparisons, we applied averaging kernel functions of TIR CO_2 data to corresponding CONTRAIL CME CO_2 profiles, as follows (Rodgers and Connor, 2003):~~

~~$$\mathbf{x}_{\text{obs-CONTRAIL}} = \mathbf{x}_{\text{a priori}} + \mathbf{A}\left(\mathbf{x}_{\text{CONTRAIL}} - \mathbf{x}_{\text{a priori}}\right). \quad (5)$$~~

~~Here, $\mathbf{x}_{\text{CONTRAIL}}$ and $\mathbf{x}_{\text{a priori}}$ are CONTRAIL CME and a priori CO_2 profiles. Figure 2a shows a comparison of the V1.0 L2 CO_2 product (i.e., the result of a comparison of CO_2 retrievals based on TANSO-FTS TIR L1B spectra corrected through the simultaneous retrieval of both~~

~~surface temperature and surface emissivity). Figure 2b and 2c show the results of a comparison of CO_2 retrievals that used TIR L1B spectra corrected only by surface temperature and surface emissivity, respectively. Figure 2d shows the result of a comparison of CO_2 retrievals from uncorrected original TIR L1B spectra. The existence of a relatively large spectral bias around the CO_2 15 μm absorption band in TANSO-FTS TIR L1B spectra (Kataoka et al., 2014) resulted in a decrease in the number of normally retrieved CO_2 profiles. In the V1.0 case (Figure 2a), CO_2 profiles were normally retrieved for 74 of the 114 coincident pairs. The comparison between Figure 2a and 2c (Figure 2b and 2d) demonstrated T that t~~he correction of the TIR L1B spectral bias through the simultaneous retrieval of surface temperature ~~could~~ increase~~d~~ the number of normally retrieved CO_2 profiles ~~(in this case, from 48 to 74)~~. This implies that a wavelength-independent component of the spectral bias in CO_2 absorption bands could be reduced by adjusting the value of surface temperature at the bands. In contrast, ~~the comparisons between Figure 2a and 2b and Figure 2c and 2d showed that~~ the spectral bias correction ~~of the TIR L1B spectral bias~~ through the simultaneous retrieval of surface emissivity~~–~~ did not increase the number of normally retrieved CO_2 profiles~~had a relatively small impact on TIR L2 CO_2 retrieval~~. If the TIR L1B spectral bias has a wavelength dependence, ~~Nevertheless,~~ surface emissivity ~~, which has a wavelength dependence,~~ could~~an~~ be effective for correcting such a wavelength-dependent bias~~the wavelength-dependent L1B spectral bias~~. A more effective method of L1B spectral bias correction based on surface emissivity should be considered in the next version of the TIR L2 CO_2 retrieval algorithm, if a future version of the TIR L1B spectral data still has a bias.

5 Comparison ~~methods of TANSO-FTS TIR V1.0 upper atmospheric CO_2 data with CME CO_2 data~~

5.1 Area comparisons

Here, we used the level flight CO_2 data of CONTRAIL CME observations in 2010 to validate the quality of UTLS CO_2 data from the TANSO-FTS TIR ~~V1.0~~V1 L2 CO_2 product. The level flight data obtained from~~in~~ the following eight airline routes of the CONTRAIL CME observations were used in this study: Tokyo–Amsterdam (NRT–AMS) and Tokyo–Moscow (NRT–DME), Tokyo–Vancouver (NRT–VYR), Tokyo–Honolulu (NRT–HNL), Tokyo–Bangkok (NRT–BKK), Tokyo–Singapore (NRT–SIN) and Tokyo–Jakarta (NRT–CGK), and

Tokyo–Sydney (NRT–SYD). We merged the level flight data of Tokyo–Amsterdam and Tokyo–Moscow into "Tokyo–Europe", and the data of Tokyo–Singapore and Tokyo–Jakarta into "Tokyo–East Asia". ~~, and the data of Tokyo–Singapore and Tokyo–Jakarta into "Tokyo–East Asia".~~ Figure 2~~3~~ shows the flight tracks of all of the CONTRAIL CME observations in 2010 used in this study. As shown in the figure, we divided the CONTRAIL CME level flight data into 40 areas following Niwa et al. (2012), and compared them with TANSO-FTS TIR CO_2 data in each area in each season. ~~The level flight data in each area were averaged for each season (MAM, JJA, SON, and JF/DJF).~~ The amount of level flight data varied depending on the area and season. The largest amount of data was obtained in area 15 over Narita Airport, where 4,694–9,306 data points were obtained. A relatively small amount of level flight data, 79–222 data points, was obtained in area 1 over Amsterdam. In all 40 areas, we collected sufficient level flight data to undertake comparison analysis based on the average values, except for seasons and regions with no flights.

5.2 Comparisons of CME profiles with and without averaging kernels

In comparisons of TIR V1 L2 CO_2 data with the CONTRAIL CME level flight data, it is difficult to smooth the CME data by applying TIR CO_2 averaging kernels, because CO_2 concentrations below and above the CME flight levels were not observed. Here, we evaluated the impact of considering averaging kernel functions on CO_2 concentrations using the CME profile data. We regarded the CME data obtained during the ascent and descent flights over the nine airports as part of CO_2 vertical profiles, and investigated differences between TIR and CME CO_2 data with and without applying averaging kernel functions in the altitude regions around the CME level flight observations. We assumed the CME ascending/descending CO_2 concentration at the uppermost altitude level to be constant up to the tropopause height, following the method proposed by Araki et al. (2010). We used stratospheric CO_2 data taken from the Nonhydrostatic Icosahedral Atmospheric Model (NICAM)–Transport Model (TM) (Niwa et al., 2011; 2012) to create whole CO_2 vertical profiles over the airports. The NICAM-TM CO_2 data used here introduced CONTRAIL CO_2 data to the inverse model in addition to surface CO_2 data, and therefore could simulate upper atmospheric CO_2 concentrations well (Niwa et al., 2012). We determined the stratospheric CO_2 profile by assuming the CO_2 concentration gradients, calculated on the basis of the NICAM-TM CO_2 data above the tropopause height.

To compare these CME CO_2 profiles with TIR CO_2 data, we calculated a weighted average of all the CME CO_2 data included in each of the 28 retrieval grid layers with respect to altitude, and defined the CO_2 data in the 28 layers as "CONTRAIL (raw)" data. Then, we selected TIR CO_2 data that coincided with each of the CONTRAIL (raw) profiles. The criteria for the coincident pairs were a 300 km distance from Narita airport, and a 3-day difference of each other observation. We applied TIR CO_2 averaging kernel functions to the corresponding CONTRAIL (raw) profile, as follows (Rodgers and Connor, 2003):

$$\mathbf{x}_{\mathrm{CONTRAIL\,(AK)}} = \mathbf{x}_{\mathrm{a\,priori}} + \mathbf{A}\left(\mathbf{x}_{\mathrm{CONTRAIL\,(raw)}} - \mathbf{x}_{\mathrm{a\,priori}}\right). \quad (5)$$

Here, $\mathbf{x}_{\mathrm{CONTRAIL\,(raw)}}$ and $\mathbf{x}_{\mathrm{a\,priori}}$ are CONTRAIL (raw) and a priori CO_2 profiles. We defined the CONTRAIL (raw) data with TIR CO_2 averaging kernel functions as "CONTRAIL (AK)" data.

5.3 Level flight comparisons

In this study, we made comparisons between TIR and CONTRAIL CME level flight CO_2 data in two ways. The first was a direct comparison with original CME CO_2 data, i.e., CONTRAIL (raw) data. The second was a comparison with CONTRAIL (AK) data in the altitude regions around the CME level flight observations that were based on "assumed CO_2 profiles" created at each of the measurement locations of all the CME level flight data. In the first comparison with CONTRAIL (raw) data, the CME level flight data in each of the 40 areas were averaged for each season (MAM, JJA, SON, and JF/DJF). ~~In all 40 areas, we collected an enough amount of level flight data to undertake a comparative analysis based on the average values, except for seasons and regions with no flights.~~ The average altitude of all of the ~~CONTRAIL~~ CME level flight data used here was 11.245 km. The airline routes of Tokyo–Europe, Tokyo–Vancouver, and Tokyo–Honolulu contained both tropospheric and stratospheric data in the areas along their routes; therefore, we calculated the average and standard deviation values separately. Here, we differentiated between the tropospheric and stratospheric level flight data on the basis of temperature lapse rates from the JMA GPV data that were interpolated to the CONTRAIL CME measurement locations. The average altitudes of the tropospheric and stratospheric level flight data from the airline route between Tokyo and Europe were 10.84 km and 11.18 km, respectively.

In the comparison with CONTRAIL (raw) data, ~~Next,~~ we selected TANSO-FTS TIR ~~V1.0~~V1 L2 CO_2 data that were in the altitude range within ±1 km of the average altitude of the

CME~~ONTRAIL~~ level flight data for each area for each season, and calculated their averages and standard deviations. Similarly, we calculated the averages and standard deviations of the corresponding a priori CO_2 data for each area for each season. For the airline routes of Tokyo–Europe, Tokyo–Vancouver, and Tokyo–Honolulu, the averages and standard deviations of TIR ~~V1.0~~V1 CO_2 data and the corresponding a priori CO_2 data were calculated separately for the tropospheric and stratospheric data. In this calculation, we first selected TIR ~~V1.0~~V1 CO_2 data that were collected in a range within ±1 km of the average altitudes of the CONTRAIL tropospheric and stratospheric CO_2 data for each area. Then, we classified each of the selected TIR CO_2 data points into tropospheric and stratospheric data on the basis of the temperature lapse rates from the JMA GPV data that were interpolated to the TANSO-FTS measurement locations, and calculated the seasonal averages and standard deviations for the reselected tropospheric and stratospheric TIR CO_2 data. This procedure was required for two reasons~~:~~. (1)~~One was that a~~ tropopause height at each TANSO-FTS measurement location should differ on a daily basis, and (2)~~. The other was that~~ because ~~TANSO-FTS~~ TIR CO_2 data were selected within the range of 2 km, some tropospheric TIR CO_2 data were selected on the basis of the CONTRAIL stratospheric level flight data, and vice versa. Figure 3~~4~~ shows the number of TANSO-FTS TIR CO_2 data points that were finally selected in each retrieval layer for each of the airline routes. The TIR CO_2 data used in the comparative analysis were mainly from layers 9 and ~~layer~~ 10 (from 287 to 196 hPa) for the tropospheric comparison and from layers 10 and ~~layer~~ 11 (from 237 to 162 hPa) for the stratospheric comparison.

In the second comparison, we assumed a CO_2 vertical profile on the basis of CONTRAIL (raw) data at each of the CONTRAIL CME level flight locations, and applied TIR CO_2 averaging kernel functions to the assumed profiles. For this purpose, realistic CO_2 vertical profiles were required along the eight airline routes. In this study, we created a CO_2 profile at each CME level flight measurement location from CarbonTracker CT2013B monthly-mean CO_2 data (Peters et al., 2007). The CarbonTracker CT2013B CO_2 data are available to the public, and therefore readers can refer to the dataset that we used as a CO_2 climatological dataset. The method for creating a CO_2 vertical profile from the CONTRAIL (raw) and CarbonTracker CT2013B data is as follows. We first averaged all of the CarbonTracker CT2013B monthly-mean data included in each of the 40 areas to create area-averaged CarbonTracker CT2013B profiles. Then, we shifted the area-averaged CarbonTracker CT2013B profile so that its concentration fit to each of the CONTRAIL (raw) data at CME

level flight altitude. Finally, we applied area-averaged TIR CO_2 averaging kernel functions to each of the shifted area-averaged CO_2 profiles, and created profiles of CONTRAIL (AK) at all the CME level flight measurement locations.

We compared the CONTRAIL (AK) data with TIR CO_2 data at the altitude regions around the CME level flight observations for each area in each season. We extracted CONTRAIL (AK) data that corresponded to the TIR retrieval layers where TIR CO_2 data were compared to CONTRAIL (raw) data, and averaged them for each area for each season. For the airline routes of Tokyo–Europe, Tokyo–Vancouver, and Tokyo–Honolulu, we separately averaged CONTRAIL (AK) data created from tropospheric and stratospheric CONTRAIL (raw) data, and defined the averages as tropospheric and stratospheric CONTRAIL (AK) data, respectively. As shown in Figure 3, the CONTRAIL (AK) data used for the comparison during flights between Tokyo and Sydney consisted of CO_2 concentrations in layers 9 and 10 of the CONTRAIL (AK) profiles. For the flights between Tokyo and Europe, the CONTRAIL (AK) data used for the tropospheric and stratospheric comparisons were based on CO_2 concentrations in layers 9 and 10 and in layers 10 and 11 of CONTRAIL (AK) profiles, respectively.

~~We did not apply TIR CO_2 averaging kernels to CONTRAIL CME CO_2 data in the following UTLS analysis. Because CO_2 concentrations below and above the CONTRAIL CME flight levels were not observed except over airports, assuming a CO_2 vertical profile for each of CONTRAIL CME level flight data points and applying averaging kernels to the assumed CONTRAIL CO_2 profiles would increase the uncertainty in the CONTRAIL CO_2 data. Here, we assess the effect of not applying averaging kernels to CONTRAIL CME level flight data. Figure 5a shows the means of the averaging kernels of each of the three layers 9, 10, and 11 of all of the TANSO-FTS TIR CO_2 profiles used in the comparisons in summer. In Figure 5, we show examples of area 40 in the airline route between Tokyo and Honolulu, where we had a large amount of data for comparison, and area 1 in the airline route between Tokyo and Amsterdam, where we had data for comparison both in the troposphere and stratosphere. Considering the half value width of the averaging kernels in Figure 5a, the TANSO-FTS TIR CO_2 retrieval results in layers 9–11 would be affected by CO_2 concentrations from ~400 to ~120–130 hPa. As shown in the CONTRAIL CME ascending/descending CO_2 profiles in Figure 5b, the variability in the CO_2 concentration from ~400 to ~200 hPa was relatively small in summer; the same was true in the other three seasons. This indicates that CO_2~~

~~concentrations below layer 9 had a small impact on the TIR CO_2 retrieval results in layers 9 and 10, which suggests that the following results do not change much, even when considering the averaging kernels related to the layers below layer 9. Consequently, we determined not to apply TIR CO_2 averaging kernels to CONTRAIL CME CO_2 data in this study. However, because we did not have CONTRAIL CME CO_2 data above ~200 hPa, we could not evaluate the impact of the CO_2 concentration above ~200 hPa on TANSO-FTS TIR CO_2 retrieval results in layers 9–11 on the basis of observation data. Thus, we should discuss again the effect of not applying averaging kernels to CONTRAIL CME data on the following comparison results in Section 6.~~

~~5.2 Results of the comparisons~~

6 Comparison results

6.1 Impacts of averaging kernels on CME profiles

Figure 4 shows comparisons of the differences between TANSO-FTS TIR and CONTRAIL (raw) CO_2 data, and the differences between TIR and CONTRAIL (AK) CO_2 data in low (BKK), middle (NRT and SYD), and high (DME) latitudes in layers 9, 10, and 11. In low latitudes, the differences between CONTRAIL (raw) and CONTRAIL (AK) were mostly less than 0.5 ppm in all seasons. This is because the tropopause heights there were much higher than the altitude levels of CONTRAIL CME level flight measurements, and CO_2 concentrations did not change much in the altitude regions where we compared TIR and CONTRAIL CME data. The same was true for other airports in low latitudes. While the differences between CONTRAIL (raw) and CONTRAIL (AK) were larger in middle and high latitudes than in low latitudes, they were in most cases less than 1 ppm in all seasons. In conclusion, the impact of applying the TIR CO_2 averaging kernels on CONTRAIL CME CO_2 data at around the CME level flight altitudes (~11 km) was on average less than 0.5 ppm in low latitudes and less than 1 ppm in middle and high latitudes.

6.2 Comparisons during level flight

The airline route between Tokyo and Sydney covered a wide latitude range from the northern mid-latitudes (35°N) to southern mid-latitudes (34°S). Figure 5~~6~~ shows ~~the~~ comparisons among CONTRAIL (raw), CONTRAIL (AK)~~CME level flight~~, TANSO-FTS TIR, and a

priori CO_2 data during flights between Tokyo and Sydney in spring. In this case, we averaged CO_2 data mainly from layers 9 and 10 of the TIR retrieval layer levels. The 1-σ values of the averages show the variability of CO_2 concentrations in these UTLS layers. The average of the TIR CO_2 data agreed better with~~to~~ the averages of the CONTRAIL (raw) and (AK) CO_2 data than the a priori CO_2 data in all ~~of the~~ latitudes. The differences between CONTRAIL (raw) and CONTRAIL (AK) were approximately 0.5 ppm, which is consistent with the result shown in Figure 4, despite the fact that CONTRAIL (AK) data here were evaluated on the basis of CarbonTracker monthly-mean data. In the Southern Hemisphere, the average of the TIR CO_2 data was within 0.1% of the ~~average~~ averages of the CONTRAIL~~–~~ (raw) and CONTRAIL (AK) CO_2 data. In the Northern Hemisphere, the average of the TIR CO_2 data agreed with the averages of the CONTRAIL (raw) and CONTRAIL (AK) CO_2 data to within 0.5%, although the~~ir~~ agreement was~~became~~ slightly worse there than in~~compared to~~ the Southern Hemisphere.

Along the airline route between Tokyo and Europe, both tropospheric and stratospheric CO_2 data were obtained in the CONTRAIL CME observations. Therefore, we were able to validate the quality of TANSO-FTS TIR CO_2 data for this route both in the upper troposphere and lower stratosphere using the UTLS ~~UTLS~~ CME~~ONTRAIL~~ CO_2 data. Here, we averaged CO_2 data mainly from layers 9 and 10 for the upper tropospheric comparison and from layers 10 and 11 for the lower stratospheric comparison. As shown in Figure 6, the differences between CONTRAIL (raw) and CONTRAIL (AK) were again approximately 0.5 ppm when CONTRAIL CME data were divided into the upper troposphere and lower stratosphere, which is consistent with the result shown in Figure 4. Figure 6~~7~~b and 6~~7~~c shows that the differences between the upper tropospheric and lower stratospheric CO_2 concentrations of CONTRAIL CME data were approximately 2–3 ppm in ~~the~~ winter (maximum of 4.24 ppm in area 14). The upper tropospheric and lower stratospheric CO_2 concentrations from TANSO-FTS TIR ~~V1.0~~V1 data also clearly differed ~~clearly~~, while the upper tropospheric and lower stratospheric CO_2 concentrations from a priori data were similar. The upper tropospheric TIR CO_2 concentrations were in a ~~fairly~~ good agreement within 1 ppm with the corresponding CONTRAIL (raw) and CONTRAIL (AK)~~CME~~ data (Figure 6~~7~~b). In the lower stratosphere in winter (Figure 6~~7~~c), the averages of the CONTRAIL (raw), CONTRAIL (AK)~~CME level flight~~, TANSO-FTS TIR, and a priori CO_2 data were all within 0.5–1 ppm of each other.~~nearly identical.~~

Figure 78 shows the results of all of the comparisons among CONTRAIL (raw), CONTRAIL (AK)CME, TANSO-FTS TIR, and a priori CO_2 data in the upper troposphere (left) and lower stratosphere (right) for each of the six (eight) airline routes for each season. We divided the data for all four datasets in each of the 40 areas into six latitude bands: 40°S–20°S (areas 30 and 31), 20°S–0° (areas 21, 28, and 29), 0°–20°N (areas 16, 17, 20, 22, 23, 26, and 27), 20°N–40°N (areas 15, 18, 19, 24, 25, and 37–40), 40°N–60°N (areas 1, 2, 14, and 32–36), and 60°N–70°N (areas 3–13). As for the lower stratosphere, we showed the results at northern latitudes of 40°N where an adequate amount of data was obtained. The thick and dashed lines indicate the differences between CONTRAIL CME and TANSO-FTS TIR CO_2 data (TIR ave. minus CONTRAIL ave.) and the differences between CONTRAIL CME and a priori CO_2 data (a priori ave. minus CONTRAIL ave.) for each of the areas along the airline routes. All of the results with more than three data points are presented. Overall, the thick black and gray lines (TIR ave. minus CONTRAIL (raw) ave. and TIR ave. minus CONTRAIL (AK) ave.) lines wereare closer to zero than the dashed linesgreen lines (a priori ave. minus CONTRAIL (raw) ave.),, which means that TIR CO_2 data agreed better withto CONTRAIL CME CO_2 data than a priori CO_2 data.

The left panels of Figure 7 show that the agreements between TIR and CONTRAIL (raw) and CONTRAIL (AK) CO_2 average data were worse in spring and summer than in fall and winter in the Northern Hemisphere in the upper troposphere. The differences between TIR and CONTRAIL (raw) and CONTRAIL (AK) CO_2 data were on average within 1 ppm in fall and winter in the northern troposphere. At 0°–40°N in summer, in contrast, the TIR and a priori CO_2 average data were 2.3 ppm lower than the CONTRAIL (AK) CO_2 average data. At 20°N–40°N in spring, the differences between TIR and CONTRAIL (AK) CO_2 average data were 2.4 ppm, although the TIR CO_2 data had a better agreement with CONTRAIL CME CO_2 data than a priori CO_2 data. On the other hand, the averages of the TIR CO_2 data were within 0-0.7 ppm of the averages of the CONTRAIL (AK) CO_2 data in the Southern Hemisphere in all seasons, as in the comparison in spring shown in Figure 5.

In the lower stratosphere, the agreements between the average TANSO-FTS TIR and CONTRAIL CME CO_2 data did not have a smaller seasonality than in the upper troposphere. The averages of TIR and CONTRAIL (raw) and CONTRAIL (AK) CO_2 data agreed with each other within 0.5% in all seasons.For the airline route between Tokyo and Europe (Figure 8a), the agreement between tropospheric TANSO-FTS TIR and CONTRAIL CME CO_2

~~average data seemed slightly better in winter, although comparisons among seasons in the troposphere were difficult because of the lack of CONTRAIL CME data in high latitudes in the spring and summer (Figure 8a1). In the stratosphere (Figure 8a2), the averages of TIR and CONTRAIL CO_2 data agreed well with each other, and their differences were within ~0.5–1 ppm in the spring, summer, and winter. The differences between the two averages were slightly larger in the fall (approximately 2 ppm). For the airline route between Tokyo and Vancouver (Figure 8b), the averages of the TIR CO_2 data were more similar to the averages of the CONTRAIL CO_2 data than the a priori CO_2 data both in the upper troposphere and lower stratosphere in the fall and winter; the differences between the TIR and CONTRAIL CO_2 average data were approximately within 1 ppm. For the airline route between Tokyo and Honolulu (Figure 8c), the agreement between TIR and CONTRAIL CO_2 average data did not show clear seasonal differences in the lower stratosphere (Figure 8c2), because of a small number of stratospheric data. In contrast, in the upper troposphere (Figure 8c1), the differences between the two were clearly larger in the spring and summer than in the fall and winter. In particular, both the differences between TIR and CONTRAIL CO_2 data and between a priori and CONTRAIL CO_2 data were larger in spring, as was the case for the results of the comparison for the airline route between Tokyo and Vancouver (Figure 8b1).~~

~~Then, we focused on the results of the comparison between TANSO-FTS TIR and CONTRAIL CME upper tropospheric CO_2 data obtained in northern low and middle latitudes. Figure 8d shows that the agreement between TIR and CONTRAIL CO_2 average data was worse in the spring and summer than in the fall and winter for the airline route between Tokyo and Bangkok. The differences between TIR and CONTRAIL CO_2 data exceeded the 1-σ standard deviations of the averages of TIR CO_2 data, and were larger than the differences between a priori and CONTRAIL CO_2 data at 23–34°N (area 20) in the summer. Similarly, the agreement between the averages of TIR and CONTRAIL CO_2 data was worse in the spring and summer than in the fall and winter for the airline route between Tokyo and East Asia (Figure 8e).~~

~~For the airline route between Tokyo and Sydney (Figure 8f), the average of the TANSO-FTS TIR CO_2 data was within 1 ppm of the average of the CONTRAIL CME CO_2 data in the Southern Hemisphere in all of the seasons, as in the comparison in the spring shown in Figure 6. However, in the Northern Hemisphere, the agreement between the two was not as strong in all of the seasons. In the comparisons in the northern summer, although the differences~~

~~between the average TIR and CONTRAIL CO_2 data were less than 1% (3 ppm), there was a relatively large negative bias in the TIR CO_2 data against the CONTRAIL CO_2 data compared to the other seasons. In the upper troposphere in northern summer, TIR CO_2 data showed a significantly good agreement with CONTRAIL CO_2 data compared to a priori CO_2 data in the Southern Hemisphere. However, in northern low and middle latitudes, TIR and a priori CO_2 data had a negative bias of up to 1% against CONTRAIL CO_2 data.~~

~~67~~ Discussion

As shown in Figure 7, TANSO-FTS TIR V1 L2 CO_2 data had a negative bias of 2.3–2.4 ppm against CONTRAIL CME CO_2 data in the northern low and middle latitudes in spring and summer. Uncertainties in surface parameters and temperature profiles could affect CO_2 retrieval in thermal infrared spectral regions. As described above, retrieving surface parameters simultaneously instead of using initial surface parameters did not affect ~~there was no clear difference in~~ CO_2 concentrations in the UTLS regions ~~between the case of using initial surface parameters and the case of simultaneously retrieving surface parameters~~ in the ~~the~~ TIR ~~V1~~ V1 CO_2 retrieval. We compared ~~Here, we compared~~ simultaneously retrieved temperature profiles with~~with~~ a priori JMA GPV temperature profiles ~~used as a priori data~~ in the UTLS region, and did not find any difference ~~. The differences~~ between the two which could explain~~did not show any correlation with~~ the largest TIR CO_2 negative bias in the northern low and middle latitudes in spring and summer. In the UTLS regions, temperature variability~~.~~ is relatively large, and therefore comprehensive validation analysis of both ~~This suggests that the simultaneous retrieval of temperatures are unlikely a main cause of the TIR CO_2 negative bias of 2.3–2.4 ppm in the northern low and middle latitudes in the spring and summer, although~~ the a priori and retrieved temperature profiles should be required~~validated~~ using reliable and independent temperature data such as radiosonde data~~a.~~.

Uncertainty in a priori data could result in uncertainty in retrieved CO_2 data. Here, we arbitrarily decreased the a priori concentration by 1% in a test TIR CO_2 retrieval, and then compared the retrieved CO_2 concentrations with those retrieved using the original a priori data. In the northern low and middle latitudes in spring and summer where the DF values of TIR V1 CO_2 data were around 1.8 and more, a 1% negative bias in a priori data could yield up to a 0.7% negative bias in retrieved CO_2 concentrations in the altitude regions where we did comparisons between TIR and CONTRAIL CME data, although the magnitude of the bias

varied depending on retrievals. As shown by the green lines in Figure 7, a priori CO_2 concentrations were underestimated by 2–4 ppm in the northern low and middle latitudes in spring and summer. The test TIR CO_2 retrieval demonstrated that the negative bias of a priori CO_2 data against CONTRAIL CME data is a possible cause of the TIR CO_2 negative bias in the UTLS regions in the northern low and middle latitudes in spring and summer.

In general, the information content of CO_2 observations made by TIR sensors is higher in middle and high latitudes in spring and summer than in fall and winter because of the thermal contrast in the atmosphere, with less seasonal dependence in low latitudes. Therefore, in spring and summer, retrieved CO_2 data contain more measurement information and are less constrained by a priori data at all latitudes. However, as shown in Figure 7, the retrieved TIR CO_2 data in the northern low and middle latitudes did not sufficiently reduce the negative bias of the a priori CO_2 data in the UTLS regions in spring and summer. This implies the existence of factors that worsened CO_2 retrieval results other than the a priori data, especially in spring and summer. Another possible factor that worsened CO_2 retrieval results is the uncertainty in the calibration of TIR V161.160 L1B spectra. As reported in Kataoka et al. (2014), TANSO-FTS TIR V130.130 L1B radiance spectra had a wavelength-dependent bias ranging from 0.1 to 2 K. Although the characteristics of the spectral bias in V161.160 L1B data used in TIR V1 L2 CO_2 retrievals are still under investigation, we assumed the same degree of bias in V161.160 L1B spectra, and evaluated the effect of the L1B spectral bias on the TIR CO_2 retrieval using the following equation:

$$\mathbf{d}_{CO2} = \mathbf{G}_{CO2}\mathbf{d}_{spec}. \quad (6)$$

Here, $\mathbf{G}_{CO2}$ is a gain matrix for CO_2 retrieval, $\mathbf{d}_{spec}$ is a spectral bias vector based on the evaluation by Kataoka et al. (2014), and $\mathbf{d}_{CO2}$ is a vector of bias errors in retrieved CO_2 concentrations attributable to the spectral bias. The result showed that a wavelength-dependent bias comparable to V130.130 L1B spectra could yield up to 0.3% and 0.5% uncertainties in retrieved CO_2 concentration in the UTLS regions in the northern middle latitude in spring and in the northern low latitude in summer, respectively. Uncertainty in the radiometric calibration of TANSO-FTS L1B spectra causes the spectral bias inherent in TIR L1B spectra. The temperatures of the internal blackbody on board the TANSO-FTS instrument partly reflect the environmental thermal conditions inside the instrument. The temperatures of FTS-mechanics and aft-optics on the optical bench of the TANSO-FTS

instrument are precisely controlled at 23 °C. The difference in temperature between the environment inside the instrument and the optical bench could cause the uncertainty in the radiometric calibration of TANSO-FTS L1B spectra. Thus, the temperatures of the internal blackbody on board the TANSO-FTS instrument could be a parameter used to evaluate the TANSO-FTS TIR L1B spectral bias.

Figure 8~~9~~ shows the averages of the partial degree of freedom of TANSO-FTS TIR ~~V1.0~~V1 L2 CO_2 data for each of the areas along the airline routes between Tokyo and Europe in the upper troposphere (a) and the lower stratosphere (b) for each season. The partial DF is defined as the diagonal element~~trace of a submatrix~~ of the averaging kernels~~s~~ corresponding to ~~a partial column of~~ TIR CO_2 data ~~-~~that were compared to CONTRAIL CME level flight data, which is equal to ~~the averages of~~ the 9th, 10th, or 11th diagonal element of matrix **A**. As shown in Figure 8~~9~~, the average values of the partial DF of TIR lower stratospheric CO_2 data were clearly lower than those of TIR upper tropospheric CO_2 data for all of the fights between Tokyo and Europe. TIR upper tropospheric CO_2 data were from layers 9 and 10, and TIR lower stratospheric CO_2 data were from layers 10 and 11, as shown in Figure 3~~4~~, which led to a clear difference in partial DF values between the TIR upper tropospheric and lower stratospheric CO_2 data. The partial DF values of TIR upper tropospheric CO_2 data were 0.13–0.20 in all of the areas for all seasons. In contrast, the partial DF values of TIR lower stratospheric CO_2 data in ~~the~~ spring, fall, and winter were ~0.05 in almost all of the areas, although they were as high as 0.1–0.14 in ~~the~~ summer. From the results shown in Figure 6c and Figure 8, we conclude that TIR CO_2 retrieval results in the lower stratosphere in winter were constrained to the relatively good a priori CO_2 data due to the low information content, and consequently had a good agreement with CONTRAIL CME CO_2 data. The comparisons in the areas during the airline route between Tokyo and Europe were included in the comparison results of 60°N–70°N in the right panels of Figure 7. In this region, the average differences between a priori and CONTRAIL (raw) data were 1-2 ppm in summer and fall, while they were less than 0.5 ppm in spring and winter. In summer, TIR CO_2 retrievals had a relatively high information content compared to the other seasons, which led to an agreement between TIR and CONTRAIL (raw) and CONTRAIL (AK) CO_2 data of within 0.5 ppm. In fall, TIR CO_2 retrieval results in the lower stratosphere were more constrained to the a priori CO_2 data, and therefore had a negative bias of approximately 1-2 ppm against CONTRAIL (raw) and CONTRAIL (AK) CO_2 data. In conclusion, the quality of TIR V1 CO_2 data in the lower stratosphere depends largely on the information content compared to the upper

troposphere. In the case of high latitude measurements, TIR V1 lower stratospheric CO_2 data are only valid in summer.

~~The thick lines in Figure 8a2 show that the agreement of TIR and CONTRAIL CO_2 data in the lower stratosphere was better in the spring, summer, and winter than in the fall. The dashed lines in Figure 8a2 also show that a priori CO_2 data agreed better with CONTRAIL CME CO_2 data in the lower stratosphere in the spring and winter than in the summer and fall. From the results shown in Figure 8a2 and Figure 9, we conclude that TIR CO_2 retrieval results in the lower stratosphere in the spring and winter were constrained to the relatively good a priori CO_2 data due to the low information content, and consequently had a good agreement with CONTRAIL CO_2 data. In the fall, TIR CO_2 retrieval results in the lower stratosphere were constrained to the relatively poor a priori CO_2 data, and therefore had a negative bias of approximately 2 ppm against CONTRAIL CO_2 data. In the summer, TIR CO_2 retrievals had a relatively high information content compared to the other seasons, which led to a good agreement between TIR and CONTRAIL CO_2 data despite the relatively poor a priori CO_2 data. In conclusion, the quality of TIR V1.0 CO_2 data in the lower stratosphere depends largely on the information content compared to the upper troposphere. In the case of high latitude measurements, TIR V1.0 lower stratospheric CO_2 data are only valid in the summer.~~

~~As shown in Figure 8d, 8e, and 8f, the agreement between TANSO-FTS TIR and CONTRAIL CME CO_2 data was worse in the spring and summer than in the fall and winter in northern low and middle latitudes. At these latitudes, TIR upper tropospheric CO_2 data had a negative bias of up to ~1% against CONTRAIL upper tropospheric CO_2 data. This characteristic was also seen in the data from flights between Tokyo and Honolulu where there was a large amount of upper tropospheric data available in all of the seasons (Figure 8c1). Overall, as shown in Figure 8, a priori CO_2 data used in TIR V1.0 CO_2 retrievals had a negative bias against CONTRAIL CO_2 data. The a priori CO_2 data in the spring and summer in Figure 8d, 8e, and 8f clearly had a larger negative bias against the corresponding CONTRAIL CO_2 data. The results show that a priori CO_2 data taken from NIES TM 05 underestimate the increase in the CO_2 concentration in the upper atmosphere in spring and summer, which results in a larger negative bias of TIR V1.0 upper tropospheric CO_2 data in the spring and summer than in the fall and winter in northern low and middle latitudes.~~

~~In general, information content of CO_2 observations made by TIR sensors is higher in middle and high latitudes in the spring and summer than in the fall and winter because of thermal contrast in the atmosphere, with less seasonal dependence in low latitudes. Therefore, in the spring and summer, retrieved CO_2 data contain more measurement information and are less constrained by a priori data in all latitudes. However, as shown in Figure 8, the retrieved TIR CO_2 data in the Northern Hemisphere did not sufficiently reduce the negative bias of the a priori CO_2 data in the spring and summer. The degree of improvement in the spring and summer was comparable to or worse than in the fall and winter. This implies the existence of factors that worsened CO_2 retrieval results other than the poor a priori data in the spring and summer. One of the possible factors is uncertainty in JMA GPV temperature profiles used in TIR V1.0 L2 CO_2 retrieval. If they have some seasonal bias, seasonally dependent bias in retrieved CO_2 data would be produced. However, the TIR V1.0 algorithm simultaneously retrieved temperature profiles other than CO_2, and therefore the effect of temperature uncertainty on retrieved CO_2 data should be reduced.~~

~~Another possible factor that worsened CO_2 retrieval results is uncertainty in the calibration of TIR V161.160 L1B spectra. This means that the amount of TIR V161.160 L1B spectral bias has some seasonal dependence. Therefore, we investigated an appropriate parameter to evaluate the uncertainty in TANSO-FTS TIR L1B spectra. The temperatures of the internal blackbody on board the TANSO-FTS instrument partly reflect the environmental thermal condition inside the instrument. The temperatures of FTS-mechanics and aft-optics on the optical bench of the TANSO-FTS instrument are precisely controlled at 23 degrees Celsius. The difference in temperature between the environment inside the instrument and the optical bench would cause the uncertainty in radiometric calibration of TANSO-FTS L1B spectra. Thus, the temperatures of the internal blackbody on board the TANSO-FTS instrument could be a parameter to evaluate the TANSO-FTS TIR L1B spectral bias.~~

~~Figure 10 is a scatter-plot of the average temperatures of the onboard internal blackbody and the average differences between TANSO-FTS TIR and CONTRAIL CME CO_2 data shown in Figure 8 for each area for each season. The average temperatures of the on-board internal blackbody were lower in the spring and summer than in the fall and winter in all of the areas. It can be seen from Figure 10 that the internal blackbody temperatures in the summer (diamonds) were lower than those in the other seasons (crosses). As discussed above, a priori CO_2 data had a larger negative bias against CONTRAIL CME CO_2 data particularly in~~

~~northern low and middle latitudes in the spring and summer, which led to a larger negative bias in retrieved TIR CO_2 data at these latitudes. In addition, retrieved TIR CO_2 data had a larger bias in summer when the internal blackbody temperatures were lower, even if the amount of negative bias in a priori CO_2 data in summer was comparable to that in the other seasons, as shown in Figure 10. As stated above, the temperature of the onboard internal blackbody could be a candidate for evaluating the spectral bias. At this moment, however, there is no definite evidence of a clear correlation between the temperatures of the onboard internal blackbody and the bias in TANSO-FTS V161.160 L1B spectra that would subsequently cause the seasonally dependent bias in the TIR V1.0 L2 CO_2 data, because the correlation between the average temperatures of the onboard internal blackbody and the average differences between TIR and CONTRAIL CO_2 data is not very strong.~~

~~The TANSO-FTS TIR V1.0 L2 CO_2 algorithm simultaneously retrieves surface temperature and surface emissivity as a corrective parameter of the bias in TIR L1B spectra. Therefore, the uncertainty in these surface parameters would have a large impact on retrieved TIR CO_2 profiles. Figure 7d and 7e in Saitoh et al. (2009) show that the uncertainty of retrieved UTLS CO_2 concentrations in layers 9–11 is much less than 1% when the surface parameters have 1% uncertainty, although the uncertainty of CO_2 concentrations at ~400 hPa reaches 3% for the same condition. We conclude that the uncertainty of the surface parameters has a relatively small impact on the TIR UTLS CO_2 concentrations that were the focus of this study. The uncertainties in surface parameters and water vapor in lower atmosphere largely affect lower and middle tropospheric TIR CO_2 data, and therefore should be discussed when validating the quality of TIR CO_2 data in the lower and middle troposphere, which is beyond the scope of this paper.~~

~~We compared TANSO-FTS TIR V1.0 L2 upper tropospheric and lower stratospheric CO_2 data that were mainly from layers 9 and 10 and from layers 10 and 11 with the corresponding CONTRAIL CME tropospheric and stratospheric CO_2 data without applying the TIR CO_2 averaging kernels to the CONTRAIL CO_2 data. As discussed above, CO_2 concentrations below layer 9 have a small impact on TIR CO_2 retrieval results in layers 9 and 10, because the variability in the CO_2 concentration from ~400 to ~200 hPa was relatively small in all of the seasons. However, in layer 11, TIR CO_2 retrieval results could be overestimated by the effect of the CO_2 concentration below layer 9, if the atmosphere in layer 11 is stratospheric air with relatively low CO_2 concentrations. On the other hand, TIR CO_2 retrieval results in layers 9–11~~

~~could also be affected by CO_2 concentration from ~200 to ~120–130 hPa, judging from the half-value width of the averaging kernels in Figure 5a. If the atmosphere from ~200 to ~120–130 hPa is stratospheric air with low CO_2 concentrations, retrieved TIR CO_2 concentrations in layers 9–11 could be underestimated. In summary, retrieved TIR CO_2 concentrations could be underestimated in layers 9–10, and face the conflicting possibility of being overestimated and/or underestimated in layer 11. However, because we did not have CO_2 observation data below and above the CONTRAIL CME flight levels, we cannot reach a definite conclusion. As shown in Figure 8, TIR upper tropospheric CO_2 data had a slightly negative bias against CONTRAIL CME CO_2 data. In the comparison of the airline route of Tokyo–Sydney as shown in Figure 6, the differences between the averages of TIR CO_2 data and the averages of CONTAIL CO_2 data were slightly larger in the Northern Hemisphere (0.5%) than in the Southern Hemisphere (0.1%). The difference between upper tropospheric and lower stratospheric CO_2 concentrations is larger in the Northern Hemisphere in spring (Sawa et al., 2012), which would cause a slightly larger negative bias in the Northern Hemisphere than in the Southern Hemisphere. The effect of lower CO_2 concentrations from ~200 to ~120–130 hPa on TIR CO_2 retrieval results in layers 9–10 could be one of the causes of a negative bias in retrieved CO_2 data other than the negative bias of a priori CO_2 data and the spectral bias of TIR V161.160 L1B spectra.~~

We investigated the differences between TIR and CONTRAIL CO_2 comparison results in layers 9–11 with and without applying averaging kernel functions ~~although in limited areas~~ over the nine~~several~~ airports where CO_2 vertical profiles were observed during ascent and descent. In the northern middle latitudes in spring (NRT in Figure 4), CONTRAIL (AK) was on average 0.2 and 1.2 ppm lower than CONTRAIL (raw) in layers 9 and 10. In contrast, the tendency was the opposite in the southern middle latitudes in spring (SYD in Figure 4); CONTRAIL (AK) was on average 1.1 and 0.4 ppm higher than CONTRAIL (raw) in layers 9 and 10. This means that CO_2 concentrations in layers 9 and 10 were more affected by stratospheric air with relatively low CO_2 concentrations in the northern middle latitude in spring, when considering averaging kernels. This is consistent with the result of Sawa et al. (2012) showing that the difference between upper tropospheric and lower stratospheric CO_2 concentrations was larger in the Northern Hemisphere in spring. ~~Following the method proposed by Araki et al. (2010), we used CONTRAIL ascending/descending CO_2 data below a tropopause and stratospheric CO_2 concentrations taken from the Nonhydrostatic Icosahedral Atmospheric Model (NICAM) Transport Model (TM) (Niwa et al., 2011) to create CO_2~~

~~profiles over airports. In northern middle latitudes in the spring (over NRT airport), considering averaging kernel functions by using Expression (5) decreased a negative bias in TIR CO_2 data in layers 9 and 10 by ~1 ppm. On the other hand, the same tendency was not seen in southern middle latitudes in the spring (SYD) when considering averaging kernel functions. This is consistent with the above discussion related to Sawa et al. (2012). In the summer and fall in middle latitudes in both hemispheres, the effect of considering averaging kernel functions on TIR and CONTRAIL CO_2 comparison results was negligible (less than ~0.5 ppm), although CONTRAIL CO_2 data in layers 9 and 10 with averaging kernel functions became slightly larger there. In low latitudes (BKK, SIN, and CGK), differences between TIR and CONTRAIL CO_2 comparison results in layers 9 and 10 with and without considering averaging kernel functions were also negligible in every season. In northern high latitudes (AMS and YVR), bias of TIR lower stratospheric CO_2 data against CONTRAIL CO_2 data in layers 10 and 11 tended to diminish when considering averaging kernel functions, and the effect of considering averaging kernel functions on TIR and CONTRAIL upper tropospheric CO_2 comparison results in layers 9 and 10 was again negligible.~~

Using CONTRAIL CME level flight observations that covered wide spatial areas allowed~~makes~~ us to discuss ~~the~~a longitudinal differences in the characteristics of TIR UTLS CO_2 data. In the comparison results of the airline routes of Tokyo–Europe (Figure 6) and Tokyo–Vancouver (not shown here)~~shown in Figure 8a and 8b~~, the magnitudes of the differences between TIR and CONTRAIL (raw) and (AK) CO_2 data did not have a clear longitudinal dependence. Table 2 summarizes the latitudinal dependence of the magnitudes of the differences between TIR and CONTRAIL (AK) CO_2 data.~~were similar in every longitude in the fall and winter in the upper troposphere and in every season in the lower stratosphere, although there is little logic to discuss the longitudinal differences in the spring and summer in the upper troposphere because of a small number of the data. On the other hand, in the comparison results of Tokyo–Honolulu, differences between TIR and CONTRAIL CO_2 data became larger toward ~165°W (195° in Figure 8c1) in the spring. This area is located at 25°N, and differences between TIR and CONTRAIL CO_2 data were also large in area 20 (in the airline route of Tokyo–Bangkok), area 27 (Tokyo–East Asia), and area 28 (Tokyo–Sydney) located in the same latitude region, which implies that these biases depended on latitude, not on longitude. We conclude that the data quality of TIR V1.0 L2 UTLS CO_2 data does not have a clear longitudinal dependence. Finally, we evaluated bias values of TIR V1.0 CO_2 data against CONTRAIL CME CO_2 data for each season for each of the latitude regions: 60–70°N~~

~~(areas 3–13), 40–60°N (areas 1, 2, 14, 35, 37, 41–43), 20–40°N (areas 15, 20, 21, 27, 28, 36, 38–40), 0–20°N (areas 18, 22, 19, 25, 26, 29, 30), 0–20°S (areas 23, 31, 32), and 20–40°S (areas 33, 34). The bias values are the weighted averages of differences between TIR and CONTRAIL averaged CO_2 data of the areas located in each latitude region with considering the number of TIR CO_2 data in each of the areas.~~ In the upper troposphere in ~~2~~0–60°N, negative biases in TIR CO_2 data against CONTRAIL CME CO_2 data ranged~~ing~~ from 1~~2~~.2~~2~~ to 2.4~~7~~ ppm ~~and from 1.2 to 1.6 ppm were seen~~ in ~~the~~ spring and summer~~, respectively~~, when applying averaging kernels to the assumed CME CO_2 profiles created based on CarbonTracker CT2013B monthly-mean profiles.~~as summarized in Table 2. Although the evaluation on the basis of NICAM-TM stratospheric CO_2 concentrations in limited areas over several airports, considering averaging kernel functions decreased a negative bias in TIR CO_2 data by ~1 ppm in the spring and slightly increased a negative bias in the summer in northern middle latitudes. Thus, the following negative biases should be considered when incorporating TIR V1.0 upper tropospheric CO_2 data in inverse models which usually consider averaging kernel functions: ~2.0 ppm in both spring and summer in 20–40°N, ~1.0 ppm in spring and ~1.5 ppm in summer in 40–60°N. In northern low latitudes (0–20°N), the negative bias of 2.0 ppm should be taken into account in summer, as presented in Table 2. In the lower stratosphere in northern high latitudes, bias of TIR CO_2 data against CONTRAIL CME CO_2 data tended to diminish when considering averaging kernel functions.~~ It is the negative biases in the northern low and middle latitudes that we should in particular~~mainly~~ be concerned~~care~~ about when using TIR ~~V1.0~~V1 L2 CO_2 data in any scientific analysis. In the upper troposphere in the northern middle latitudes, CO_2 concentrations reach the maximum from spring through early summer. The negative biases in TIR CO_2 data resulted in ~~there make~~ the maximum ~~of~~ TIR CO_2 concentrations being lower than that~~hat~~ of the CONTRAIL CME CO_2 concentrations, which le~~dads~~ to an underestimate of the amplitude of the CO_2 seasonal variation when using TIR CO_2 data without taking their negative biases into account.

~~7~~8 Summary

In this study, we conducted a comprehensive validation of the UTLS CO_2 concentrations from the GOSAT/TANSO-FTS TIR ~~V1.0~~V1 L2 CO_2 product. The TIR ~~V1.0~~V1 L2 CO_2 algorithm used both the CO_2 10 μm and 15 μm absorption bands (690–750 cm^{-1}, 790–795 cm^{-1}, 930–990 cm^{-1}, and 1040–1090 cm^{-1}), and simultaneously retrieved vertical profiles of CO_2, water

vapor, ozone, and temperature in these wavelength regions. Because the TANSO-FTS TIR V161.160 L1B radiance data used in the TIR ~~V1.0~~V1 L2 CO_2 retrieval had a spectral bias, we simultaneously derived surface temperature and surface emissivity in the same wavelength regions ~~just~~ as a corrective parameter, other than temperature and gas profiles, to correct the spectral bias. The simultaneous retrieval of surface temperature greatly increased the number of normally retrieved CO_2 profiles.

To validate the quality of TIR ~~V1.0~~V1 upper atmospheric CO_2 data, we compared them with the level flight CO_2 data of ~~the~~ CONTRAIL CME observations along the following airline routes in 2010: Tokyo–Europe (Amsterdam and Moscow), Tokyo–Vancouver, Tokyo–Honolulu, Tokyo–Bangkok, Tokyo–East Asia (Singapore and Jakarta), and Tokyo–Sydney. For the CONTRAIL data obtained during the northern high latitude flights, we made comparisons among CONTRAIL, TIR, and a priori CO_2 data separately in the upper troposphere and in the lower stratosphere. The TIR upper tropospheric and lower stratospheric CO_2 data that were compared were mainly from layers 9 and 10 (287–196 hPa) and from layers 10 and 11 (237–162 hPa), respectively. In this study, we evaluated the impact of considering TIR CO_2 averaging kernel functions on CO_2 concentrations using the CME profile data over the nine airports; the impact at around the CME level flight altitudes (~11 km) was on average less than 0.5 ppm in low latitudes and less than 1 ppm in middle and high latitudes.

In the Southern Hemisphere, the averages of TANSO-FTS TIR V1 upper atmospheric CO_2 data were within 0.1% of the averages of CONTRAIL CO_2 data with and without TIR CO_2 averaging kernels for all ~~of the~~ seasons, from the limited comparisons made during flights between Tokyo and Sydney, while ~~. In the Northern Hemisphere,~~ TIR CO_2 data had a better agreement with CONTRAIL CO_2 data than a priori CO_2 data, with the agreement being on average within 0.5% in the Northern Hemisphere. The~~The~~ northern high latitude comparisons suggest that the quality of TIR lower stratospheric CO_2 data depends largely on the information content. In high latitudes, TIR ~~V1.0~~ lower stratospheric CO_2 data are only valid in ~~the~~ summer when their information content is highest. Overall, the agreements of TIR and CONTRAIL CME CO_2 data were worse in spring and summer than in fall and winter in the Northern Hemisphere in the upper troposphere. TIR CO_2 data had a negative bias up to 2.4 ppm against CONTRAIL CO_2 data with TIR CO_2 averaging kernels in the northern low and middle latitudes in spring and summer. This is ~~In the northern low and middle latitudes, the~~

~~agreement between TIR and CONTRAIL CO_2 data in the upper troposphere was worse in the spring and summer than that in the fall and winter,~~ partly because of ~~the~~a larger negative bias in the a priori CO_2 data ~~in the spring and summer than in the fall and winter~~. The~~In addition, a seasonal dependence of the~~ spectral bias inherent to TANSO-FTS TIR L1B radiance data could cause a negative bias in retrieved CO_2 concentrations, particularly in summer. TIR sensors can make more observations than SWIR sensors. When using the TIR UTLS CO_2 data,~~The combined use of TIR UTLS CO_2 data and XCO_2 data from the SWIR bands of TANSO-FTS can be useful for studies of CO_2 surface flux inversion and atmospheric transport, provided that~~ the seasonally and regionally dependent negative biases of the TIR ~~V1.0~~V1 L2 CO_2 data presented here should be~~are~~ taken into account.

Acknowledgements

We thank all of the members of the GOSAT Science Team and their associates. We are also grateful to the engineers of Japan Airlines, the JAL Foundation, and JAMCO Tokyo for supporting the CONTRAIL project. We thank Dr. Y. Niwa for providing the outputs of NICAM-TM CO_2 simulations. We thank Dr. Saeki and Dr. Maksyutov to provide information on a priori dataset. CarbonTracker CT2013B results were provided by NOAA Earth System Research Laboratory (ESRL), Boulder, Colorado, USA from the website at http://carbontracker.noaa.gov. This~~is~~ study was supported by the Green Network of Excellence (GRENE-ei) of the Ministry of Education, Culture, Sports, and ~~X~~Technology. This study was performed within the framework of the GOSAT Research Announcement.

References

Araki, M., Morino, I., Machida, T., Sawa, Y., Hatsueda, H., Ohyama, H., Yokota, T., and Uchino, O.: CO_2 column-averaged volume mixing ratio derived over Tsukuba from measurements by commercial airlines, Atmos. Chem. Phys., 10, 7659-7667, 2010.

Bakwin, P. S., Tans, P. P., Hurst, D. F., and Zhao, C.: Measurements of carbon dioxide on very tall towers: results of the NOAA/CMDL program, Tellus, 50B, 401-415, 1998.

Baldridge, A. M., Hook, S. J., Grove, C. I., and Rivera, G.: The ASTER spectral library version 2.0, Remote Sens. Env., 10.1016/jrse.2008.11.007, 2009.

Barkley, M. P., Frieß, U., and Monks, P. S.: Measuring atmospheric CO_2 from space using Full Spectral Initiation (FSI) WFM-DOAS, Atmos. Chem. Phys., 6, 3517-3534, 2006.

Basu, S., Guerlet, S., Butz, A., Houweling, S., Hasekamp, O., Aben, I., Krummel, P., Steele, P., Langenfelds, R., Torn, M., Biraud, S., Stephens, B., Andrews, A., and Worthy, D.: Global CO_2 fluxes estimated from GOSAT retrievals of total column CO_2, Atmos. Chem. Phys., 13, 8695-8717, 2013.

Basu, S., Krol, M., Butz, A., Clerbaux, C., Sawa, Y., Machida, T., Matsueda, H., Frankenberg, C., Hasekamp, O. P., and Aben, I.: The seasonal variation of the CO_2 flux over Tropical Asia estimated from GOSAT, CONTRAIL, and IASI, Geophys. Res. Lett., 41, 1809-1815, 2014.

Brenninkmeijer, C. A. M. et al.: Civil Aircraft for the regular investigation of the atmosphere based on an instrumented container: The new CARIBIC system, Atmos. Chem. Phys., 7, 4953-4976, 2007.

Buchwitz, M., de Beek, R., Burrows, J. P., Bovensmann, H., Warneke, T., Notholt, J., Meirink, J. F., Goede, A. P. H., Bergamaschi, P., Körner, S., Heimann, M., and Schulz, A.: Atmospheric methane and carbon dioxide from SCIAMACHY satellite data: initial comparison with chemistry and transport models, Atmos. Chem. Phys., 5, 941-962, 2005.

Butz, A. et al.: Toward accurate CO_2 and CH_4 observations from GOSAT, Geophys. Res. Lett., 38, doi:10.1029/2011GL047888, 2011.

Chahine, M., Barnet, C., Olsen, E. T., Chen, L., and Maddy, E.: On the determination of atmospheric minor gases by the method of vanishing partial derivatives with application to CO_2, Geophys. Res. Lett., 32, doi:10.1029/2005GL024165, 2005.

Chédin, A., Serrar, S., Armante, R., Scott, N. A., and Hollingsworth, A.: Signatures of annual and seasonal variations of CO_2 and other greenhouse gases from comparisons between NOAA TOVS observations and radiation model simulations, J. Climate, 15, 95-116, 2002.

Chédin, A., Serrar, S., Scott, N. A., Crevoisier, C., and Armante, R.: First global measurement of midtropospheric CO_2 from NOAA polar satellites, J. Geophys. Res., 108, doi:10.1029/2003JD003439, 2003.

Chédin, A., Serrar, S., Scott, N. A., Pierangelo, C., and Ciais, P.: Impact of tropical biomass burning emissions on the diurnal cycle of upper tropospheric CO_2 retrieved from NOAA 10 satellite observations, J. Geophys. Res., 110, doi:10.1029/2004JD005540, 2005.

Chevallier, F., Fisher, M., Peylin, P., Serrar, S., Bousquet, P., Bréon, F.-M., Chédin, A., and Ciais, P.: Inferring CO_2 sources and sinks from satellite observations: Method and application to TOVS data, J. Geophys. Res., 110, doi:10.1029/2005JD006390, 2005.

Chevallier, F., Palmer, P. I., Feng, L., Boesch, H., O'Dell, C. W., and Bousquet, P.: Toward robust and consistent regional CO_2 flux estimates from in situ and spaceborne measurements of atmospheric CO_2, Geophys. Res. Lett., 41, 1065-1070, 2014.

Climate Modeling and Diagnostics Laboratory (CMDL): Climate Modeling and Diagnostics Laboratory Summary Report No. 27 2002-2003, Boulder, Colorado, USA, 2004.

Cogan, A. J., Boesch, H., Parker, R. J., Feng, L., Palmer, P. I., Blavier, J.-F. L., Deutscher, N. M., Macatangay, R., Notholt, J., Roehl, C., Warneke, T., and Wunch, D.: Atmospheric carbon dioxide retrieved from the Greenhouse gases Observing SATellite (GOSAT): Comparison with ground-based TCCON observations and GEOS-Chem model calculations, J. Geophys. Res., 117, doi:10.1029/2012JD018087, 2012.

Crevoisier, C., Heilliette, S., Chédin, A., Serrar, S., Armante, R., and Scott, N. A.: Midtropospheric CO_2 concentration retrieval from AIRS observations in the tropics, Geophys. Res. Lett., 31, doi:10.1029/2004GL020141, 2004.

Crevoisier, C., Chédin, A., Matsueda, H., Machida, T., Armante, R., and Scott, N. A.: First year of upper tropospheric integrated content of CO_2 from IASI hyperspectral infrared observations Atmos. Chem. Phys., 9, 4797-4810, 2009.

Crevoisier, C., Sweeney, C., Gloor, M., Sarmiento, J. L., and Tans, P. P.: Regional US carbon sinks from three-dimensional atmospheric CO_2 sampling, PNAS, 107, 18,348-18,353, 2010.

Hamazaki, T., Kaneko, Y., Kuze, A., and Kondo, K.: Fourier transform spectrometer for Greenhouse Gases Observing Satellite (GOSAT), Proc. of Soc. Photo Opt. Instrum. Eng., 73-80, 2005.

Imasu, R., Hayashi, Y., Inagoya, A., Saitoh, N., and Shiomi, K.: Retrieval of minor constituents from thermal infrared spectra observed by GOSAT TANSO-FTS sensor, Proc. of Soc. Photo Opt. Instrum. Eng., 7857, doi:10.1117/12.870684, 2010.

Inoue, M., Morino, I., Uchino, O., Miyamoto, Y., Yoshida, Y., Yokota, T., Machida, T., Sawa, Y., Matsueda, H., Sweeney, C., Tans, P. P., Andrews, A. E., Biraud, S. C., Tanaka, T., Kawakami, S., and Patra, P. K.: Validation of XCO_2 derived from SWIR spectra of GOSAT TANSO-FTS with aircraft measurement data, Atmos. Chem. Phys., 13, 9771-9788, 2013.

Ishida, H. and Nakajima, T. Y.: Development of an unbiased cloud detection algorithm for a spaceborne multispectral imager, J. Geophys. Res., 114, doi:10.1029/2008JD010710, 2009.

Ishida, H., Nakjima, T. Y., Yokota, T., Kikuchi, N., and Watanabe, H.: Investigation of GOSAT TANSO-CAI Cloud Screening Ability through an Intersatellite Comparison, J. Appl. Meteo. Clim., 50, 1571-1586, 2011.

Intergovernmental Panel on Climate Change (IPCC): Contribution of Working Group I to the Fifth Assessment Report of the Intergovernmental Panel on Climate Change, Cambridge University Press, Cambridge, United Kingdom and New York, NY, USA, 2013.

Karion, A., Sweeney, C., and Tans, P. P.; AirCore: An innovative atmospheric sampling system, J. Atmos. Ocean Tech., 27, 1839-1853, 2010.

Kataoka, F., Knuteson, R. O., Kuze, A., Suto, H., Shiomi, K., Harada, M., Garms, E. M., Roman, J. A., Tobin, D. C., Taylor, J. K., Revercomb, H. E., Sekio, N., Higuchi, R., and Mitomi, Y.: TIR spectral radiance calibration of the GOSAT satellite borne TANSO-FTS with the aircraft-based S-HIS and the ground-based S-AERI at the Railroad Valley desert playa, IEEE T. Geosci. Remote, 52, 89-105, 2014.

Keeling, C. D., Bacastow, R. B., Bainbridge, A. E., Ekdahl, C. A., Guenther, P. R., Waterman, L. S., and Chin, J. F. S.; Atmospheric carbon dioxide variations at Mauna Loa Observatory, Hawaii, Tellus, 28, 538-551, 1976a.

Keeling, C. D., Adams, J. A., Ekdahl, C. A., and Guenther, P. R.: Atmospheric carbon dioxide variations at the South Pole, Tellus, 28, 553-564, 1976b.

Keeling, C. D., Chin, J. F. S., and Whorf, T. P.: Increased activity of northern vegetation inferred from atmospheric CO_2 measurements, Nature, 382, 146-149, 1996.

Kulawik, S. S., Jones, D. B. A., Nassar, R., Irion, F. W., Worden, J. R., Bowman, K. W., Machida, T., Matsueda, H., Sawa, Y., Biraud, S. C., Fischer, M. L., and Jacobson, A. R.: Characterization of Tropospheric Emission Spectrometer (TES) CO_2 for carbon cycle science, Atmos. Chem. Phys., 10, 5601-5623, 2010.

Kulawik, S. S. et al.: Comparison of improved Aura Tropospheric Emission Spectrometer CO_2 with HIPPO and SGP aircraft profile measurements, Atmos. Chem. Phys., 13, 3205-3225, 2013.

Kuze, A., Suto, H., Nakajima, M., and Hamazaki, T.: Thermal and near infrared sensor for carbon observation Fourier-transform spectrometer on the Greenhouse Gases Observing Satellite for greenhouse gases monitoring, Appl. Optics, 48, 6716-6733, 2009.

Kuze, A., Suto, H., Shiomi, K., Urabe, T., Nakajima, M., Yoshida, J., Kawashima, T., Yamamoto, Y., Kataoka, F., and Buijs, H.: Level 1 algorithms for TANSO on GOSAT: processing and on-orbit calibrations, Atmos. Meas. Tech., 5, 2447-2467, 2012.

Machida, T., Matsueda, H., Sawa, Y., Nakagawa, Y., Hirotani, K., Kondo, N., Goto, K., Nakazawa, T., Ishikawa, K., and Ogawa, T.: Worldwide measurements of atmospheric CO_2 and other trace gas species using commercial airlines, J. Atmos. Ocean Tech., 25, 1744-1754, 2008.

Machida, T., Tohjima, Y., Katsumata, K., and Mukai, H.: A new CO_2 calibration scale based on gravimetric one-step dilution cylinders in National Institute for Environmental Studies - NIES 09 CO_2 Scale, 15th WMO/IAEA Meeting of Experts on Carbon Dioxide, Other Greenhouse Gases and Related Tracers Measurement Techniques, GAW Rep., 194, 165-169, World Meteorological Organization, Geneva, Switzerland, 2011.

McPeters, R. D., Labow, G. J., and Logan, J. A.: Ozone climatological profiles for satellite retrieval algorithms, J. Geophys. Res., 112, doi:10.1029/2005JD006823, 2007.

Maddy, E. S., Barnet, C. D., Goldberg, M., Sweeney, C., and Liu, X.: CO_2 retrievals from the Atmospheric Infrared Sounder: Methodology and validation, J. Geophys. Res., 113, doi:10.1029/2007JD009402, 2008.

Maksyutov, S., Takagi, H., Valsala, V. K., Saito, M., Oda, T., Saeki, T., Belikov, D. A., Saito, R., Ito, A., Yoshida, Y., Morino, I., Uchino, O., Andres, R. J., and Yokota, T.: Regional CO_2 flux estimates for 2009-2010 based on GOSAT and ground-based CO_2 observations, Atmos. Chem. Phys., 13, 9351-9373, 2013.

Matsueda, H., Machida, T., Sawa, Y., Nakagawa, Y., Hirotani, K., Ikeda, H., Kondo, N., and Goto, K.: Evaluation of atmospheric CO_2 measurements from new flask air sampling of JAL airliner observations, Pap. Meteorol. Geophys., 59, 1-17, 2008.

Matsueda, H., Machida, T., Sawa, Y., and Niwa, Y.: Long-term change of CO_2 latitudinal distribution in the upper troposphere, Geophys. Res. Lett., 42, 2508-2514, 2015.

Nassar1, R., Jones, D. B. A., Kulawik, S. S., Worden, J. R., Bowman, K. W., Andres, R. J., Suntharalingam, P., Chen, J. M., Brenninkmeijer, C. A. M., Schuck, T. J., Conway, T. J., and Worthy, D. E.: Inverse modeling of CO_2 sources and sinks using satellite observations of CO_2 from TES and surface flask measurements, Atmos. Chem. Phys., 11, 6029-6047, 2011.

Niwa, Y., Tomita, H., Satoh, M., and Imasu, R.: A threedimensional icosahedral grid advection scheme preserving monotonicity and consistency with continuity for atmospheric tracer transport, J. Meteor. Soc. Jpn., 89, 255–268, 2011.

Niwa, Y., Machida, T., Sawa, Y., Matsueda, H., Schuck, T. J., Brenninkmeijer, C. A. M., Imasu, R., and Satoh, M.: Imposing strong constraints on tropical terrestrial CO_2 fluxes using passenger aircraft based measurements, J. Geophys. Res., 117, doi:10.1029/2012JD017474, 2012.

O'Dell1, C. W. et al.: The ACOS CO_2 retrieval algorithm - Part 1: Description and validation against synthetic observations Atmos. Meas. Tech., 5, 99-121, 2012.

Ohyama, H., Kawakami, S., Shiomi, K., and Miyagawa, K.: Retrievals of Total and Tropospheric Ozone From GOSAT Thermal Infrared Spectral Radiances, IEEE T. Geosci. Remote, 50, 1770-1784, 2012.

Ohyama, H., Kawakami, S., Shiomi, K., Morino, I., and Uchino, O.: Atmospheric Temperature and Water Vapor Retrievals from GOSAT Thermal Infrared Spectra and Initial Validation with Coincident Radiosonde Measurements, SOLA, 9, 143-147, 2013.

Pak, B. C., and Prather, M. J.: CO_2 sources inversions using satellite observations of the upper troposphere, Geophys. Res. Lett., 28, 4571-4574, 2001.

Peters, W., Jacobson, A. R., Sweeney, C., Andrews, A. E., Conway, T. J., Masarie, K., Miller, J. B., Bruhwiler, L. M. P., Petron, G., Hirsch, A. I., Worthy, D. E. J., van der Werf, G. R., Randerson, J. T., Wennberg, P. O., Krol, M. C., and Tans, P. P.: An atmospheric perspective on North American carbon dioxide exchange: CarbonTracker", PNAS, 48, 104, 18925-18930, with updates documented at http://carbontracker.noaa.gov.

Rayner, P. J. and O'Brien, D. M.: The utility of remotely sensed CO_2 concentration data in surface source inversions, Geophys. Res. Lett., 28, 175-178, 2001.

Rodgers, C. D.: Inverse method for atmospheric sounding, World Scientific Publishing, 2000.

Rodgers, C. D. and Connor, B. J.: Intercomparison of remote sounding instruments, J. Geophys. Res., 108, 10.1029/2002JD002299, 2003.

Rodgers, C. D. and Connor, B. J.: Intercomparison of remote sounding instruments, J. Geophys. Res., 108, 10.1029/2002JD002299, 2003.

Saeki, T., Maksyutov, S., Saito, M., Valsala, V., Oda, T., Andres, R. J., Belikov, D., Tans, P., Dlugokencky, E., Yoshida, Y., Morino, I., Uchino, O., and Yokota, T.: Inverse Modeling of CO_2 Fluxes Using GOSAT Data and Multi-Year Ground-Based Observations, SOLA, 9, 45-50, 2013.

Saeki, T., Saito, R., Belikov, D., and Maksyutov, S.: Global high-resolution simulations of CO_2 and CH_4 using a NIES transport model to produce a priori concentrations for use in satellite data retrievals, Geosci. Model Dev., 6, 81-100, 2013.

Saitoh, N., Imasu, R., Ota, Y., and Niwa, Y.: CO_2 retrieval algorithm for the thermal infrared spectra of the Greenhouse Gases Observing Satellite: potential of retrieving CO_2 vertical profile from high-resolution FTS sensor, J. Geophys. Res., 114, doi:10.1029/2007JD011500, 2009.

Saitoh, N., Touno, M., Hayashida, S., Imasu, R., Shiomi, K., Yokota, T., Yoshida, Y., Machida, T., Matsueda, H., and Sawa, Y.: Comparisons between XCH_4 from GOSAT Shortwave and Thermal Infrared Spectra and Aircraft CH_4 Measurements over Guam, SOLA, 8, 145-149, 2012.

Sawa, Y., Machida, and T., Matsueda, H.: Aircraft observation of the seasonal variation in the transport of CO_2 in the upper atmosphere, J. Geophys. Res., 117, doi:10.1029/2011JD016933, 2012.

Strow, L. L. and Hannon, S. E.: A 4-year zonal climatology of lower tropospheric CO_2 derived from ocean-only Atmospheric Infrared Sounder observations, J. Geophys. Res., 113, doi:10.1029/2007JD009713, 2008.

Takagi, H. et al.: Influence of differences in current GOSAT XCO_2 retrievals on surface flux estimation, Geophys. Res. Lett., 41, 2598-2605, 2014.

Yokota, T., Yoshida, Y., Eguchi, N., Ota, Y., Tanaka, T., Watanabe, H., and Maksyutov, S.: Global Concentrations of CO_2 and CH_4 Retrieved from GOSAT: First Preliminary Results, SOLA, 5, 160-163, 2009.

Yoshida, Y., Ota, Y., Eguchi, N., Kikuchi, N., Nobuta, K., Tran, H., Morino, I., and Yokota, T.: Retrieval algorithm for CO_2 and CH_4 column abundances from short-wavelength infrared spectral observations by the Greenhouse gases observing satellite, Atmos. Meas. Tech., 4, 717-734, 2011.

Yoshida, Y. et al.: Improvement of the retrieval algorithm for GOSAT SWIR XCO_2 and XCH_4 and their validation using TCCON data, Atmos. Meas. Tech., 6, 1533-1547, 2013.

Table 1. Retrieval grid layers of GOSAT/TANSO-FTS TIR CO_2 ~~V1.0~~V1 data.

Layer level	Lower presure level (hPa)	Upper pressure level (hPa)
1	1165.91	857.70
2	857.70	735.64
3	735.64	630.96
4	630.96	541.17
5	541.17	464.16
6	464.16	398.11
7	398.11	341.45
8	341.45	287.30
9	287.30	237.14
10	237.14	195.73
11	195.73	161.56
12	161.56	133.35
13	133.35	110.07
14	110.07	90.85
15	90.85	74.99
16	74.99	61.90
17	61.90	51.09
18	51.09	42.17
19	42.17	34.81
20	34.81	28.73
21	28.73	23.71
22	23.71	19.57
23	19.57	16.16
24	16.16	13.34
25	13.34	10.00
26	10.00	5.62
27	5.62	1.00
28	1.00	0.10

Table 2. Bias values of GOSAT/TANSO-FTS TIR ~~V1.0~~V1 CO_2 data against CONTRAIL (AK) ~~CME~~ CO_2 data for each season and each latitude region in the upper troposphere and lower stratosphere in the unit of ppm. Significant bias values larger than ±2~~1.0~~ ppm are indicated by boldface.

UT	LS	MAM		JJA		SON		JF	
60–70°N		-1.0	-0.8	-0.2	-0.5	-1.0	-1.1	0.3	-0.5
40–60°N		-1.7	0.3	-1.6	-1.3	-1.1	-0.9	-0.5	-0.5
20–40°N		**-2.4**		**-2.3**		-1.1		0.3	
0–20°N		-1.2		**-2.3**		-0.5		0.5	
20°S–0		-0.1		-0.6		0.4		0.0	
40–20°S		-0.2		-0.4		-0.7		-0.5	

~~The evaluation of the bias values does not consider TIR CO_2 averaging kernel functions.~~

~~UT~~	~~LS~~	~~MAM~~		~~JJA~~		~~SON~~		~~JF (DJF)~~	
~~60–70°N~~		~~-0.8~~	~~0.3~~	~~0.2~~	~~-0.3~~	~~-0.6~~	~~**-2.0**~~	~~0.3~~	~~-0.1~~
~~40–60°N~~		~~**-2.2**~~	~~**1.2**~~	~~**-1.2**~~	~~**-1.2**~~	~~-0.7~~	~~**-1.0**~~	~~0.2~~	~~-0.4~~
~~20–40°N~~		~~**-2.7**~~		~~**-1.6**~~		~~-0.4~~		~~0.2~~	
~~0–20°N~~		~~-0.8~~		~~**-2.0**~~		~~-0.2~~		~~0.8~~	
~~20°S–0~~		~~0.3~~		~~-0.2~~		~~0.5~~		~~0.4~~	
~~40–20°S~~		~~0.5~~		~~-0.1~~		~~-0.5~~		~~0.1~~	

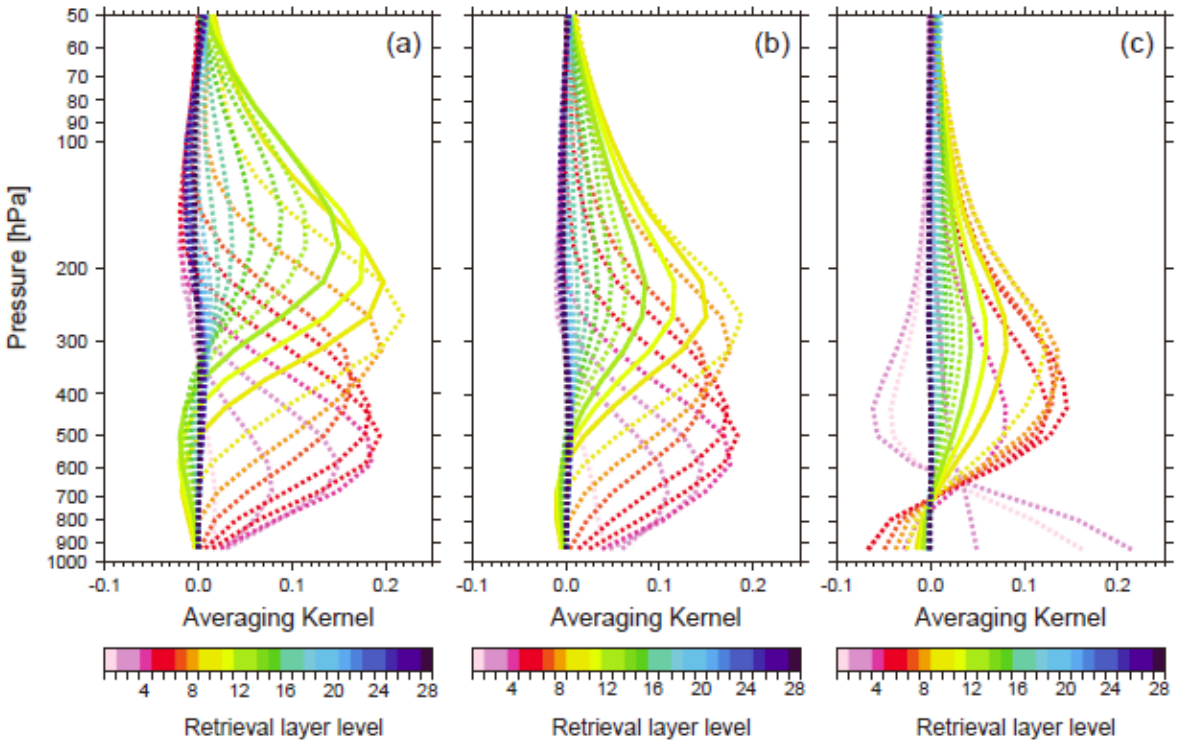
(a)
(b)
(c)
Pressure [hPa]
50
60
70
80
90
100
200
300
400
500
600
700
800
900
1000
-0.1
0.0
0.1
0.2
Averaging Kernel
4
8
12
16
20
24
28
Retrieval layer level

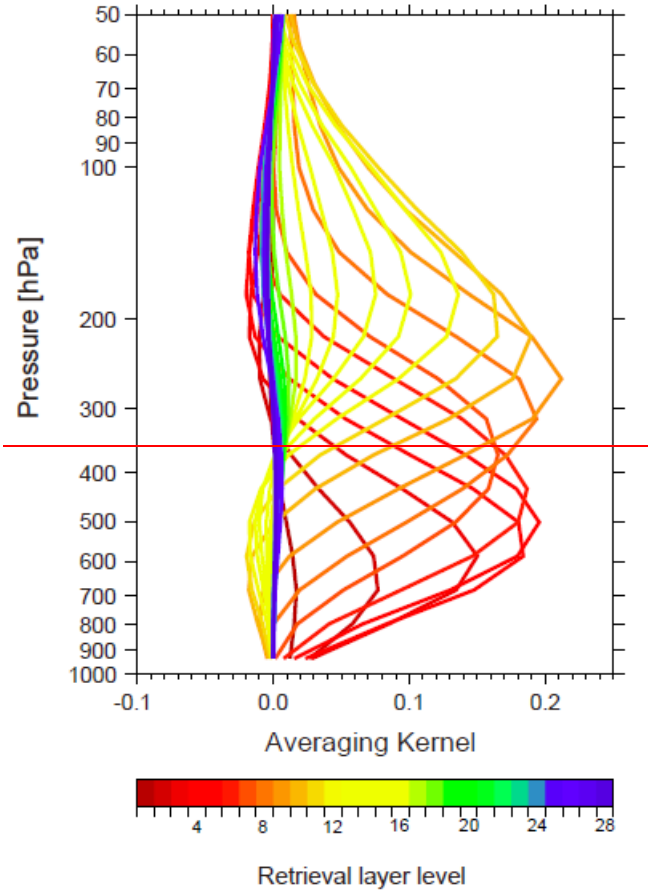
Pressure [hPa]
50
60
70
80
90
100
200
300
400
500
600
700
800
900
1000
-0.1
0.0
0.1
0.2
Averaging Kernel
4
8
12
16
20
24
28
Retrieval layer level

Figure 1. Averaging kernel functions of GOSAT/TANSO-FTS TIR V1.0 CO_2 retrieval in the 28 retrieval grid layers shown in Table 1:. (a) low latitudes in summer, (b) mid-latitudes in spring, and (c) high latitudes in winter. Solid orange, yellow, and green lines indicate averaging kernel functions of each of the three layer levels 9, 10, and 11, respectively..

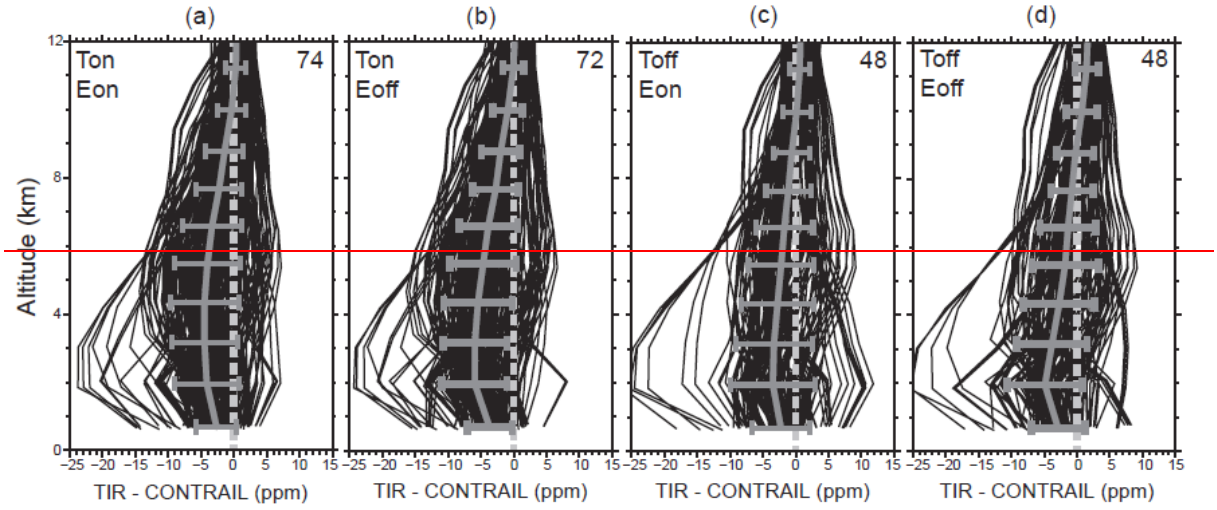

Figure 2. Differences between GOSAT/TANSO-FTS TIR retrieved CO_2 profiles and the corresponding CONTRAIL CME ascending/descending data over Narita airport with considering TIR CO_2 averaging kernel functions. Thin black lines show individual comparisons. Thick gray lines and horizontal bars show the means and 1-σ standard deviations of the comparisons. The upper right number of each panel indicates the number of all of the GOSAT/TANSO-FTS TIR CO_2 profiles among the 141 pairs that were normally retrieved under each retrieval condition: (a) Ton & Eon, (b) Ton & Eoff, (c) Toff & Eon, and (d) Toff & Eoff. See the text for details of the retrieval conditions.

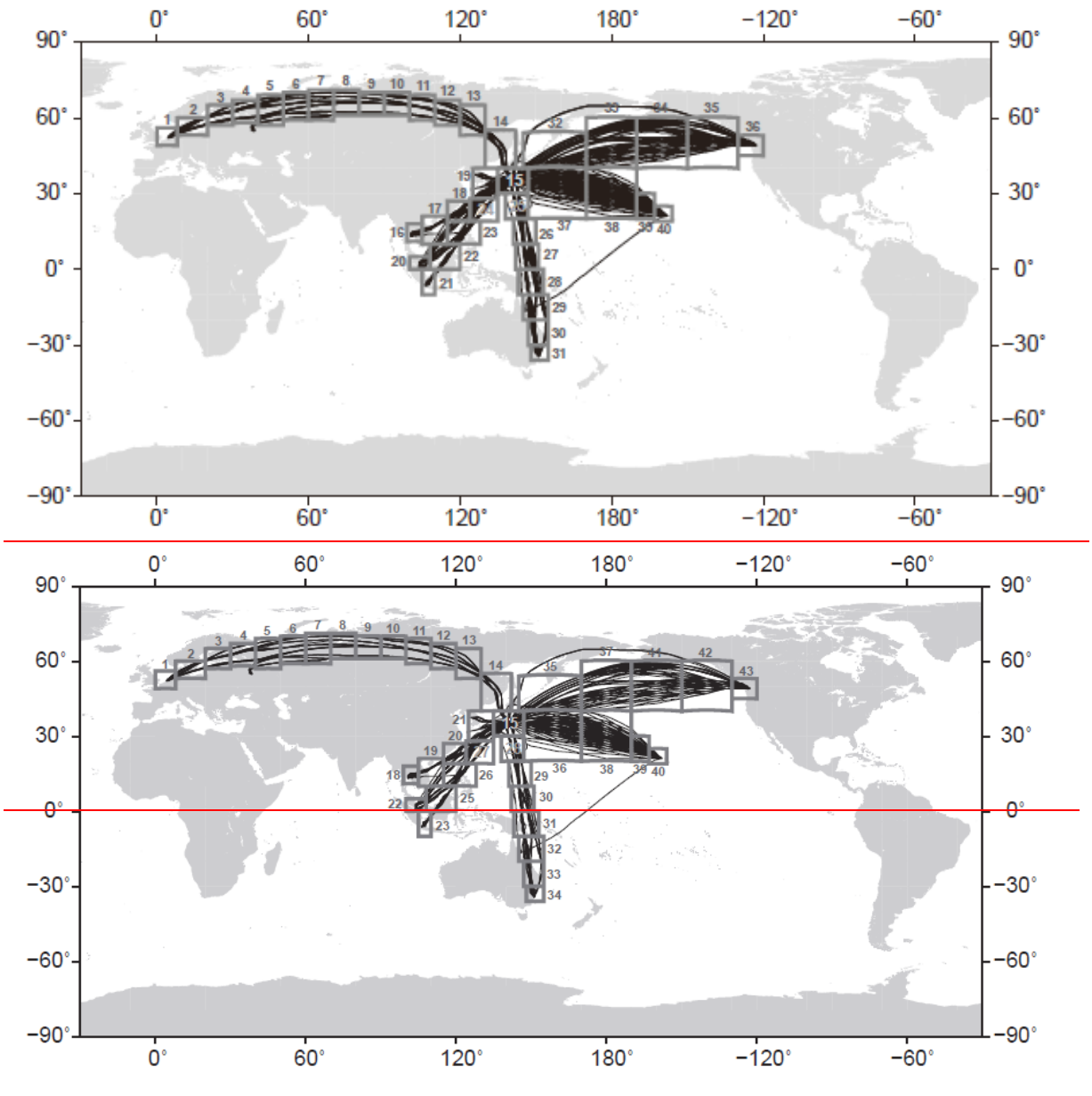

Figure 2~~3~~. Flight tracks of all of the CONTRAIL CME observations in 2010 used in this study. A number next to a box area indicates each area number.

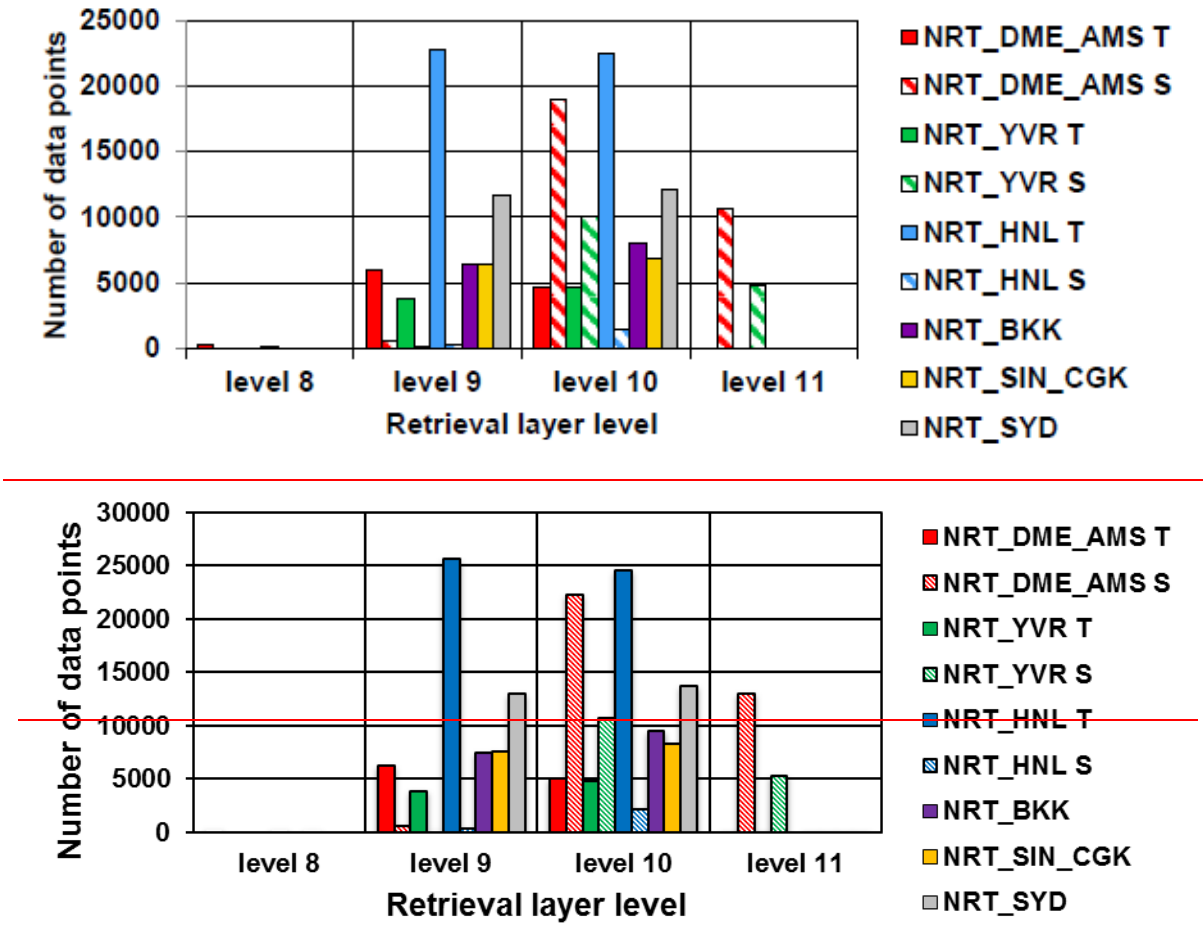

Figure 34. The number of GOSAT/TANSO-FTS TIR CO_2 data points compared to the CONTRAIL CME level flight data for each retrieval grid layer level for each flight. The numbers of TIR CO_2 data points in the troposphere ("T") and stratosphere ("S") are shown separately for the Tokyo–Europe (NRT_DME_AMS), Tokyo–Vancouver (NRT_YVR), and Tokyo–Honolulu (NRT_HNL) flight routes.

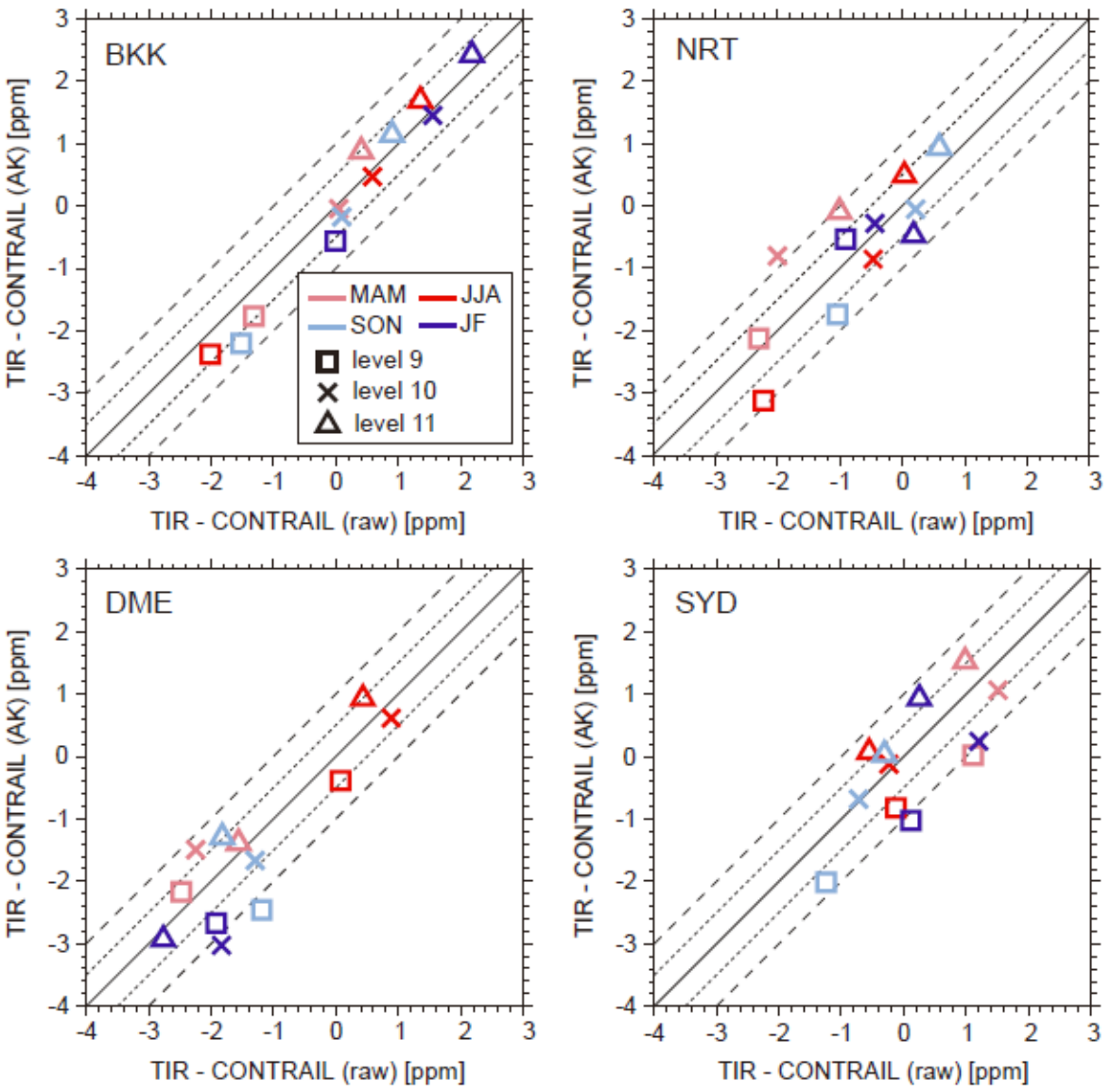
BKK
NRT
DME
SYD
MAM
JJA
SON
JF
level 9
level 10
level 11
TIR - CONTRAIL (AK) [ppm]
TIR - CONTRAIL (raw) [ppm]

1

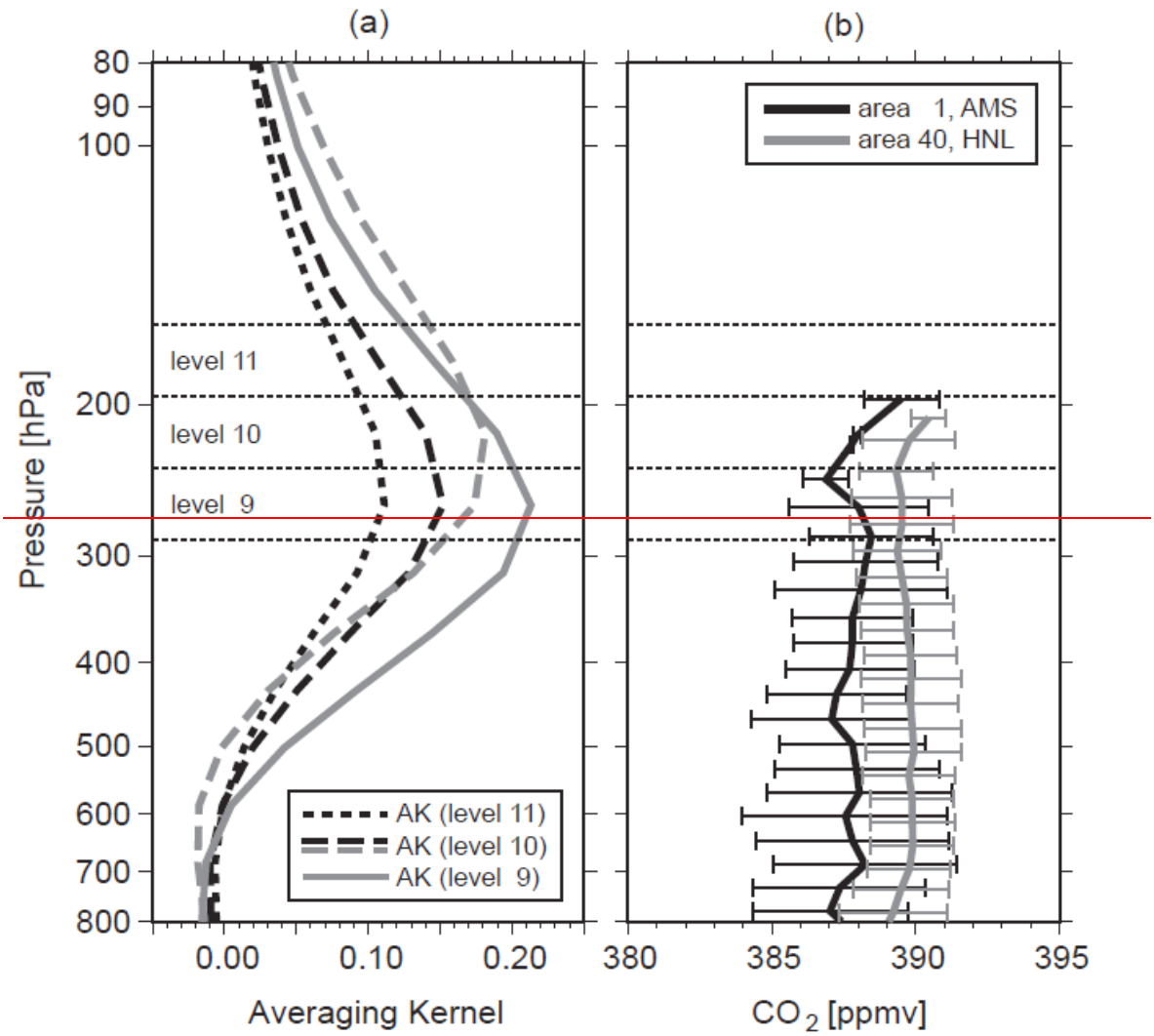

Figure 4. Scatter plots of GOSAT/TANSO-FTS TIR and CONTRAIL (raw) CO_2 differences and GOSAT/TANSO-FTS TIR and CONTRAIL (AK) CO_2 differences in layers 9, 10, and 11 for each season.~~Figure 5. (Left panel) Averaging kernel function of each of the three layer levels 9, 10, and 11, shown by solid, dashed, and dotted lines, respectively. Black and gray lines show the means of averaging kernel functions of all of the GOSAT/TANSO-FTS TIR CO_2 profiles used in the comparisons made in areas 1 and 40 in summer (JJA), respectively. (Right panel) Mean profiles with 1-σ standard deviations of CONTRAIL CME ascending/descending CO_2 data over Amsterdam (located in area 1) and Honolulu (located in area 40) airports in summer (JJA), shown by black and gray lines, respectively.~~

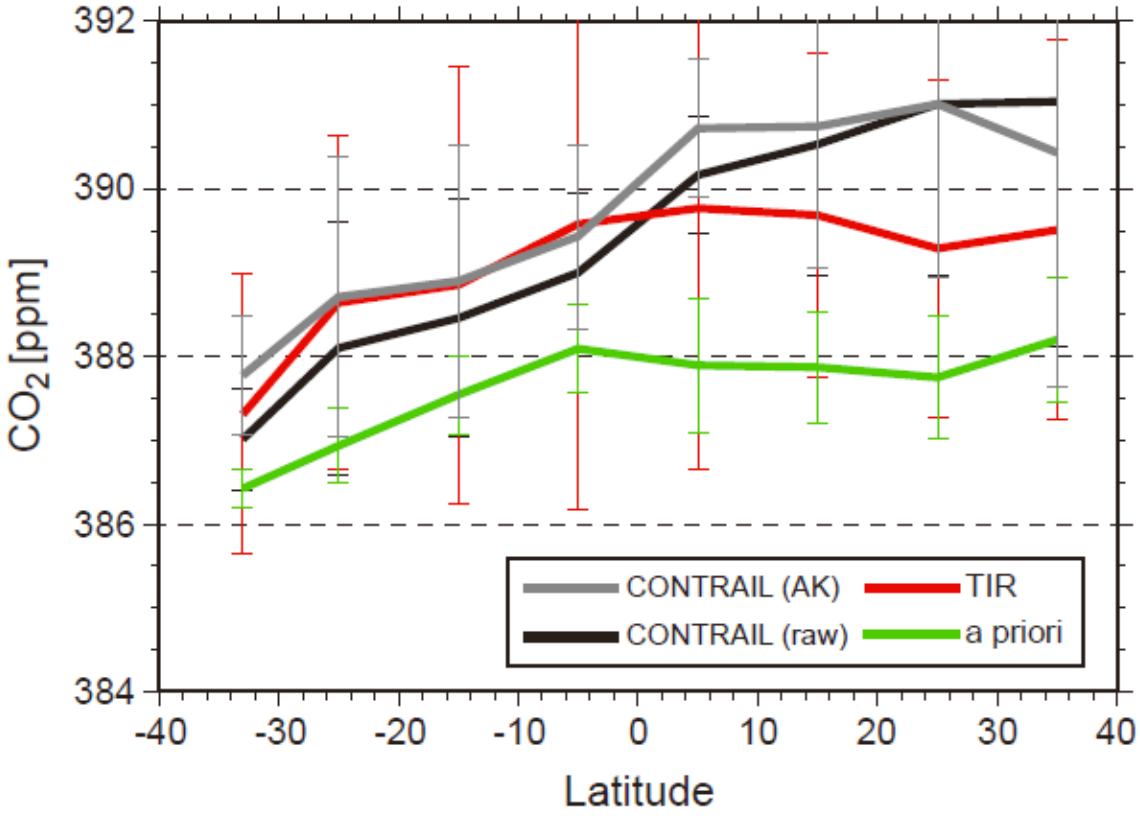
392
390
388
386
384
CO_2 [ppm]
-40
-30
-20
-10
0
10
20
30
40
Latitude
CONTRAIL (AK)
CONTRAIL (raw)
TIR
a priori

1

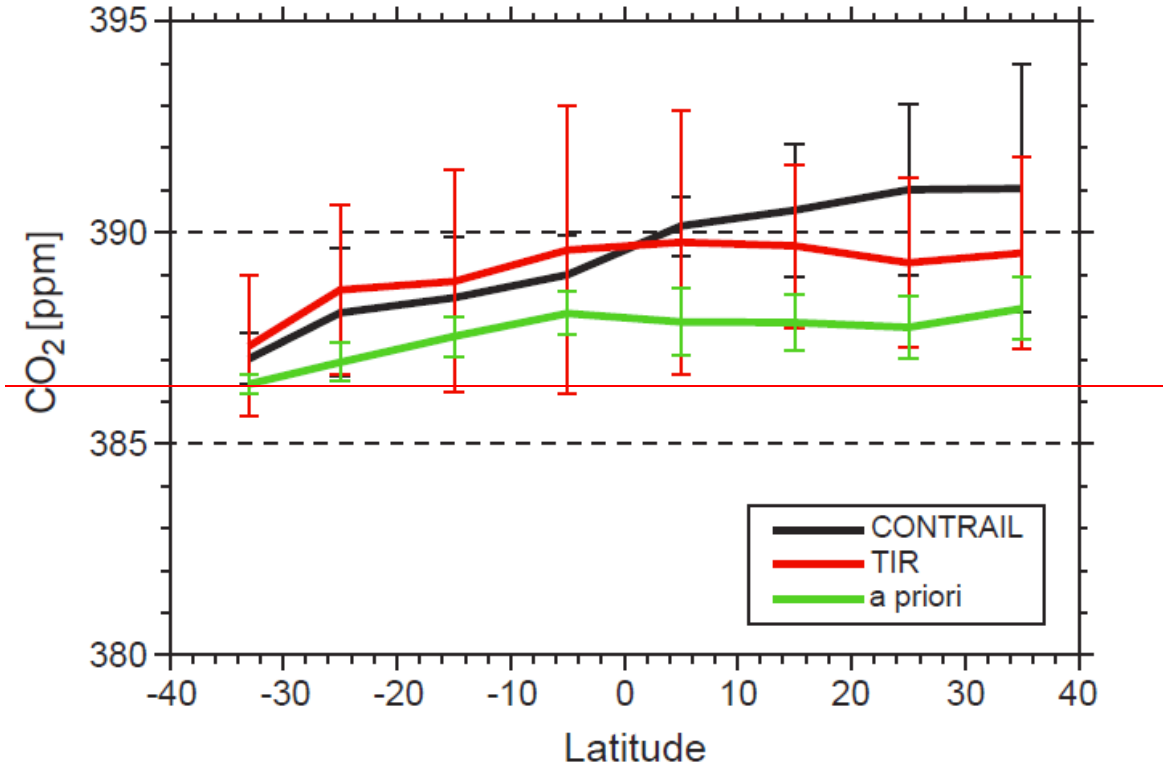
395
390
385
380
CO_2 [ppm]
-40
-30
-20
-10
0
10
20
30
40
Latitude
CONTRAIL
TIR
a priori

2

3

Figure 5~~6~~. Comparisons among CONTRAIL (raw), CONTRAIL (AK) ~~CONTRAIL CME level flight~~, GOSAT/TANSO-FTS TIR, and a priori (NIES TM 05) CO_2 data during flights between Tokyo and Sydney (NRT_SYD) in spring (MAM), shown by black, gray, red, and green lines, respectively. The means and their 1-σ standard deviations were calculated in each area during the flight for all four~~three~~ datasets.

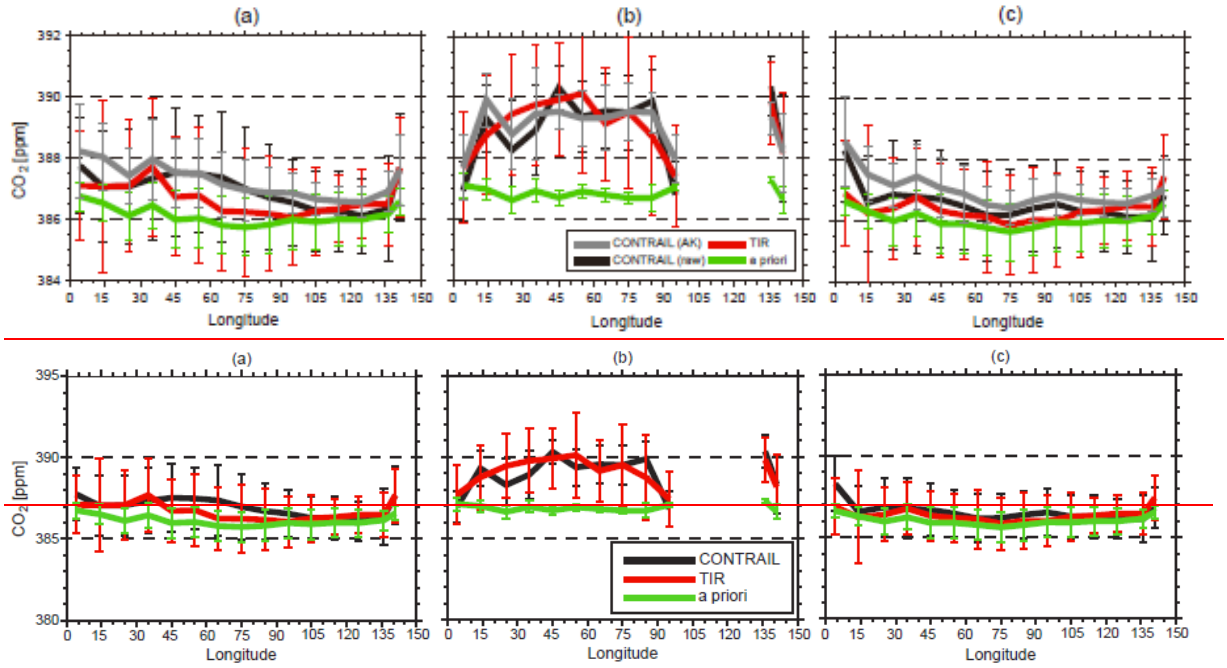

Figure 6~~7~~. Same as Figure 5~~6~~, but for flights between Tokyo and Europe (NRT_DME_AMS) in winter (JF). (a) All of the data, (b) only data in the troposphere, and (c) only data in the stratosphere. See the text for the classification of tropospheric and stratospheric data.

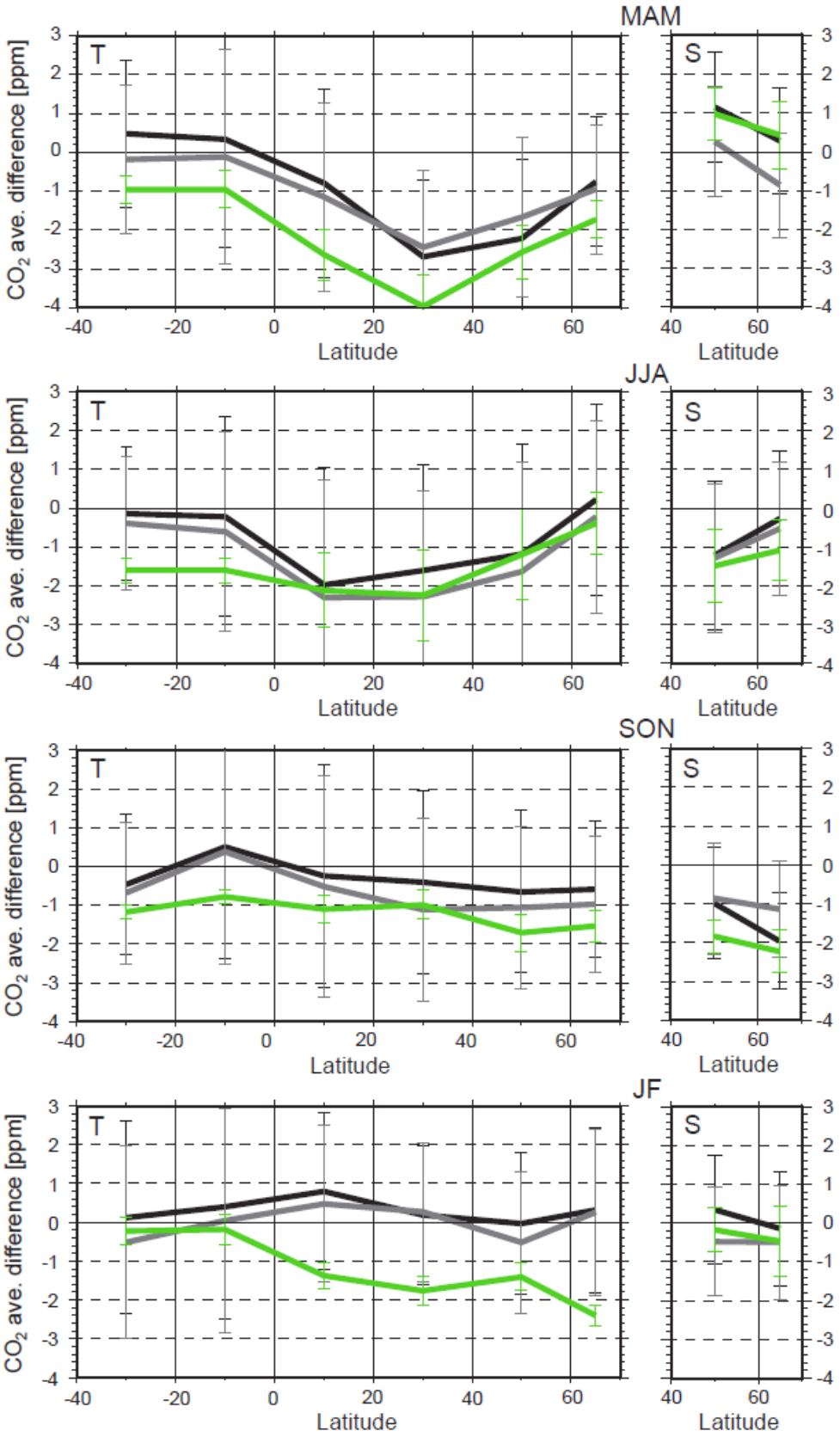

1

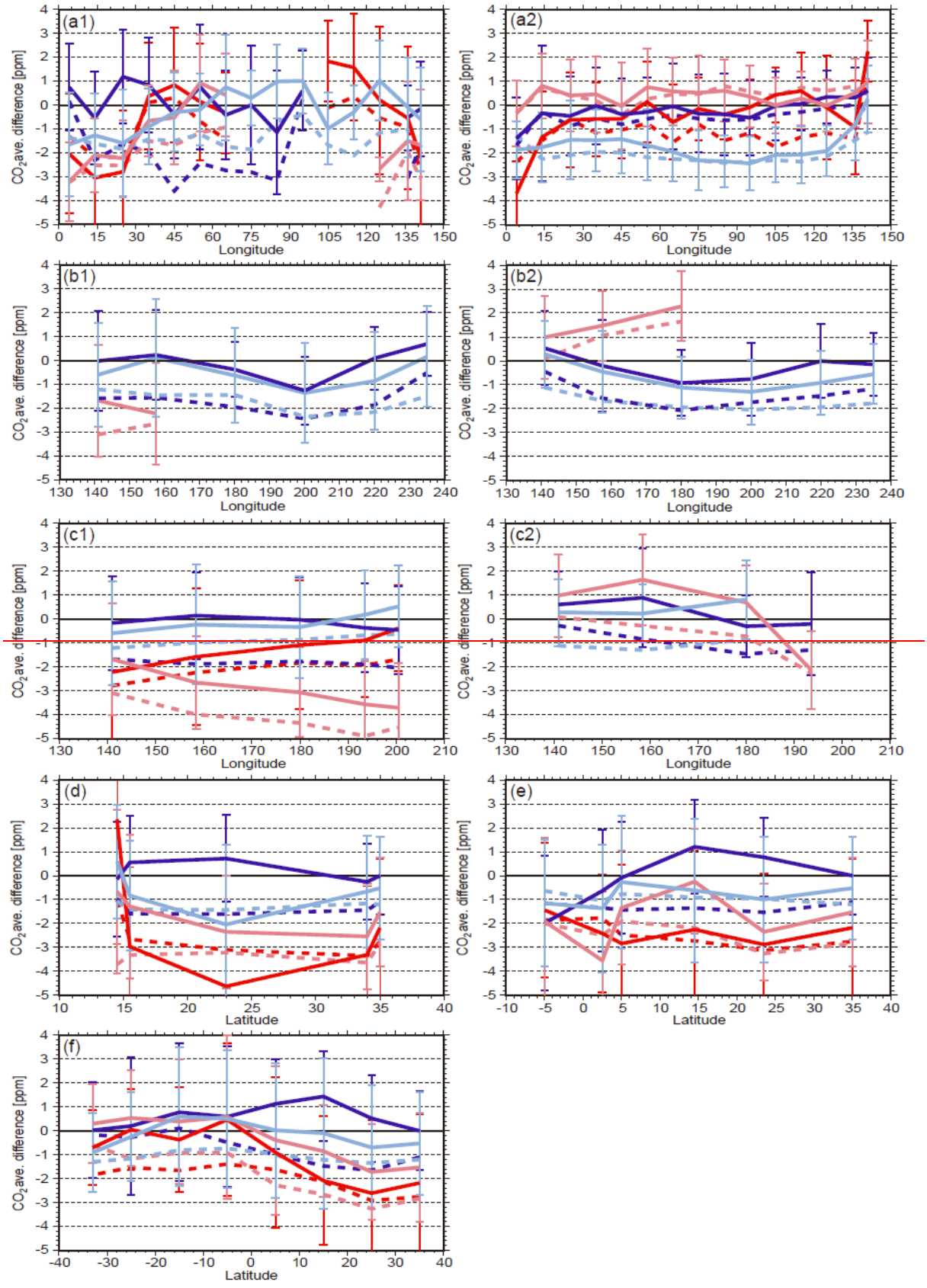
(a1)
(a2)
(b1)
(b2)
(c1)
(c2)
(d)
(e)
(f)
CO2ave. difference [ppm]
Longitude
Latitude

1

2

Figure 7~~8~~. Differences between GOSAT/TANSO-FTS TIR and CONTRAIL (raw) averaged CO_2 data (TIR ave. minus CONTRAIL (raw) ave.), TIR and CONTRAIL (AK) averaged CO_2 data (TIR ave. minus CONTRAIL (AK) ave.), and a priori (NIES TM 05) and CONTRAIL (raw) averaged CO_2 data (a priori ave. minus CONTRAIL (raw) ave.) for each season for each latitude band (40°S–20°S, 20°S–0°, 0°–20°N, 20°N–40°N, 40°N–60°N, 60°N–70°N), shown by black, gray, and green lines, respectively. Left and right panels show the differences in the upper troposphere and lower stratosphere, respectively. The 1-σ standard deviations of the latitudinal averages of TANSO-FTS TIR CO_2 data are shown by vertical bars.~~Differences between GOSAT/TANSO-FTS TIR and CONTRAIL CME averaged CO_2 data (TIR ave. minus CONTRAIL ave.) and a priori (NIES TM 05) and CONTRAIL CME averaged CO_2 data (a priori ave. minus CONTRAIL ave.) for each season and each area of all of the six flight routes, shown by thick and dashed lines, respectively: (a) Tokyo–Europe (NRT_DME_AMS), (b) Tokyo–Vancouver (NRT_YVR), (c) Tokyo–Honolulu (NRT_HNL), (d) Tokyo–Bangkok (NRT_BKK), (e) Tokyo–East Asia (NRT_SIN_CGK), and (f) Tokyo–Sydney (NRT_SYD). The means of the differences were calculated for each of the areas in spring (MAM), summer (JJA), fall (SON), and winter (JF/DJF), as shown by the pink, red, light blue, and blue lines, respectively. The 1-σ standard deviations of the averages of TANSO-FTS TIR CO2 data are shown by vertical bars. For the airline routes of Tokyo–Europe, Tokyo–Vancouver, and Tokyo–Honolulu, the results only for the tropospheric data (a1, b1, and c1) and only for the stratospheric data (a2, b2, and c2) are shown separately. Data in December 2010 were used only in the comparisons for the flight between Tokyo and Vancouver.~~

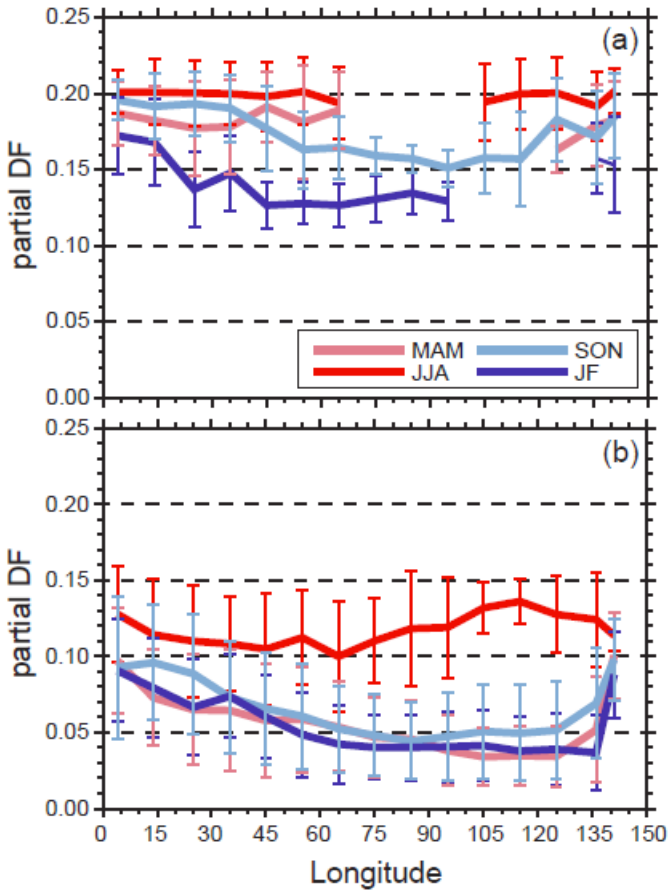

Figure 8~~9~~. Partial degree of freedom (DF) for GOSAT/TANSO-FTS TIR CO_2 data in the upper troposphere (a) and the lower stratosphere (b) for each area of the flight between Tokyo and Europe (NRT_DME_AMS). The means and their 1-σ standard deviations of the partial DF data were calculated in spring (MAM), summer (JJA), fall (SON), and winter (JF), as shown by the pink, red, light blue, and blue lines, respectively.

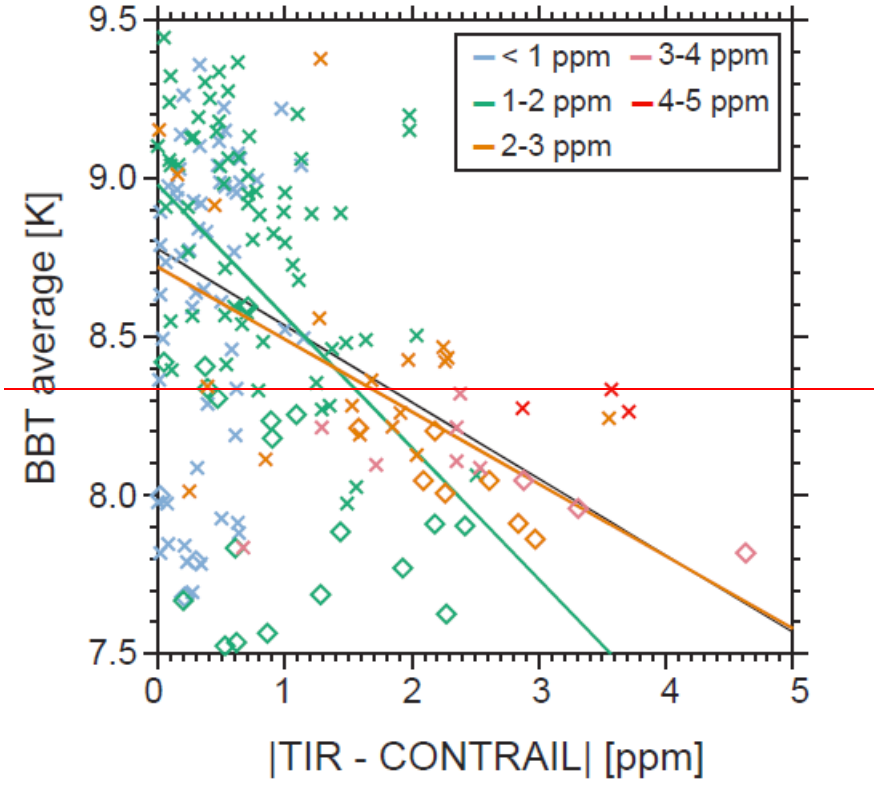

Figure 10. Correlations between the mean temperatures of the internal blackbody (BBT) on board the GOSAT/TANSO-FTS instrument and the differences between GOSAT/TANSO-FTS TIR and CONTRAIL CME averaged CO_2 data (TIR ave. minus CONTRAIL ave.) for each area of all flights for each of the four seasons. All of the data are categorized according to the differences between corresponding a priori (NIES TM 05) and CONTRAIL CME averaged CO_2 data (a priori ave. minus CONTRAIL ave.): less than 1 ppm (light blue), 1–2 ppm (green), 2–3 ppm (orange), 3–4 ppm (pink), and 4–5 ppm (red). Regression lines of the "1–2 ppm" dataset, the "2-3 ppm" dataset and all of the datasets are shown by green, orange, and black lines, respectively. The correlation coefficients of the green, orange, and black lines are -0.49, -0.56, and -0.41, respectively.

To Associate Editor and Referees,

The following attachment is the final revised manuscript.

Validation of GOSAT/TANSO-FTS TIR UTLS CO_2 data (Version 1) using CONTRAIL measurements

N. Saitoh[1], S. Kimoto[1], R. Sugimura[1], R. Imasu[2], S. Kawakami[3], K. Shiomi[3], A. Kuze[3], T. Machida[4], Y. Sawa[5], and H. Matsueda[5]

[1]{Center for Environmental Remote Sensing, Chiba University, Chiba, Japan}

[2]{Atmosphere and Ocean Research Institute, University of Tokyo, Kashiwa, Japan}

[3]{Japan Aerospace Exploration Agency, Tsukuba, Japan}

[4]{National Institute for Environmental Studies, Tsukuba, Japan}

[5]{Meteorological Research Institute, Tsukuba, Japan}

Correspondence to: N. Saitoh (nsaitoh@faculty.chiba-u.jp)

Abstract

Thermal and Near Infrared Sensor for Carbon Observation (TANSO)–Fourier Transform Spectrometer (FTS) on board the Greenhouse Gases Observing Satellite (GOSAT) has been observing carbon dioxide (CO_2) concentrations in several atmospheric layers in the thermal infrared (TIR) band since its launch. This study compared TANSO-FTS TIR V1 CO_2 data and CO_2 data obtained in the Comprehensive Observation Network for TRace gases by AIrLiner (CONTRAIL) project in the upper troposphere and lower stratosphere (UTLS), where the TIR band of TANSO-FTS is most sensitive to CO_2 concentrations, to validate the quality of the TIR V1 UTLS CO_2 data from 287 to 162 hPa. We first evaluated the impact of considering TIR CO_2 averaging kernel functions on CO_2 concentrations using CO_2 profile data obtained by the CONTRAIL Continuous CO_2 Measuring Equipment (CME), and found that the impact at around the CME level flight altitudes (~11 km) was on average less than 0.5 ppm in low latitudes and less than 1 ppm in middle and high latitudes. From a comparison made during flights between Tokyo and Sydney, the averages of the TIR upper atmospheric CO_2 data were within 0.1% of the averages of the CONTRAIL CME CO_2 data with and without TIR CO_2 averaging kernels for all seasons in the Southern Hemisphere. The results of comparisons for all of the eight airline routes showed that the agreements of TIR and CME CO_2 data were

worse in spring and summer than in fall and winter in the Northern Hemisphere in the upper troposphere. While the differences between TIR and CME CO_2 data were on average within 1 ppm in fall and winter, TIR CO_2 data had a negative bias up to 2.4 ppm against CME CO_2 data with TIR CO_2 averaging kernels in the northern low and middle latitudes in spring and summer. The negative bias in the northern middle latitudes resulted in the maximum of TIR CO_2 concentrations being lower than that of CME CO_2 concentrations, which led to an underestimate of the amplitude of CO_2 seasonal variation.

1 Introduction

Carbon dioxide (CO_2) in the atmosphere is a well-known strong greenhouse gas (IPCC, 2013, and references therein), with concentrations that have been observed both *in situ* and by satellite sensors. Its long-term observation began in Mauna Loa, Hawaii, and the South Pole in the late 1950s (Keeling et al., 1976a, 1976b, 1996). Since then, comprehensive CO_2 observations in the atmosphere have been conducted worldwide in several observatories and tall towers (Bakwin et al., 1998), by aircraft flask sampling (e.g., Crevoisier et al., 2010), and via the AirCore sampling system (Karion et al., 2010) in the framework of researches by the National Oceanic and Atmospheric Administration (NOAA). Atmospheric CO_2 concentrations have gradually increased at a globally averaged annual rate of 1.7±0.5 ppm from 1998 to 2011, although its growth rate has relatively large interannual variation (IPCC, 2013). Upper atmospheric CO_2 observations have been made in many areas by several projects using commercial airliners, such as the Comprehensive Observation Network for TRace gases by AIrLiner (CONTRAIL) project (Machida et al., 2008) and the Civil Aircraft for the Regular Investigation of the atmosphere Based on an Instrument Container (CARIBIC) project (Brenninkmeijer et a., 2007). Continuous long-term measurements of CO_2 made by several airplanes of Japan Airlines (JAL) in the CONTRAIL project have revealed details of its seasonal variation and interhemispheric transport in the upper atmosphere (Sawa et al., 2012) and interannual and long-term trends of its latitudinal gradients (Matsueda et al., 2015).

Atmospheric CO_2 observations by satellite sensors are categorized into two types: those utilizing CO_2 absorption bands in the shortwave infrared (SWIR) regions at around 1.6 and 2.0 μm, and those in the thermal infrared (TIR) regions at around 4.6, 10, and 15 μm. The Scanning Imaging Absorption Spectrometer for Atmospheric Chartography (SCIAMACHY)

on the Environmental Satellite (ENVISAT) first observed CO_2 column-averaged dry-air mole fractions (XCO_2) from spectra at 1.57 μm (Buchwitz et al., 2005; Barkley et al., 2006). The Thermal and Near Infrared Sensor for Carbon Observation (TANSO)–Fourier Transform Spectrometer (FTS) on board the Greenhouse Gases Observing Satellite (GOSAT), which was launched in 2009 (Yokota et al., 2009), has observed XCO_2 with high precision by utilizing the 1.6 and/or 2.0 μm CO_2 absorption bands (Yoshida et al., 2011, 2013; O'Dell et al., 2012; Butz et al., 2011; Cogan et al., 2012). The Orbiting Carbon Observatory 2 (OCO-2) was successfully launched in 2014, and started regular observations of XCO_2 with high spatial resolution. Satellite CO_2 observations at TIR absorption bands have a longer history beginning with the High-Resolution Infrared Sounder (HIRS) (Chédin et al., 2002, 2003, 2005). The Atmospheric Infrared Sounder (AIRS) has achieved more accurate observations of middle and upper tropospheric CO_2 concentrations (Crevoisier et al., 2004; Chahine et al., 2005; Maddy et al., 2008; Strow and Hannon, 2008). The Tropospheric Emission Spectrometer (TES) has observed CO_2 concentrations in several vertical layers with high accuracy by taking advantage of its high wavelength resolution (Kulawik et al., 2010, 2013). The Infrared Atmospheric Sounding Interferometer (IASI) has observed upper atmospheric CO_2 amounts from its TIR spectra (Crevoisier et al., 2009). TANSO-FTS also has a TIR band in addition to its three SWIR bands, and obtains vertical information of CO_2 concentrations in addition to XCO_2 in the same field of view (Saitoh et al., 2009).

Rayner and O'Brien (2001) and Pak and Prather (2001) showed the utility of global CO_2 data obtained by satellite sensors for estimating its source and sink strength, and many studies of CO_2 inversion have been conducted using a huge amount of satellite data since the 2000s. Chevallier et al. (2005) first used satellite CO_2 data, observed with the Operational Vertical Sounder (TOVS), to estimate CO_2 surface fluxes. They reported that a regional bias in satellite CO_2 data hampers the outcomes. Nassar et al. (2011) demonstrated that the wide spatial coverage of satellite CO_2 data is beneficial to CO_2 surface flux inversion through the combined use of TES and surface flask CO_2 data, particularly in regions where surface measurements are sparse. In addition to CO_2 surface inversion results using TIR observations, global XCO_2 data observed with the SWIR bands of TANSO-FTS have been actively used for estimating CO_2 source and sink strength (Maksyutov et al., 2013; Saeki et al., 2013; Chevallier et al., 2014; Basu et al., 2013, 2014; Takagi et al., 2014). One of the important things to consider when incorporating satellite data in CO_2 inversion is the accuracy of the data, as suggested by Basu et al. (2013). Uncertainties in satellite CO_2 data should be assessed

seasonally and regionally to determine the seasonal and regional characteristics of the satellite CO_2 bias.

The importance of upper atmospheric CO_2 data in the inversion analysis of CO_2 surface fluxes was discussed in Niwa et al. (2012). They used CONTRAIL CO_2 data in conjunction with surface CO_2 data to estimate surface flux, and demonstrated that adding middle and upper tropospheric data observed by the aircraft could greatly reduce the posteriori flux errors, particularly in tropical Asian regions. Middle and upper tropospheric and lower stratospheric CO_2 concentrations and column amounts of CO_2 can be simultaneously observed in the same field of view with TANSO-FTS on board GOSAT. Provided that the quality of upper atmospheric CO_2 data simultaneously obtained with TANSO-FTS is proven to be comparable to that of TANSO-FTS XCO_2 data (Yoshida et al., 2013; Inoue et al., 2013), the combined use of upper atmospheric CO_2 and XCO_2 data observed with TANSO-FTS could be a useful tool for estimating CO_2 surface flux.

GOSAT, which is the first satellite to be dedicated to greenhouse gas monitoring, was launched on January 23, 2009. As described above, TANSO-FTS on board GOSAT has been observing CO_2 concentrations in several vertical layers in the TIR band. In this study, we focused on CO_2 concentrations in the upper troposphere and lower stratosphere (UTLS), where the TIR band of TANSO-FTS is most sensitive. We validated these data by comparison with upper atmospheric CO_2 data obtained in a wide spatial coverage in the CONTRAIL project. Sections 2 and 3 explain the GOSAT and CONTRAIL measurements, respectively. Section 4 details the retrieval algorithm used in the latest version 1 (V1) CO_2 level 2 (L2) product of the TIR band of TANSO-FTS. Section 5 describes the methods of comparing TANSO-FTS TIR V1 L2 and CONTRAIL CO_2 data. Sections 6 and 7 show and discuss the results of the comparisons between TIR and CONTRAIL CO_2 data. Section 8 summarizes this study.

2 GOSAT observations

GOSAT is a joint satellite project of the National Institute for Environmental Studies (NIES), Ministry of the Environment (MOE), and Japan Aerospace Exploration Agency (JAXA) for the purpose of making global observations of greenhouse gases such as CO_2 and CH_4 (Hamazaki et al., 2005; Yokota et al., 2009). It was launched on January 23, 2009, from the Tanegashima Space Center, and has continued its observations for more than six years.

GOSAT is equipped with the TANSO-FTS for greenhouse gas monitoring and the TANSO-Cloud and Aerosol Imager (CAI) to detect clouds and aerosols in the TANSO-FTS field of view (Kuze et al., 2009). TANSO-FTS consists of three bands in the SWIR region and one band in the TIR region. Column amounts of greenhouse gases are observed in the SWIR bands and vertical information of gas concentrations are obtained in the TIR band (Yoshida et al., 2011, 2013; Saitoh et al., 2009, 2012; Ohyama et al., 2012, 2013).

Kuze et al. (2012) provided a detailed description of the methods used for the processing and calibration of level 1B (L1B) spectral data from TANSO-FTS. They explained the algorithm for the version 150.151 (V150.151) L1B spectral data. The TIR V1 L2 CO_2 product we focused on in this study was created from a later version, V161.160, of L1B spectral data. The following modifications were made to the algorithm from V150.151 to V161.160: improving the TIR radiometric calibration through the improvement of calibration parameters, turning off the sampling interval non-uniformity correction, modifying the spike noise criteria of the quality flag, and reevaluating the misalignment between the GOSAT satellite and TANSO-FTS sensor. Kataoka et al. (2014) reported that the biases of TANSO-FTS TIR V130.130 L1B radiance spectra based on comparisons with the Scanning High-resolution Interferometer Sounder (S-HIS) spectra for warm scenes were 0.5 K at 800–900 cm^{-1} and 700–750 cm^{-1}, 0.1 K at 980–1080 cm^{-1}, and more than 2 K at 650–700 cm^{-1}. Although the magnitude of the spectral bias evaluated on the basis of V130.130 L1B data would change in V161.160 L1B data, the issue of L1B spectral bias still remains. The spectral bias inherent in TIR L1B spectra would be mainly because of uncertainty of polarization correction. Another possible cause was discussed in Imasu et al. (2010). When retrieving CO_2 concentrations from the TIR band of TANSO-FTS, the spectral bias that is predominant in CO_2 absorption bands should be considered (Ohyama et al., 2013).

3 CONTRAIL Continuous Measurement Equipment (CME) observations

We used CO_2 data obtained in the CONTRAIL project to validate the quality of TANSO-FTS TIR V1 L2 CO_2 data. CONTRAIL is a project to observe atmospheric trace gases such as CO_2 and CH_4 using instruments installed on commercial aircraft operated by JAL. Observations of trace gases in this project began in 2005. Two types of measurement instruments, the Automatic Air Sampling Equipment (ASE) and the Continuous CO_2

Measuring Equipment (CME), have been installed on several JAL aircraft to measure trace gases over a wide area (Machida et al., 2008).

This study used CO_2 data obtained with CME on several airline routes from Narita Airport, Japan. CO_2 observations with CME use a LI-COR LI-840 instrument that utilizes a nondispersive infrared absorption (NDIR) method (Machida et al., 2008). In the observations, two different standard gases, with CO_2 concentration of 340 ppm and 390 ppm based on NIES09 scale, are regularly introduced into the NDIR for calibration. The accuracy of CME CO_2 measurements is 0.2 ppm. See Machida et al. (2008), Matsueda et al. (2008), and Machida et al. (2011) for details of the CME CO_2 observations and their accuracy and precision.

4 Retrieval algorithm of TANSO-FTS TIR V1 CO_2 data

4.1 Basic retrieval settings

Saitoh et al. (2009) provided an algorithm for retrieving CO_2 concentrations from the TIR band of TANSO-FTS. The first version, V00.01, of the L2 CO_2 product of the TIR band of TANSO-FTS was basically processed by the algorithm described in Saitoh et al. (2009). The V1 L2 CO_2 product that we focused on in this study also adopted a non-linear maximum a posteriori (MAP) method with linear mapping, as was the case for the V00.01 product. We utilized the following expressions in TIR CO_2 retrieval:

$$\begin{aligned} \hat{\mathbf{z}}_{\mathbf{i+1}} &= \mathbf{W}^{*}\mathbf{x}_{\mathbf{a}} + \mathbf{G}[\mathbf{y} - \mathbf{F}(\hat{\mathbf{x}}_{\mathbf{i}}) + \mathbf{K}_{\mathbf{i}}\mathbf{W}(\mathbf{W}^{*}\hat{\mathbf{x}}_{\mathbf{i}} - \mathbf{W}^{*}\mathbf{x}_{\mathbf{a}})] \\ \mathbf{G} &= [\mathbf{W}^{T}\mathbf{K}_{\mathbf{i}}{}^{T}\mathbf{S}_{\varepsilon}{}^{-1}\mathbf{K}_{\mathbf{i}}\mathbf{W} + (\mathbf{W}^{*}\mathbf{S}_{\mathbf{a}}\mathbf{W}^{*T})^{-1}]^{-1}\mathbf{W}^{T}\mathbf{K}_{\mathbf{i}}{}^{T}\mathbf{S}_{\varepsilon}{}^{-1} \end{aligned} \quad (1)$$

where $\mathbf{x_a}$ is an a priori vector, $\mathbf{S_a}$ is a covariance matrix of the a priori vector, $\mathbf{S_\varepsilon}$ is a covariance matrix of measurement noise, $\mathbf{K_i}$ is a CO_2 Jacobian matrix calculated using the i^{th} retrieval vector $\hat{\mathbf{x}}_\mathbf{i}$ on full grids, $\mathbf{F}(\hat{\mathbf{x}}_\mathbf{i})$ is a forward spectrum vector based on $\hat{\mathbf{x}}_\mathbf{i}$, $\mathbf{y}$ is a measurement spectrum vector, and $\hat{\mathbf{z}}_{\mathbf{i+1}}$ is the $i+1^{th}$ retrieval vector defined on retrieval grids. $\mathbf{W}$ is a matrix that interpolates from retrieval grids onto full grids. $\mathbf{W}^*$ is the generalized inverse matrix of $\mathbf{W}$.

The full grids are vertical layer grids for radiative transfer calculation, and the retrieval grids are defined as a subset of the full grids. In the V1 L2 CO_2 retrieval algorithm, linear mapping

between retrieval grids and full grids was also applied, but the number of full grid levels was 78 instead of 110 in the V00.01 algorithm. The determination of retrieval grids in the V1 algorithm basically followed the method of the V00.01 algorithm. It was based on the areas of a CO_2 averaging kernel matrix in the tropics, but the retrieval grid levels were fixed for all of the retrieval processing, as presented in Table 1. Averaging kernel matrix **A** is defined (Rodgers, 2000) as

$$\mathbf{A} = \mathbf{GKW} . \quad (2)$$

Figure 1 shows typical averaging kernel functions of TIR V1 L2 CO_2 retrieval. The degrees of freedom (DF) in these cases (trace of the matrix **A**) were (a) 2.22, (b) 1.81, and (c) 1.36, respectively. The seasonally averaged DF values of TIR V1 CO_2 data ranged from 1.12 to 2.35. In the low and middle latitudes between 35°N and 35°S, the CO_2 DF values were around 2.0 or more; this means that observations by the TIR band of TANSO-FTS can provide information on CO_2 concentrations in more than two vertical layers, one of which we focused on in this study.

A priori and initial values for CO_2 concentrations were taken from the outputs of the NIES transport model (NIES-TM05) (Saeki et al., 2013). A priori and initial values for temperature and water vapor were obtained from Japan Meteorological Agency (JMA) Grid Point Value (GPV) data. Basically, the retrieval processing of TANSO-FTS was only conducted under clear-sky conditions, which was judged based on a cloud flag from TANSO-CAI in the daytime (Ishida and Nakajima, 2009; Ishida et al., 2011) and on a TANSO-FTS TIR spectrum in the nighttime.

4.2 Improvements in the TIR V1 CO_2 algorithm

The following conditions are the improvements made in the TANSO-FTS TIR V1 L2 CO_2 algorithm from the V00.01 algorithm. The V1 algorithm used the CO_2 10 μm absorption band in addition to the CO_2 absorption band at around 15 μm band; the wavelength regions of 690–750 cm^{-1}, 790–795 cm^{-1}, 930–990 cm^{-1}, and 1040–1090 cm^{-1} were used in the CO_2 retrieval. We did not apply any channel selection. In these wavelength regions, temperature, water vapor, and ozone concentrations were retrieved simultaneously with CO_2 concentration. Moreover, surface temperature and surface emissivity were simultaneously derived as a

correction parameter of the spectral bias inherent in TANSO-FTS TIR V161.160 L1B spectra at the above-mentioned CO_2 absorption bands. We assumed that the spectral bias could be divided into two components: a wavelength-dependent bias whose amount varied depending on wavelength and a wavelength-independent bias whose amount was uniform in a certain wavelength region. We tried to correct such a wavelength-independent component of the spectral bias by adjusting the value of surface temperature. Similarly, a wavelength-dependent component of the spectral bias was corrected by adjusting the value of surface emissivity in each wavelength channel. Therefore the matrices of $\mathbf{K}$ and $\mathbf{S_a}$ of expression (1) are as follows:

$$\mathbf{K} = (\mathbf{K_{CO2}}\ \mathbf{K_{H2O}}\ \mathbf{K_{O3}}\ \mathbf{K_T}\ \mathbf{k}_{sT\_1}\ \mathbf{k}_{sT\_2}\ \mathbf{k}_{sT\_3}\ \mathbf{k}_{sT\_4}\ \mathbf{k}_{sT\_5}\ \mathbf{k}_{sE\_1}\ \mathbf{k}_{sE\_2}\ \mathbf{k}_{sE\_3}\ \mathbf{k}_{sE\_4}\ \mathbf{k}_{sE\_5}), \quad (3)$$

$$\mathbf{S_a} = \begin{vmatrix} \mathbf{S_{CO2}} & & & & & & & & & & & & \\ & \mathbf{S_{H2O}} & & & & & & & & & & & \\ & & \mathbf{S_{O3}} & & & & & & & & & & \\ & & & \mathbf{S_T} & & & & & & & & & \\ & & & & S_{sT\_1} & & & & & & & & \\ & & & & & S_{sT\_2} & & & & \mathbf{0} & & & \\ & & & & & & S_{sT\_3} & & & & & & \\ & & & & & & & S_{sT\_4} & & & & & \\ & & & & \mathbf{0} & & & & S_{sT\_5} & & & & \\ & & & & & & & & & S_{sE\_1} & & & \\ & & & & & & & & & & S_{sE\_2} & & \\ & & & & & & & & & & & S_{sE\_3} & \\ & & & & & & & & & & & & S_{sE\_4} \\ & & & & & & & & & & & & & S_{sE\_5} \end{vmatrix}, \quad (4)$$

where $\mathbf{K_{CO2}}$, $\mathbf{K_{H2O}}$, $\mathbf{K_{O3}}$, and $\mathbf{K_T}$ are Jacobian matrices of CO_2, water vapor, ozone, and temperature on full grids, respectively, and $\mathbf{S_{CO2}}$, $\mathbf{S_{H2O}}$, $\mathbf{S_{O3}}$, and $\mathbf{S_T}$ are a priori covariance matrices of CO_2, water vapor, ozone, and temperature on full grids, respectively. The vectors $\mathbf{k}_{sT\_1}$, $\mathbf{k}_{sT\_2}$, $\mathbf{k}_{sT\_3}$, $\mathbf{k}_{sT\_4}$, and $\mathbf{k}_{sT\_5}$ are the Jacobian vectors of surface temperature in the wavelength regions of 690–715 cm^{-1}, 715–750 cm^{-1}, 790–795 cm^{-1}, 930–990 cm^{-1}, and 1040–1090 cm^{-1}, respectively. The vectors $\mathbf{k}_{sE\_1}$, $\mathbf{k}_{sE\_2}$, $\mathbf{k}_{sE\_3}$, $\mathbf{k}_{sE\_4}$, and $\mathbf{k}_{sE\_5}$ are the Jacobian vectors of surface emissivity in each of the five wavelength regions, respectively. The elements of the Jacobian vectors of surface parameters that were defined for each of the five wavelength regions were set to be zero in the other wavelength regions. The values S_{sT_1},

S_{sT_2}, S_{sT_3}, S_{sT_4}, and S_{sT_5} and S_{sE_1}, S_{sE_2}, S_{sE_3}, S_{sE_4}, and S_{sE_5} are a priori variances of surface temperature and surface emissivity in each of the five wavelength regions, respectively. Simultaneous retrieval of the surface parameters in the V1 algorithm was conducted just for the purpose of correcting the TIR V161.160 L1B spectral bias; it had no physical meaning. We estimated the surface parameters separately in each of the five wavelength regions to consider differences in the amount of spectral bias in each wavelength region. The matrices $\mathbf{S_a}$ for CO_2, temperature, water vapor, and ozone were diagonal matrices with vertically fixed diagonal elements with a standard deviation of 2.5%, 3 K, 20%, and 30%, respectively. Here, a priori and initial values for ozone were obtained from the climatological data for each latitude bin for each month given by MacPeters et al. (2007). We assumed rather large values as a priori variances of the surface parameters (a standard deviation of 10 K for surface temperature), which could allow more flexibility in the L1B spectral bias correction by the surface parameters. The a priori and initial values for surface emissivity were calculated by linear regression analysis using the Advanced Space-borne Thermal Emission Reflection Radiometer (ASTER) Spectral Library (Baldridge et al., 2009) using land-cover classification, vegetation, and wind speed information. The a priori and initial values for surface temperature were estimated using radiance data in several channels around 900 cm^{-1} of the TIR V161.160 L1B spectra.

In the TIR V1 L2 algorithm, we estimated surface temperature and surface emissivity to correct the spectral bias inherent in the TANSO-FTS TIR L1B spectra (Kataoka et al., 2014). The existence of a relatively large spectral bias around the CO_2 15 μm absorption band in TANSO-FTS TIR L1B spectra (Kataoka et al., 2014) resulted in a decrease in the number of normally retrieved CO_2 profiles. This is probably because the TIR L1B spectral bias in the CO_2 15 μm absorption band was sometimes too large for the L2 retrieval calculation to converse in a limited iteration. The correction of the TIR L1B spectral bias through the simultaneous retrieval of the surface parameters did not affect retrieved CO_2 concentrations in the UTLS regions, which was the focus of this study, but it altered the number of normally retrieved CO_2 profiles. The correction of the TIR L1B spectral bias through the simultaneous retrieval of surface temperature increased the number of normally retrieved CO_2 profiles. This implies that a wavelength-independent component of the spectral bias in CO_2 absorption bands could be reduced by adjusting the value of surface temperature at the bands. In contrast, the spectral bias correction through the simultaneous retrieval of surface emissivity did not increase the number of normally retrieved CO_2 profiles. If the TIR L1B spectral bias has a

wavelength dependence, surface emissivity could be effective for correcting such a wavelength-dependent bias. A more effective method of L1B spectral bias correction based on surface emissivity should be considered in the next version of the TIR L2 CO_2 retrieval algorithm, if a future version of the TIR L1B spectral data still has a bias.

5 Comparison methods

5.1 Area comparisons

Here, we used the level flight CO_2 data of CONTRAIL CME observations in 2010 to validate the quality of UTLS CO_2 data from the TANSO-FTS TIR V1 L2 CO_2 product. The level flight data obtained from the following eight airline routes of the CONTRAIL CME observations were used in this study: Tokyo–Amsterdam (NRT–AMS) and Tokyo–Moscow (NRT–DME), Tokyo–Vancouver (NRT–VYR), Tokyo–Honolulu (NRT–HNL), Tokyo–Bangkok (NRT–BKK), Tokyo–Singapore (NRT–SIN) and Tokyo–Jakarta (NRT–CGK), and Tokyo–Sydney (NRT–SYD). We merged the level flight data of Tokyo–Amsterdam and Tokyo–Moscow into "Tokyo–Europe", and the data of Tokyo–Singapore and Tokyo–Jakarta into "Tokyo–East Asia". Figure 2 shows the flight tracks of all of the CONTRAIL CME observations in 2010 used in this study. As shown in the figure, we divided the CONTRAIL CME level flight data into 40 areas following Niwa et al. (2012), and compared them with TANSO-FTS TIR CO_2 data in each area in each season. The amount of level flight data varied depending on the area and season. The largest amount of data was obtained in area 15 over Narita Airport, where 4,694–9,306 data points were obtained. A relatively small amount of level flight data, 79–222 data points, was obtained in area 1 over Amsterdam. In all 40 areas, we collected sufficient level flight data to undertake comparison analysis based on the average values, except for seasons and regions with no flights.

5.2 Comparisons of CME profiles with and without averaging kernels

In comparisons of TIR V1 L2 CO_2 data with the CONTRAIL CME level flight data, it is difficult to smooth the CME data by applying TIR CO_2 averaging kernels, because CO_2 concentrations below and above the CME flight levels were not observed. Here, we evaluated the impact of considering averaging kernel functions on CO_2 concentrations using the CME profile data. We regarded the CME data obtained during the ascent and descent flights over

the nine airports as part of CO_2 vertical profiles, and investigated differences between TIR and CME CO_2 data with and without applying averaging kernel functions in the altitude regions around the CME level flight observations. We assumed the CME ascending/descending CO_2 concentration at the uppermost altitude level to be constant up to the tropopause height, following the method proposed by Araki et al. (2010). We used stratospheric CO_2 data taken from the Nonhydrostatic Icosahedral Atmospheric Model (NICAM)–Transport Model (TM) (Niwa et al., 2011; 2012) to create whole CO_2 vertical profiles over the airports. The NICAM-TM CO_2 data used here introduced CONTRAIL CO_2 data to the inverse model in addition to surface CO_2 data, and therefore could simulate upper atmospheric CO_2 concentrations well (Niwa et al., 2012). We determined the stratospheric CO_2 profile by assuming the CO_2 concentration gradients, calculated on the basis of the NICAM-TM CO_2 data above the tropopause height.

To compare these CME CO_2 profiles with TIR CO_2 data, we calculated a weighted average of all the CME CO_2 data included in each of the 28 retrieval grid layers with respect to altitude, and defined the CO_2 data in the 28 layers as "CONTRAIL (raw)" data. Then, we selected TIR CO_2 data that coincided with each of the CONTRAIL (raw) profiles. The criteria for the coincident pairs were a 300 km distance from Narita airport, and a 3-day difference of each other observation. We applied TIR CO_2 averaging kernel functions to the corresponding CONTRAIL (raw) profile, as follows (Rodgers and Connor, 2003):

$$\mathbf{x}_{\mathbf{CONTRAIL\,(AK)}} = \mathbf{x}_{\mathbf{a\,priori}} + \mathbf{A}\left(\mathbf{x}_{\mathbf{CONTRAIL\,(raw)}} - \mathbf{x}_{\mathbf{a\,priori}}\right). \quad (5)$$

Here, $\mathbf{x}_{\mathbf{CONTRAIL\,(raw)}}$ and $\mathbf{x}_{\mathbf{a\,priori}}$ are CONTRAIL (raw) and a priori CO_2 profiles. We defined the CONTRAIL (raw) data with TIR CO_2 averaging kernel functions as "CONTRAIL (AK)" data.

5.3 Level flight comparisons

In this study, we made comparisons between TIR and CONTRAIL CME level flight CO_2 data in two ways. The first was a direct comparison with original CME CO_2 data, i.e., CONTRAIL (raw) data. The second was a comparison with CONTRAIL (AK) data in the altitude regions around the CME level flight observations that were based on "assumed CO_2 profiles" created at each of the measurement locations of all the CME level flight data. In the first comparison with CONTRAIL (raw) data, the CME level flight data in each of the 40 areas were averaged for each season (MAM, JJA, SON, and JF/DJF). The average altitude of all of the CME level

flight data used here was 11.245 km. The airline routes of Tokyo–Europe, Tokyo–Vancouver, and Tokyo–Honolulu contained both tropospheric and stratospheric data in the areas along their routes; therefore, we calculated the average and standard deviation values separately. Here, we differentiated between the tropospheric and stratospheric level flight data on the basis of temperature lapse rates from the JMA GPV data that were interpolated to the CONTRAIL CME measurement locations. The average altitudes of the tropospheric and stratospheric level flight data from the airline route between Tokyo and Europe were 10.84 km and 11.18 km, respectively.

In the comparison with CONTRAIL (raw) data, we selected TANSO-FTS TIR V1 L2 CO_2 data that were in the altitude range within ±1 km of the average altitude of the CME level flight data for each area for each season, and calculated their averages and standard deviations. Similarly, we calculated the averages and standard deviations of the corresponding a priori CO_2 data for each area for each season. For the airline routes of Tokyo–Europe, Tokyo–Vancouver, and Tokyo–Honolulu, the averages and standard deviations of TIR V1 CO_2 data and the corresponding a priori CO_2 data were calculated separately for the tropospheric and stratospheric data. In this calculation, we first selected TIR V1 CO_2 data that were collected in a range within ±1 km of the average altitudes of the CONTRAIL tropospheric and stratospheric CO_2 data for each area. Then, we classified each of the selected TIR CO_2 data points into tropospheric and stratospheric data on the basis of the temperature lapse rates from the JMA GPV data that were interpolated to the TANSO-FTS measurement locations, and calculated the seasonal averages and standard deviations for the reselected tropospheric and stratospheric TIR CO_2 data. This procedure was required for two reasons: (1) tropopause height at each TANSO-FTS measurement location should differ on a daily basis, and (2) because TIR CO_2 data were selected within the range of 2 km, some tropospheric TIR CO_2 data were selected on the basis of the CONTRAIL stratospheric level flight data, and vice versa. Figure 3 shows the number of TANSO-FTS TIR CO_2 data points that were finally selected in each retrieval layer for each of the airline routes. The TIR CO_2 data used in the comparative analysis were mainly from layers 9 and 10 (from 287 to 196 hPa) for the tropospheric comparison and from layers 10 and 11 (from 237 to 162 hPa) for the stratospheric comparison.

In the second comparison, we assumed a CO_2 vertical profile on the basis of CONTRAIL (raw) data at each of the CONTRAIL CME level flight locations, and applied TIR CO_2

averaging kernel functions to the assumed profiles. For this purpose, realistic CO_2 vertical profiles were required along the eight airline routes. In this study, we created a CO_2 profile at each CME level flight measurement location from CarbonTracker CT2013B monthly-mean CO_2 data (Peters et al., 2007). The CarbonTracker CT2013B CO_2 data are available to the public, and therefore readers can refer to the dataset that we used as a CO_2 climatological dataset. The method for creating a CO_2 vertical profile from the CONTRAIL (raw) and CarbonTracker CT2013B data is as follows. We first averaged all of the CarbonTracker CT2013B monthly-mean data included in each of the 40 areas to create area-averaged CarbonTracker CT2013B profiles. Then, we shifted the area-averaged CarbonTracker CT2013B profile so that its concentration fit to each of the CONTRAIL (raw) data at CME level flight altitude. Finally, we applied area-averaged TIR CO_2 averaging kernel functions to each of the shifted area-averaged CO_2 profiles, and created profiles of CONTRAIL (AK) at all the CME level flight measurement locations.

We compared the CONTRAIL (AK) data with TIR CO_2 data at the altitude regions around the CME level flight observations for each area in each season. We extracted CONTRAIL (AK) data that corresponded to the TIR retrieval layers where TIR CO_2 data were compared to CONTRAIL (raw) data, and averaged them for each area for each season. For the airline routes of Tokyo–Europe, Tokyo–Vancouver, and Tokyo–Honolulu, we separately averaged CONTRAIL (AK) data created from tropospheric and stratospheric CONTRAIL (raw) data, and defined the averages as tropospheric and stratospheric CONTRAIL (AK) data, respectively. As shown in Figure 3, the CONTRAIL (AK) data used for the comparison during flights between Tokyo and Sydney consisted of CO_2 concentrations in layers 9 and 10 of the CONTRAIL (AK) profiles. For the flights between Tokyo and Europe, the CONTRAIL (AK) data used for the tropospheric and stratospheric comparisons were based on CO_2 concentrations in layers 9 and 10 and in layers 10 and 11 of CONTRAIL (AK) profiles, respectively.

6 Comparison results

6.1 Impacts of averaging kernels on CME profiles

Figure 4 shows comparisons of the differences between TANSO-FTS TIR and CONTRAIL (raw) CO_2 data, and the differences between TIR and CONTRAIL (AK) CO_2 data in low

(BKK), middle (NRT and SYD), and high (DME) latitudes in layers 9, 10, and 11. In low latitudes, the differences between CONTRAIL (raw) and CONTRAIL (AK) were mostly less than 0.5 ppm in all seasons. This is because the tropopause heights there were much higher than the altitude levels of CONTRAIL CME level flight measurements, and CO_2 concentrations did not change much in the altitude regions where we compared TIR and CONTRAIL CME data. The same was true for other airports in low latitudes. While the differences between CONTRAIL (raw) and CONTRAIL (AK) were larger in middle and high latitudes than in low latitudes, they were in most cases less than 1 ppm in all seasons. In conclusion, the impact of applying the TIR CO_2 averaging kernels on CONTRAIL CME CO_2 data at around the CME level flight altitudes (~11 km) was on average less than 0.5 ppm in low latitudes and less than 1 ppm in middle and high latitudes.

6.2 Comparisons during level flight

The airline route between Tokyo and Sydney covered a wide latitude range from the northern mid-latitudes (35°N) to southern mid-latitudes (34°S). Figure 5 shows comparisons among CONTRAIL (raw), CONTRAIL (AK), TANSO-FTS TIR, and a priori CO_2 data during flights between Tokyo and Sydney in spring. In this case, we averaged CO_2 data mainly from layers 9 and 10 of the TIR retrieval layer levels. The 1-σ values of the averages show the variability of CO_2 concentrations in these UTLS layers. The average of the TIR CO_2 data agreed better with the averages of the CONTRAIL (raw) and (AK) CO_2 data than the a priori CO_2 data in all latitudes. The differences between CONTRAIL (raw) and CONTRAIL (AK) were approximately 0.5 ppm, which is consistent with the result shown in Figure 4, despite the fact that CONTRAIL (AK) data here were evaluated on the basis of CarbonTracker monthly-mean data. In the Southern Hemisphere, the average of the TIR CO_2 data was within 0.1% of the averages of the CONTRAIL (raw) and CONTRAIL (AK) CO_2 data. In the Northern Hemisphere, the average of the TIR CO_2 data agreed with the averages of the CONTRAIL (raw) and CONTRAIL (AK) CO_2 data to within 0.5%, although the agreement was slightly worse there than in the Southern Hemisphere.

Along the airline route between Tokyo and Europe, both tropospheric and stratospheric CO_2 data were obtained in the CONTRAIL CME observations. Therefore, we were able to validate the quality of TANSO-FTS TIR CO_2 data for this route both in the upper troposphere and lower stratosphere using the UTLS CME CO_2 data. Here, we averaged CO_2 data mainly from layers 9 and 10 for the upper tropospheric comparison and from layers 10 and 11 for the

lower stratospheric comparison. As shown in Figure 6, the differences between CONTRAIL (raw) and CONTRAIL (AK) were again approximately 0.5 ppm when CONTRAIL CME data were divided into the upper troposphere and lower stratosphere, which is consistent with the result shown in Figure 4. Figure 6b and 6c shows that the differences between the upper tropospheric and lower stratospheric CO_2 concentrations of CONTRAIL CME data were approximately 2–3 ppm in winter (maximum of 4.24 ppm in area 14). The upper tropospheric and lower stratospheric CO_2 concentrations from TANSO-FTS TIR V1 data also clearly differed, while the upper tropospheric and lower stratospheric CO_2 concentrations from a priori data were similar. The upper tropospheric TIR CO_2 concentrations were in a good agreement within 1 ppm with the corresponding CONTRAIL (raw) and CONTRAIL (AK) data (Figure 6b). In the lower stratosphere in winter (Figure 6c), the averages of the CONTRAIL (raw), CONTRAIL (AK), TANSO-FTS TIR, and a priori CO_2 data were all within 0.5–1 ppm of each other.

Figure 7 shows the results of all of the comparisons among CONTRAIL (raw), CONTRAIL (AK), TANSO-FTS TIR, and a priori CO_2 data in the upper troposphere (left) and lower stratosphere (right) for each season. We divided the data for all four datasets in each of the 40 areas into six latitude bands: 40°S–20°S (areas 30 and 31), 20°S–0° (areas 21, 28, and 29), 0°–20°N (areas 16, 17, 20, 22, 23, 26, and 27), 20°N–40°N (areas 15, 18, 19, 24, 25, and 37–40), 40°N–60°N (areas 1, 2, 14, and 32–36), and 60°N–70°N (areas 3–13). As for the lower stratosphere, we showed the results at northern latitudes of 40°N where an adequate amount of data was obtained. Overall, the black and gray lines (TIR ave. minus CONTRAIL (raw) ave. and TIR ave. minus CONTRAIL (AK) ave.) were closer to zero than the green lines (a priori ave. minus CONTRAIL (raw) ave.), which means that TIR CO_2 data agreed better with CONTRAIL CME CO_2 data than a priori CO_2 data.

The left panels of Figure 7 show that the agreements between TIR and CONTRAIL (raw) and CONTRAIL (AK) CO_2 average data were worse in spring and summer than in fall and winter in the Northern Hemisphere in the upper troposphere. The differences between TIR and CONTRAIL (raw) and CONTRAIL (AK) CO_2 data were on average within 1 ppm in fall and winter in the northern troposphere. At 0°–40°N in summer, in contrast, the TIR and a priori CO_2 average data were 2.3 ppm lower than the CONTRAIL (AK) CO_2 average data. At 20°N–40°N in spring, the differences between TIR and CONTRAIL (AK) CO_2 average data were 2.4 ppm, although the TIR CO_2 data had a better agreement with CONTRAIL CME CO_2

data than a priori CO_2 data. On the other hand, the averages of the TIR CO_2 data were within 0-0.7 ppm of the averages of the CONTRAIL (AK) CO_2 data in the Southern Hemisphere in all seasons, as in the comparison in spring shown in Figure 5.

In the lower stratosphere, the agreements between the average TANSO-FTS TIR and CONTRAIL CME CO_2 data did not have a smaller seasonality than in the upper troposphere. The averages of TIR and CONTRAIL (raw) and CONTRAIL (AK) CO_2 data agreed with each other within 0.5% in all seasons.

7 Discussion

As shown in Figure 7, TANSO-FTS TIR V1 L2 CO_2 data had a negative bias of 2.3–2.4 ppm against CONTRAIL CME CO_2 data in the northern low and middle latitudes in spring and summer. Uncertainties in surface parameters and temperature profiles could affect CO_2 retrieval in thermal infrared spectral regions. As described above, retrieving surface parameters simultaneously instead of using initial surface parameters did not affect CO_2 concentrations in the UTLS regions in the TIR V1 CO_2 retrieval. We compared simultaneously retrieved temperature profiles with a priori JMA GPV temperature profiles in the UTLS region, and did not find any difference between the two which could explain the largest TIR CO_2 negative bias in the northern low and middle latitudes in spring and summer. In the UTLS regions, temperature variability is relatively large, and therefore comprehensive validation analysis of both the a priori and retrieved temperature profiles should be required using reliable and independent temperature data such as radiosonde data.

Uncertainty in a priori data could result in uncertainty in retrieved CO_2 data. Here, we arbitrarily decreased the a priori concentration by 1% in a test TIR CO_2 retrieval, and then compared the retrieved CO_2 concentrations with those retrieved using the original a priori data. In the northern low and middle latitudes in spring and summer where the DF values of TIR V1 CO_2 data were around 1.8 and more, a 1% negative bias in a priori data could yield up to a 0.7% negative bias in retrieved CO_2 concentrations in the altitude regions where we did comparisons between TIR and CONTRAIL CME data, although the magnitude of the bias varied depending on retrievals. As shown by the green lines in Figure 7, a priori CO_2 concentrations were underestimated by 2–4 ppm in the northern low and middle latitudes in spring and summer. The test TIR CO_2 retrieval demonstrated that the negative bias of a priori

CO_2 data against CONTRAIL CME data is a possible cause of the TIR CO_2 negative bias in the UTLS regions in the northern low and middle latitudes in spring and summer.

In general, the information content of CO_2 observations made by TIR sensors is higher in middle and high latitudes in spring and summer than in fall and winter because of the thermal contrast in the atmosphere, with less seasonal dependence in low latitudes. Therefore, in spring and summer, retrieved CO_2 data contain more measurement information and are less constrained by a priori data at all latitudes. However, as shown in Figure 7, the retrieved TIR CO_2 data in the northern low and middle latitudes did not sufficiently reduce the negative bias of the a priori CO_2 data in the UTLS regions in spring and summer. This implies the existence of factors that worsened CO_2 retrieval results other than the a priori data, especially in spring and summer. Another possible factor that worsened CO_2 retrieval results is the uncertainty in the calibration of TIR V161.160 L1B spectra. As reported in Kataoka et al. (2014), TANSO-FTS TIR V130.130 L1B radiance spectra had a wavelength-dependent bias ranging from 0.1 to 2 K. Although the characteristics of the spectral bias in V161.160 L1B data used in TIR V1 L2 CO_2 retrievals are still under investigation, we assumed the same degree of bias in V161.160 L1B spectra, and evaluated the effect of the L1B spectral bias on the TIR CO_2 retrieval using the following equation:

$$\mathbf{d}_{\mathbf{CO2}} = \mathbf{G}_{\mathbf{CO2}}\mathbf{d}_{\mathbf{spec}} . \quad (6)$$

Here, $\mathbf{G}_{\mathbf{CO2}}$ is a gain matrix for CO_2 retrieval, $\mathbf{d}_{\mathbf{spec}}$ is a spectral bias vector based on the evaluation by Kataoka et al. (2014), and $\mathbf{d}_{\mathbf{CO2}}$ is a vector of bias errors in retrieved CO_2 concentrations attributable to the spectral bias. The result showed that a wavelength-dependent bias comparable to V130.130 L1B spectra could yield up to 0.3% and 0.5% uncertainties in retrieved CO_2 concentration in the UTLS regions in the northern middle latitude in spring and in the northern low latitude in summer, respectively. Uncertainty in the radiometric calibration of TANSO-FTS L1B spectra causes the spectral bias inherent in TIR L1B spectra. The temperatures of the internal blackbody on board the TANSO-FTS instrument partly reflect the environmental thermal conditions inside the instrument. The temperatures of FTS-mechanics and aft-optics on the optical bench of the TANSO-FTS instrument are precisely controlled at 23 °C. The difference in temperature between the environment inside the instrument and the optical bench could cause the uncertainty in the radiometric calibration of TANSO-FTS L1B spectra. Thus, the temperatures of the internal

blackbody on board the TANSO-FTS instrument could be a parameter used to evaluate the TANSO-FTS TIR L1B spectral bias.

Figure 8 shows the averages of the partial degree of freedom of TANSO-FTS TIR V1 L2 CO_2 data for each of the areas along the airline routes between Tokyo and Europe in the upper troposphere (a) and the lower stratosphere (b) for each season. The partial DF is defined as the diagonal element of the averaging kernels corresponding to TIR CO_2 data that were compared to CONTRAIL CME level flight data, which is equal to the 9^{th}, 10^{th}, or 11^{th} diagonal element of matrix **A**. As shown in Figure 8, the average values of the partial DF of TIR lower stratospheric CO_2 data were clearly lower than those of TIR upper tropospheric CO_2 data for all of the fights between Tokyo and Europe. TIR upper tropospheric CO_2 data were from layers 9 and 10, and TIR lower stratospheric CO_2 data were from layers 10 and 11, as shown in Figure 3, which led to a clear difference in partial DF values between the TIR upper tropospheric and lower stratospheric CO_2 data. The partial DF values of TIR upper tropospheric CO_2 data were 0.13–0.20 in all of the areas for all seasons. In contrast, the partial DF values of TIR lower stratospheric CO_2 data in spring, fall, and winter were ~0.05 in almost all of the areas, although they were as high as 0.1–0.14 in summer. From the results shown in Figure 6c and Figure 8, we conclude that TIR CO_2 retrieval results in the lower stratosphere in winter were constrained to the relatively good a priori CO_2 data due to the low information content, and consequently had a good agreement with CONTRAIL CME CO_2 data. The comparisons in the areas during the airline route between Tokyo and Europe were included in the comparison results of 60°N–70°N in the right panels of Figure 7. In this region, the average differences between a priori and CONTRAIL (raw) data were 1-2 ppm in summer and fall, while they were less than 0.5 ppm in spring and winter. In summer, TIR CO_2 retrievals had a relatively high information content compared to the other seasons, which led to an agreement between TIR and CONTRAIL (raw) and CONTRAIL (AK) CO_2 data of within 0.5 ppm. In fall, TIR CO_2 retrieval results in the lower stratosphere were more constrained to the a priori CO_2 data, and therefore had a negative bias of approximately 1-2 ppm against CONTRAIL (raw) and CONTRAIL (AK) CO_2 data. In conclusion, the quality of TIR V1 CO_2 data in the lower stratosphere depends largely on the information content compared to the upper troposphere. In the case of high latitude measurements, TIR V1 lower stratospheric CO_2 data are only valid in summer.

We investigated the differences between TIR and CONTRAIL CO_2 comparison results in layers 9–11 with and without applying averaging kernel functions over the nine airports where CO_2 vertical profiles were observed during ascent and descent. In the northern middle latitudes in spring (NRT in Figure 4), CONTRAIL (AK) was on average 0.2 and 1.2 ppm lower than CONTRAIL (raw) in layers 9 and 10. In contrast, the tendency was the opposite in the southern middle latitudes in spring (SYD in Figure 4); CONTRAIL (AK) was on average 1.1 and 0.4 ppm higher than CONTRAIL (raw) in layers 9 and 10. This means that CO_2 concentrations in layers 9 and 10 were more affected by stratospheric air with relatively low CO_2 concentrations in the northern middle latitude in spring, when considering averaging kernels. This is consistent with the result of Sawa et al. (2012) showing that the difference between upper tropospheric and lower stratospheric CO_2 concentrations was larger in the Northern Hemisphere in spring.

Using CONTRAIL CME level flight observations that covered wide spatial areas allowed us to discuss the longitudinal differences in the characteristics of TIR UTLS CO_2 data. In the comparison results of the airline routes of Tokyo–Europe (Figure 6) and Tokyo–Vancouver (not shown here), the magnitudes of the differences between TIR and CONTRAIL (raw) and (AK) CO_2 data did not have a clear longitudinal dependence. Table 2 summarizes the latitudinal dependence of the magnitudes of the differences between TIR and CONTRAIL (AK) CO_2 data. In the upper troposphere in 0–60°N, negative biases in TIR CO_2 data against CONTRAIL CME CO_2 data ranged from 1.2 to 2.4 ppm in spring and summer, when applying averaging kernels to the assumed CME CO_2 profiles created based on CarbonTracker CT2013B monthly-mean profiles. It is the negative biases in the northern low and middle latitudes that we should in particular be concerned about when using TIR V1 L2 CO_2 data in any scientific analysis. In the upper troposphere in the northern middle latitudes, CO_2 concentrations reach the maximum from spring through early summer. The negative biases in TIR CO_2 data resulted in the maximum TIR CO_2 concentrations being lower than that of the CONTRAIL CME CO_2 concentrations, which led to an underestimate of the amplitude of the CO_2 seasonal variation when using TIR CO_2 data without taking their negative biases into account.

8 Summary

In this study, we conducted a comprehensive validation of the UTLS CO_2 concentrations from the GOSAT/TANSO-FTS TIR V1 L2 CO_2 product. The TIR V1 L2 CO_2 algorithm used both the CO_2 10 μm and 15 μm absorption bands (690–750 cm^{-1}, 790–795 cm^{-1}, 930–990 cm^{-1}, and 1040–1090 cm^{-1}), and simultaneously retrieved vertical profiles of CO_2, water vapor, ozone, and temperature in these wavelength regions. Because the TANSO-FTS TIR V161.160 L1B radiance data used in the TIR V1 L2 CO_2 retrieval had a spectral bias, we simultaneously derived surface temperature and surface emissivity in the same wavelength regions as a corrective parameter, other than temperature and gas profiles, to correct the spectral bias. The simultaneous retrieval of surface temperature greatly increased the number of normally retrieved CO_2 profiles.

To validate the quality of TIR V1 upper atmospheric CO_2 data, we compared them with the level flight CO_2 data of CONTRAIL CME observations along the following airline routes in 2010: Tokyo–Europe (Amsterdam and Moscow), Tokyo–Vancouver, Tokyo–Honolulu, Tokyo–Bangkok, Tokyo–East Asia (Singapore and Jakarta), and Tokyo–Sydney. For the CONTRAIL data obtained during the northern high latitude flights, we made comparisons among CONTRAIL, TIR, and a priori CO_2 data separately in the upper troposphere and in the lower stratosphere. The TIR upper tropospheric and lower stratospheric CO_2 data that were compared were mainly from layers 9 and 10 (287–196 hPa) and from layers 10 and 11 (237–162 hPa), respectively. In this study, we evaluated the impact of considering TIR CO_2 averaging kernel functions on CO_2 concentrations using the CME profile data over the nine airports; the impact at around the CME level flight altitudes (~11 km) was on average less than 0.5 ppm in low latitudes and less than 1 ppm in middle and high latitudes.

In the Southern Hemisphere, the averages of TANSO-FTS TIR V1 upper atmospheric CO_2 data were within 0.1% of the averages of CONTRAIL CO_2 data with and without TIR CO_2 averaging kernels for all seasons, from the limited comparisons made during flights between Tokyo and Sydney, while TIR CO_2 data had a better agreement with CONTRAIL CO_2 data than a priori CO_2 data, with the agreement being on average within 0.5% in the Northern Hemisphere. The northern high latitude comparisons suggest that the quality of TIR lower stratospheric CO_2 data depends largely on the information content. In high latitudes, TIR lower stratospheric CO_2 data are only valid in summer when their information content is highest. Overall, the agreements of TIR and CONTRAIL CME CO_2 data were worse in spring

and summer than in fall and winter in the Northern Hemisphere in the upper troposphere. TIR CO_2 data had a negative bias up to 2.4 ppm against CONTRAIL CO_2 data with TIR CO_2 averaging kernels in the northern low and middle latitudes in spring and summer. This is partly because of the larger negative bias in the a priori CO_2 data. The spectral bias inherent to TANSO-FTS TIR L1B radiance data could cause a negative bias in retrieved CO_2 concentrations, particularly in summer. TIR sensors can make more observations than SWIR sensors. When using the TIR UTLS CO_2 data, the seasonally and regionally dependent negative biases of the TIR V1 L2 CO_2 data presented here should be taken into account.

Acknowledgements

We thank all of the members of the GOSAT Science Team and their associates. We are also grateful to the engineers of Japan Airlines, the JAL Foundation, and JAMCO Tokyo for supporting the CONTRAIL project. We thank Dr. Y. Niwa for providing the outputs of NICAM-TM CO_2 simulations. We thank Dr. Saeki and Dr. Maksyutov to provide information on a priori dataset. CarbonTracker CT2013B results were provided by NOAA Earth System Research Laboratory (ESRL), Boulder, Colorado, USA from the website at http://carbontracker.noaa.gov. This study was supported by the Green Network of Excellence (GRENE-ei) of the Ministry of Education, Culture, Sports, and Technology. This study was performed within the framework of the GOSAT Research Announcement.

References

Araki, M., Morino, I., Machida, T., Sawa, Y., Hatsueda, H., Ohyama, H., Yokota, T., and Uchino, O.: CO_2 column-averaged volume mixing ratio derived over Tsukuba from measurements by commercial airlines, Atmos. Chem. Phys., 10, 7659-7667, 2010.

Bakwin, P. S., Tans, P. P., Hurst, D. F., and Zhao, C.: Measurements of carbon dioxide on very tall towers: results of the NOAA/CMDL program, Tellus, 50B, 401-415, 1998.

Baldridge, A. M., Hook, S. J., Grove, C. I., and Rivera, G.: The ASTER spectral library version 2.0, Remote Sens. Env., 10.1016/jrse.2008.11.007, 2009.

Barkley, M. P., Frieß, U., and Monks, P. S.: Measuring atmospheric CO_2 from space using Full Spectral Initiation (FSI) WFM-DOAS, Atmos. Chem. Phys., 6, 3517-3534, 2006.

Basu, S., Guerlet, S., Butz, A., Houweling, S., Hasekamp, O., Aben, I., Krummel, P., Steele, P., Langenfelds, R., Torn, M., Biraud, S., Stephens, B., Andrews, A., and Worthy, D.: Global CO_2 fluxes estimated from GOSAT retrievals of total column CO_2, Atmos. Chem. Phys., 13, 8695-8717, 2013.

Basu, S., Krol, M., Butz, A., Clerbaux, C., Sawa, Y., Machida, T., Matsueda, H., Frankenberg, C., Hasekamp, O. P., and Aben, I.: The seasonal variation of the CO_2 flux over Tropical Asia estimated from GOSAT, CONTRAIL, and IASI, Geophys. Res. Lett., 41, 1809-1815, 2014.

Brenninkmeijer, C. A. M. et al.: Civil Aircraft for the regular investigation of the atmosphere based on an instrumented container: The new CARIBIC system, Atmos. Chem. Phys., 7, 4953-4976, 2007.

Buchwitz, M., de Beek, R., Burrows, J. P., Bovensmann, H., Warneke, T., Notholt, J., Meirink, J. F., Goede, A. P. H., Bergamaschi, P., Körner, S., Heimann, M., and Schulz, A.: Atmospheric methane and carbon dioxide from SCIAMACHY satellite data: initial comparison with chemistry and transport models, Atmos. Chem. Phys., 5, 941-962, 2005.

Butz, A. et al.: Toward accurate CO_2 and CH_4 observations from GOSAT, Geophys. Res. Lett., 38, doi:10.1029/2011GL047888, 2011.

Chahine, M., Barnet, C., Olsen, E. T., Chen, L., and Maddy, E.: On the determination of atmospheric minor gases by the method of vanishing partial derivatives with application to CO_2, Geophys. Res. Lett., 32, doi:10.1029/2005GL024165, 2005.

Chédin, A., Serrar, S., Armante, R., Scott, N. A., and Hollingsworth, A.: Signatures of annual and seasonal variations of CO_2 and other greenhouse gases from comparisons between NOAA TOVS observations and radiation model simulations, J. Climate, 15, 95-116, 2002.

Chédin, A., Serrar, S., Scott, N. A., Crevoisier, C., and Armante, R.: First global measurement of midtropospheric CO_2 from NOAA polar satellites, J. Geophys. Res., 108, doi:10.1029/2003JD003439, 2003.

Chédin, A., Serrar, S., Scott, N. A., Pierangelo, C., and Ciais, P.: Impact of tropical biomass burning emissions on the diurnal cycle of upper tropospheric CO_2 retrieved from NOAA 10 satellite observations, J. Geophys. Res., 110, doi:10.1029/2004JD005540, 2005.

Chevallier, F., Fisher, M., Peylin, P., Serrar, S., Bousquet, P., Bréon, F.-M., Chédin, A., and Ciais, P.: Inferring CO_2 sources and sinks from satellite observations: Method and application to TOVS data, J. Geophys. Res., 110, doi:10.1029/2005JD006390, 2005.

Chevallier, F., Palmer, P. I., Feng, L., Boesch, H., O'Dell, C. W., and Bousquet, P.: Toward robust and consistent regional CO_2 flux estimates from in situ and spaceborne measurements of atmospheric CO_2, Geophys. Res. Lett., 41, 1065-1070, 2014.

Climate Modeling and Diagnostics Laboratory (CMDL): Climate Modeling and Diagnostics Laboratory Summary Report No. 27 2002-2003, Boulder, Colorado, USA, 2004.

Cogan, A. J., Boesch, H., Parker, R. J., Feng, L., Palmer, P. I., Blavier, J.-F. L., Deutscher, N. M., Macatangay, R., Notholt, J., Roehl, C., Warneke, T., and Wunch, D.: Atmospheric carbon dioxide retrieved from the Greenhouse gases Observing SATellite (GOSAT): Comparison with ground-based TCCON observations and GEOS-Chem model calculations, J. Geophys. Res., 117, doi:10.1029/2012JD018087, 2012.

Crevoisier, C., Heilliette, S., Chédin, A., Serrar, S., Armante, R., and Scott, N. A.: Midtropospheric CO_2 concentration retrieval from AIRS observations in the tropics, Geophys. Res. Lett., 31, doi:10.1029/2004GL020141, 2004.

Crevoisier, C., Chédin, A., Matsueda, H., Machida, T., Armante, R., and Scott, N. A.: First year of upper tropospheric integrated content of CO_2 from IASI hyperspectral infrared observations Atmos. Chem. Phys., 9, 4797-4810, 2009.

Crevoisier, C., Sweeney, C., Gloor, M., Sarmiento, J. L., and Tans, P. P.: Regional US carbon sinks from three-dimensional atmospheric CO_2 sampling, PNAS, 107, 18,348-18,353, 2010.

Hamazaki, T., Kaneko, Y., Kuze, A., and Kondo, K.: Fourier transform spectrometer for Greenhouse Gases Observing Satellite (GOSAT), Proc. of Soc. Photo Opt. Instrum. Eng., 73-80, 2005.

Imasu, R., Hayashi, Y., Inagoya, A., Saitoh, N., and Shiomi, K.: Retrieval of minor constituents from thermal infrared spectra observed by GOSAT TANSO-FTS sensor, Proc. of Soc. Photo Opt. Instrum. Eng., 7857, doi:10.1117/12.870684, 2010.

Inoue, M., Morino, I., Uchino, O., Miyamoto, Y., Yoshida, Y., Yokota, T., Machida, T., Sawa, Y., Matsueda, H., Sweeney, C., Tans, P. P., Andrews, A. E., Biraud, S. C., Tanaka, T., Kawakami, S., and Patra, P. K.: Validation of XCO_2 derived from SWIR spectra of GOSAT TANSO-FTS with aircraft measurement data, Atmos. Chem. Phys., 13, 9771-9788, 2013.

Ishida, H. and Nakajima, T. Y.: Development of an unbiased cloud detection algorithm for a spaceborne multispectral imager, J. Geophys. Res., 114, doi:10.1029/2008JD010710, 2009.

Ishida, H., Nakjima, T. Y., Yokota, T., Kikuchi, N., and Watanabe, H.: Investigation of GOSAT TANSO-CAI Cloud Screening Ability through an Intersatellite Comparison, J. Appl. Meteo. Clim., 50, 1571-1586, 2011.

Intergovernmental Panel on Climate Change (IPCC): Contribution of Working Group I to the Fifth Assessment Report of the Intergovernmental Panel on Climate Change, Cambridge University Press, Cambridge, United Kingdom and New York, NY, USA, 2013.

Karion, A., Sweeney, C., and Tans, P. P.; AirCore: An innovative atmospheric sampling system, J. Atmos. Ocean Tech., 27, 1839-1853, 2010.

Kataoka, F., Knuteson, R. O., Kuze, A., Suto, H., Shiomi, K., Harada, M., Garms, E. M., Roman, J. A., Tobin, D. C., Taylor, J. K., Revercomb, H. E., Sekio, N., Higuchi, R., and Mitomi, Y.: TIR spectral radiance calibration of the GOSAT satellite borne TANSO-FTS with the aircraft-based S-HIS and the ground-based S-AERI at the Railroad Valley desert playa, IEEE T. Geosci. Remote, 52, 89-105, 2014.

Keeling, C. D., Bacastow, R. B., Bainbridge, A. E., Ekdahl, C. A., Guenther, P. R., Waterman, L. S., and Chin, J. F. S.; Atmospheric carbon dioxide variations at Mauna Loa Observatory, Hawaii, Tellus, 28, 538-551, 1976a.

Keeling, C. D., Adams, J. A., Ekdahl, C. A., and Guenther, P. R.: Atmospheric carbon dioxide variations at the South Pole, Tellus, 28, 553-564, 1976b.

Keeling, C. D., Chin, J. F. S., and Whorf, T. P.: Increased activity of northern vegetation inferred from atmospheric CO_2 measurements, Nature, 382, 146-149, 1996.

Kulawik, S. S., Jones, D. B. A., Nassar, R., Irion, F. W., Worden, J. R., Bowman, K. W., Machida, T., Matsueda, H., Sawa, Y., Biraud, S. C., Fischer, M. L., and Jacobson, A. R.: Characterization of Tropospheric Emission Spectrometer (TES) CO_2 for carbon cycle science, Atmos. Chem. Phys., 10, 5601-5623, 2010.

Kulawik, S. S. et al.: Comparison of improved Aura Tropospheric Emission Spectrometer CO_2 with HIPPO and SGP aircraft profile measurements, Atmos. Chem. Phys., 13, 3205-3225, 2013.

Kuze, A., Suto, H., Nakajima, M., and Hamazaki, T.: Thermal and near infrared sensor for carbon observation Fourier-transform spectrometer on the Greenhouse Gases Observing Satellite for greenhouse gases monitoring, Appl. Optics, 48, 6716-6733, 2009.

Kuze, A., Suto, H., Shiomi, K., Urabe, T., Nakajima, M., Yoshida, J., Kawashima, T., Yamamoto, Y., Kataoka, F., and Buijs, H.: Level 1 algorithms for TANSO on GOSAT: processing and on-orbit calibrations, Atmos. Meas. Tech., 5, 2447-2467, 2012.

Machida, T., Matsueda, H., Sawa, Y., Nakagawa, Y., Hirotani, K., Kondo, N., Goto, K., Nakazawa, T., Ishikawa, K., and Ogawa, T.: Worldwide measurements of atmospheric CO_2 and other trace gas species using commercial airlines, J. Atmos. Ocean Tech., 25, 1744-1754, 2008.

Machida, T., Tohjima, Y., Katsumata, K., and Mukai, H.: A new CO_2 calibration scale based on gravimetric one-step dilution cylinders in National Institute for Environmental Studies - NIES 09 CO_2 Scale, 15th WMO/IAEA Meeting of Experts on Carbon Dioxide, Other Greenhouse Gases and Related Tracers Measurement Techniques, GAW Rep., 194, 165-169, World Meteorological Organization, Geneva, Switzerland, 2011.

McPeters, R. D., Labow, G. J., and Logan, J. A.: Ozone climatological profiles for satellite retrieval algorithms, J. Geophys. Res., 112, doi:10.1029/2005JD006823, 2007.

Maddy, E. S., Barnet, C. D., Goldberg, M., Sweeney, C., and Liu, X.: CO_2 retrievals from the Atmospheric Infrared Sounder: Methodology and validation, J. Geophys. Res., 113, doi:10.1029/2007JD009402, 2008.

Maksyutov, S., Takagi, H., Valsala, V. K., Saito, M., Oda, T., Saeki, T., Belikov, D. A., Saito, R., Ito, A., Yoshida, Y., Morino, I., Uchino, O., Andres, R. J., and Yokota, T.: Regional CO_2 flux estimates for 2009-2010 based on GOSAT and ground-based CO_2 observations, Atmos. Chem. Phys., 13, 9351-9373, 2013.

Matsueda, H., Machida, T., Sawa, Y., Nakagawa, Y., Hirotani, K., Ikeda, H., Kondo, N., and Goto, K.: Evaluation of atmospheric CO_2 measurements from new flask air sampling of JAL airliner observations, Pap. Meteorol. Geophys., 59, 1-17, 2008.

Matsueda, H., Machida, T., Sawa, Y., and Niwa, Y.: Long-term change of CO_2 latitudinal distribution in the upper troposphere, Geophys. Res. Lett., 42, 2508-2514, 2015.

Nassar1, R., Jones, D. B. A., Kulawik, S. S., Worden, J. R., Bowman, K. W., Andres, R. J., Suntharalingam, P., Chen, J. M., Brenninkmeijer, C. A. M., Schuck, T. J., Conway, T. J., and Worthy, D. E.: Inverse modeling of CO_2 sources and sinks using satellite observations of CO_2 from TES and surface flask measurements, Atmos. Chem. Phys., 11, 6029-6047, 2011.

Niwa, Y., Tomita, H., Satoh, M., and Imasu, R.: A threedimensional icosahedral grid advection scheme preserving monotonicity and consistency with continuity for atmospheric tracer transport, J. Meteor. Soc. Jpn., 89, 255–268, 2011.

Niwa, Y., Machida, T., Sawa, Y., Matsueda, H., Schuck, T. J., Brenninkmeijer, C. A. M., Imasu, R., and Satoh, M.: Imposing strong constraints on tropical terrestrial CO_2 fluxes using passenger aircraft based measurements, J. Geophys. Res., 117, doi:10.1029/2012JD017474, 2012.

O'Dell1, C. W. et al.: The ACOS CO_2 retrieval algorithm - Part 1: Description and validation against synthetic observations Atmos. Meas. Tech., 5, 99-121, 2012.

Ohyama, H., Kawakami, S., Shiomi, K., and Miyagawa, K.: Retrievals of Total and Tropospheric Ozone From GOSAT Thermal Infrared Spectral Radiances, IEEE T. Geosci. Remote, 50, 1770-1784, 2012.

Ohyama, H., Kawakami, S., Shiomi, K., Morino, I., and Uchino, O.: Atmospheric Temperature and Water Vapor Retrievals from GOSAT Thermal Infrared Spectra and Initial Validation with Coincident Radiosonde Measurements, SOLA, 9, 143-147, 2013.

Pak, B. C., and Prather, M. J.: CO_2 sources inversions using satellite observations of the upper troposphere, Geophys. Res. Lett., 28, 4571-4574, 2001.

Peters, W., Jacobson, A. R., Sweeney, C., Andrews, A. E., Conway, T. J., Masarie, K., Miller, J. B., Bruhwiler, L. M. P., Petron, G., Hirsch, A. I., Worthy, D. E. J., van der Werf, G. R., Randerson, J. T., Wennberg, P. O., Krol, M. C., and Tans, P. P.: An atmospheric perspective on North American carbon dioxide exchange: CarbonTracker", PNAS, 48, 104, 18925-18930, with updates documented at http://carbontracker.noaa.gov.

Rayner, P. J. and O'Brien, D. M.: The utility of remotely sensed CO_2 concentration data in surface source inversions, Geophys. Res. Lett., 28, 175-178, 2001.

Rodgers, C. D.: Inverse method for atmospheric sounding, World Scientific Publishing, 2000.

Rodgers, C. D. and Connor, B. J.: Intercomparison of remote sounding instruments, J. Geophys. Res., 108, 10.1029/2002JD002299, 2003.

Rodgers, C. D. and Connor, B. J.: Intercomparison of remote sounding instruments, J. Geophys. Res., 108, 10.1029/2002JD002299, 2003.

Saeki, T., Maksyutov, S., Saito, M., Valsala, V., Oda, T., Andres, R. J., Belikov, D., Tans, P., Dlugokencky, E., Yoshida, Y., Morino, I., Uchino, O., and Yokota, T.: Inverse Modeling of CO_2 Fluxes Using GOSAT Data and Multi-Year Ground-Based Observations, SOLA, 9, 45-50, 2013.

Saeki, T., Saito, R., Belikov, D., and Maksyutov, S.: Global high-resolution simulations of CO_2 and CH_4 using a NIES transport model to produce a priori concentrations for use in satellite data retrievals, Geosci. Model Dev., 6, 81-100, 2013.

Saitoh, N., Imasu, R., Ota, Y., and Niwa, Y.: CO_2 retrieval algorithm for the thermal infrared spectra of the Greenhouse Gases Observing Satellite: potential of retrieving CO_2 vertical profile from high-resolution FTS sensor, J. Geophys. Res., 114, doi:10.1029/2007JD011500, 2009.

Saitoh, N., Touno, M., Hayashida, S., Imasu, R., Shiomi, K., Yokota, T., Yoshida, Y., Machida, T., Matsueda, H., and Sawa, Y.: Comparisons between XCH_4 from GOSAT Shortwave and Thermal Infrared Spectra and Aircraft CH_4 Measurements over Guam, SOLA, 8, 145-149, 2012.

Sawa, Y., Machida, and T., Matsueda, H.: Aircraft observation of the seasonal variation in the transport of CO_2 in the upper atmosphere, J. Geophys. Res., 117, doi:10.1029/2011JD016933, 2012.

Strow, L. L. and Hannon, S. E.: A 4-year zonal climatology of lower tropospheric CO_2 derived from ocean-only Atmospheric Infrared Sounder observations, J. Geophys. Res., 113, doi:10.1029/2007JD009713, 2008.

Takagi, H. et al.: Influence of differences in current GOSAT XCO_2 retrievals on surface flux estimation, Geophys. Res. Lett., 41, 2598-2605, 2014.

Yokota, T., Yoshida, Y., Eguchi, N., Ota, Y., Tanaka, T., Watanabe, H., and Maksyutov, S.: Global Concentrations of CO_2 and CH_4 Retrieved from GOSAT: First Preliminary Results, SOLA, 5, 160-163, 2009.

Yoshida, Y., Ota, Y., Eguchi, N., Kikuchi, N., Nobuta, K., Tran, H., Morino, I., and Yokota, T.: Retrieval algorithm for CO_2 and CH_4 column abundances from short-wavelength infrared spectral observations by the Greenhouse gases observing satellite, Atmos. Meas. Tech., 4, 717-734, 2011.

Yoshida, Y. et al.: Improvement of the retrieval algorithm for GOSAT SWIR XCO_2 and XCH_4 and their validation using TCCON data, Atmos. Meas. Tech., 6, 1533-1547, 2013.

Table 1. Retrieval grid layers of GOSAT/TANSO-FTS TIR CO_2 V1 data.

Layer level	Lower presure level (hPa)	Upper pressure level (hPa)
1	1165.91	857.70
2	857.70	735.64
3	735.64	630.96
4	630.96	541.17
5	541.17	464.16
6	464.16	398.11
7	398.11	341.45
8	341.45	287.30
9	287.30	237.14
10	237.14	195.73
11	195.73	161.56
12	161.56	133.35
13	133.35	110.07
14	110.07	90.85
15	90.85	74.99
16	74.99	61.90
17	61.90	51.09
18	51.09	42.17
19	42.17	34.81
20	34.81	28.73
21	28.73	23.71
22	23.71	19.57
23	19.57	16.16
24	16.16	13.34
25	13.34	10.00
26	10.00	5.62
27	5.62	1.00
28	1.00	0.10

Table 2. Bias values of GOSAT/TANSO-FTS TIR V1 CO_2 data against CONTRAIL (AK) CO_2 data for each season and each latitude region in the upper troposphere and lower stratosphere in the unit of ppm. Significant bias values larger than ±2 ppm are indicated by boldface.

UT	LS	MAM		JJA		SON		JF	
60–70°N		-1.0	-0.8	-0.2	-0.5	-1.0	-1.1	0.3	-0.5
40–60°N		-1.7	0.3	-1.6	-1.3	-1.1	-0.9	-0.5	-0.5
20–40°N		**-2.4**		**-2.3**		-1.1		0.3	
0–20°N		-1.2		**-2.3**		-0.5		0.5	
20°S–0		-0.1		-0.6		0.4		0.0	
40–20°S		-0.2		-0.4		-0.7		-0.5	

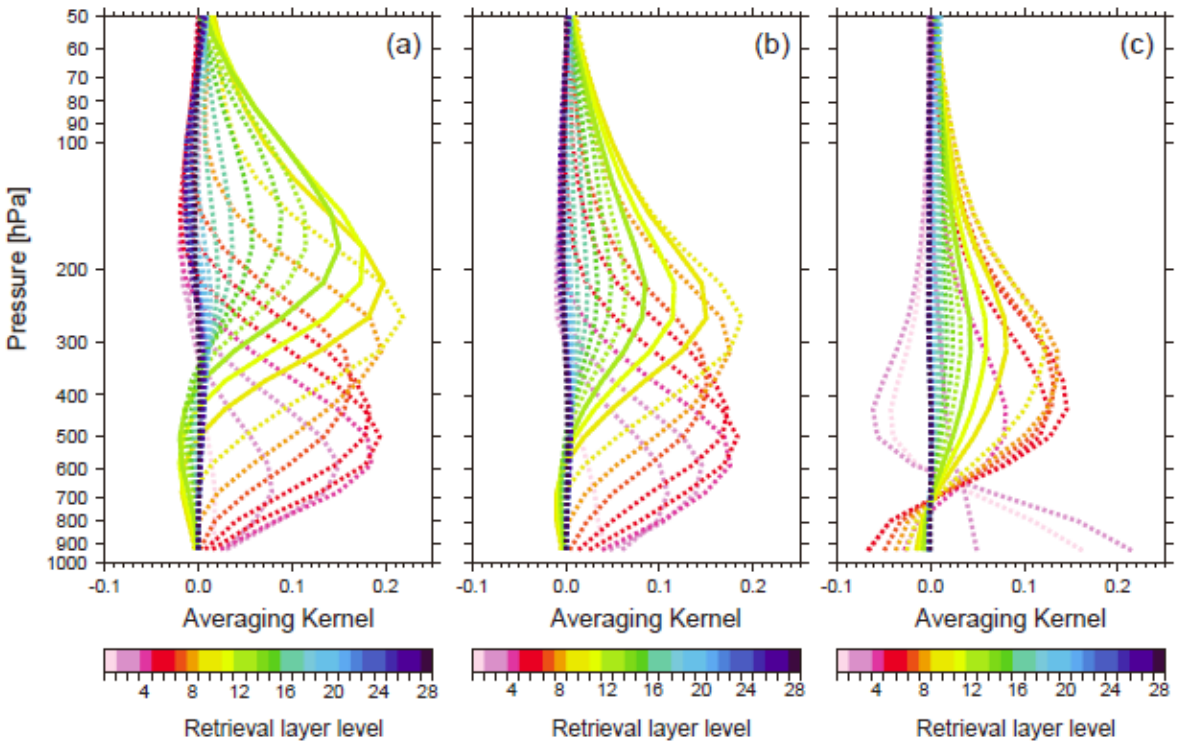

Figure 1. Averaging kernel functions of GOSAT/TANSO-FTS TIR V1 CO_2 retrieval in the 28 retrieval grid layers shown in Table 1: (a) low latitudes in summer, (b) mid-latitudes in spring, and (c) high latitudes in winter. Solid orange, yellow, and green lines indicate averaging kernel functions of each of the three layer levels 9, 10, and 11, respectively.

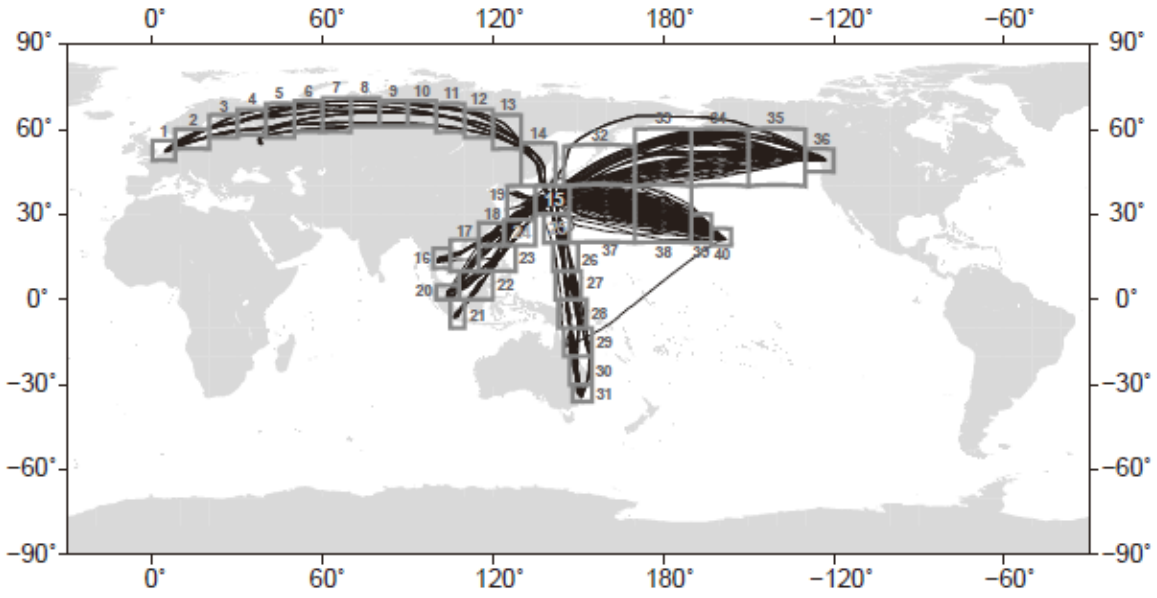

Figure 2. Flight tracks of all of the CONTRAIL CME observations in 2010 used in this study. A number next to a box area indicates each area number.

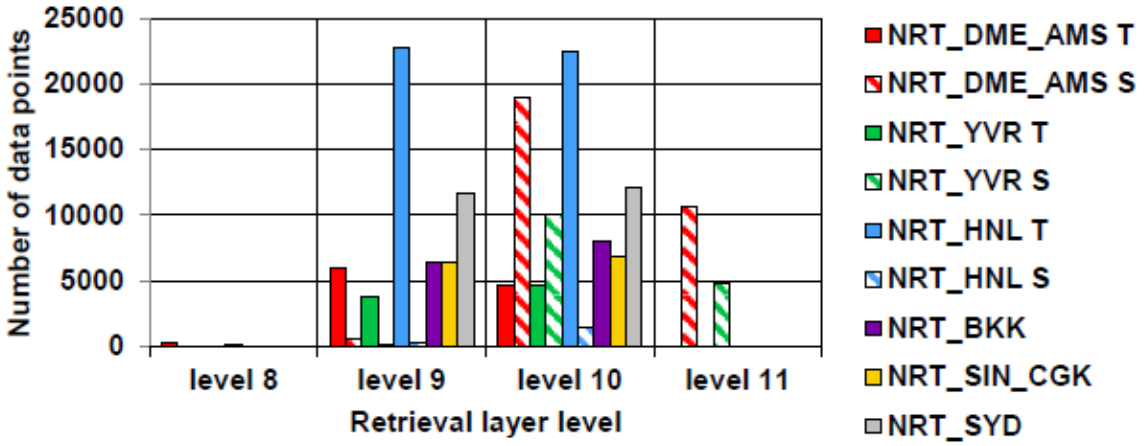

Figure 3. The number of GOSAT/TANSO-FTS TIR CO_2 data points compared to the CONTRAIL CME level flight data for each retrieval grid layer level for each flight. The numbers of TIR CO_2 data points in the troposphere ("T") and stratosphere ("S") are shown separately for the Tokyo–Europe (NRT_DME_AMS), Tokyo–Vancouver (NRT_YVR), and Tokyo–Honolulu (NRT_HNL) flight routes.

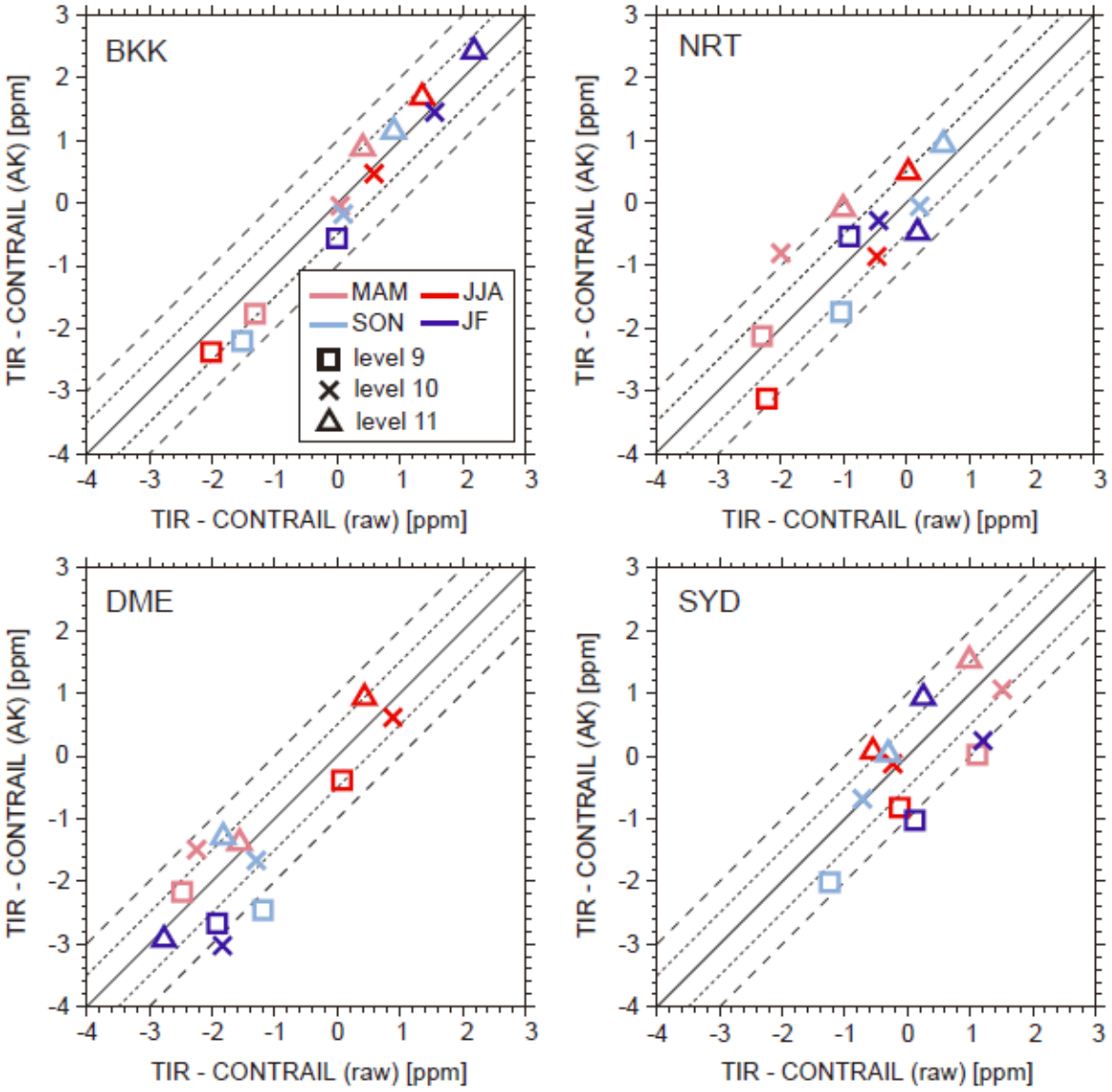

Figure 4. Scatter plots of GOSAT/TANSO-FTS TIR and CONTRAIL (raw) CO_2 differences and GOSAT/TANSO-FTS TIR and CONTRAIL (AK) CO_2 differences in layers 9, 10, and 11 for each season.

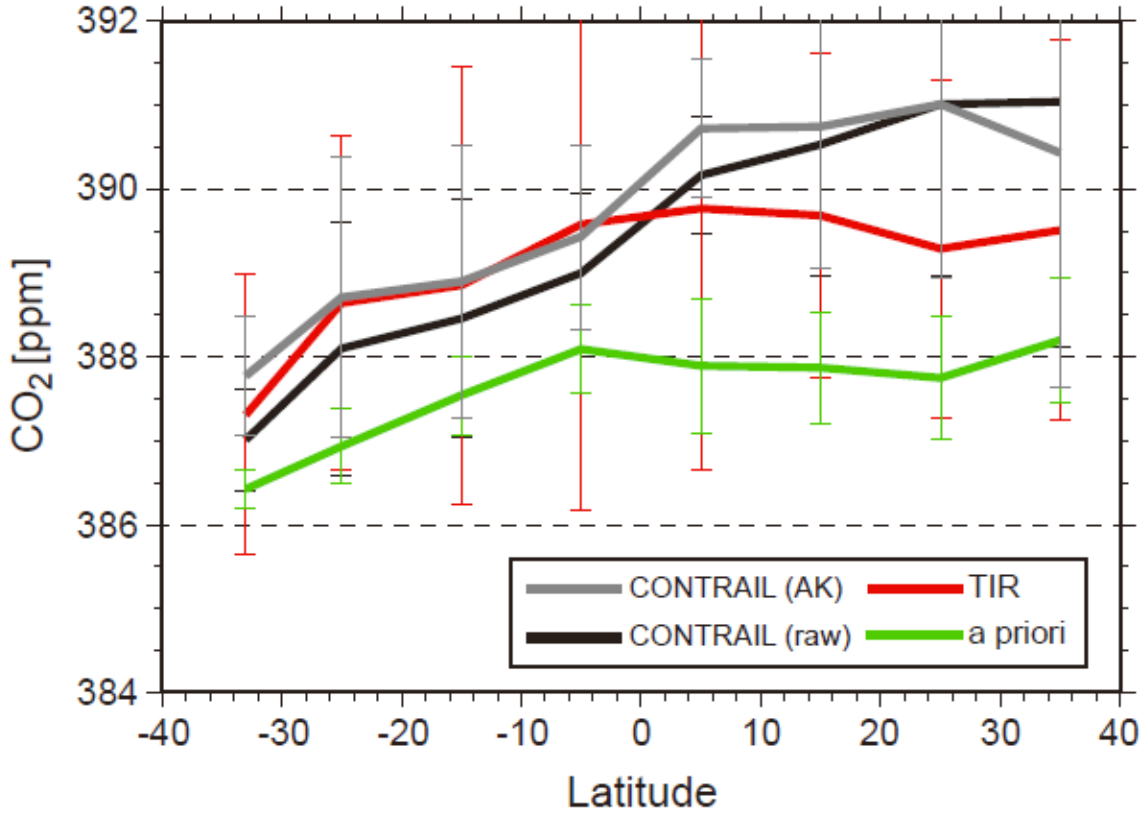

Figure 5. Comparisons among CONTRAIL (raw), CONTRAIL (AK), GOSAT/TANSO-FTS TIR, and a priori (NIES TM 05) CO_2 data during flights between Tokyo and Sydney (NRT_SYD) in spring (MAM), shown by black, gray, red, and green lines, respectively. The means and their 1-σ standard deviations were calculated in each area during the flight for all four datasets.

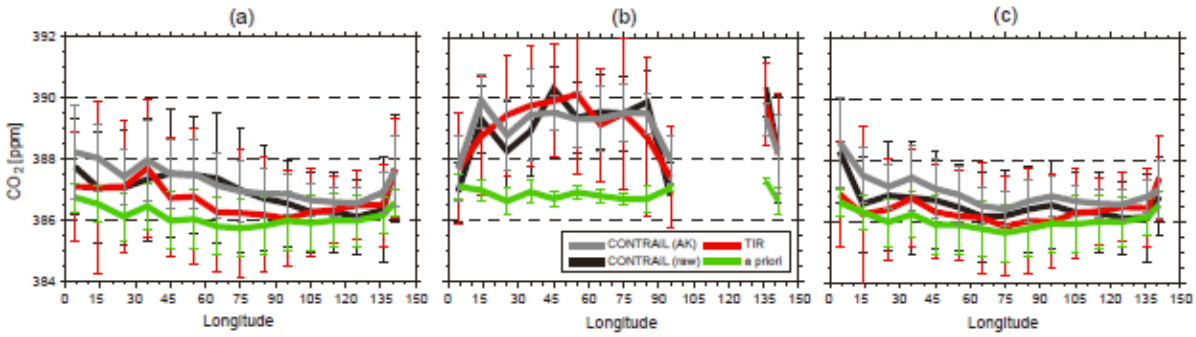

Figure 6. Same as Figure 5, but for flights between Tokyo and Europe (NRT_DME_AMS) in winter (JF). (a) All of the data, (b) only data in the troposphere, and (c) only data in the stratosphere. See the text for the classification of tropospheric and stratospheric data.

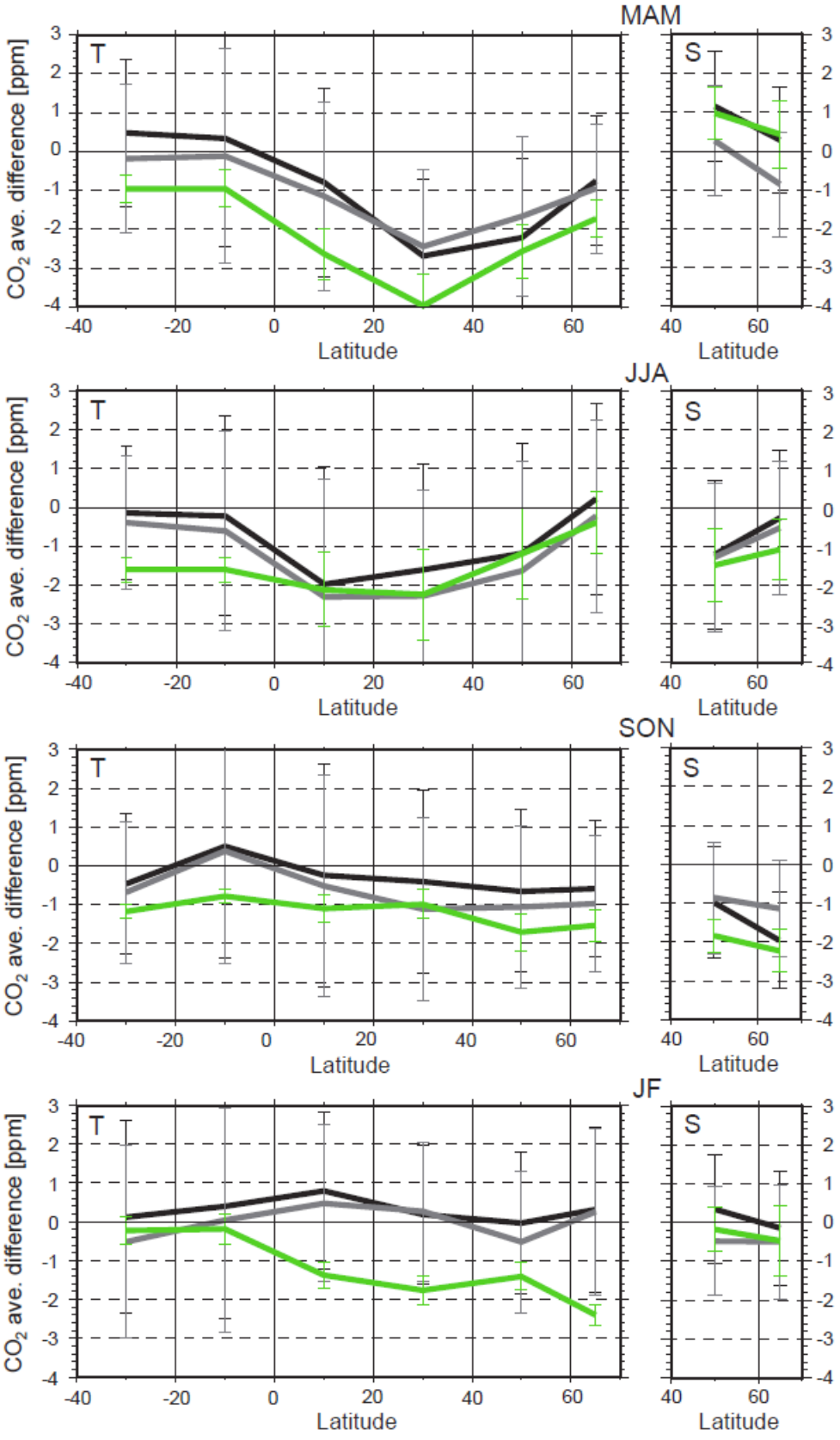

1

2

Figure 7. Differences between GOSAT/TANSO-FTS TIR and CONTRAIL (raw) averaged CO_2 data (TIR ave. minus CONTRAIL (raw) ave.), TIR and CONTRAIL (AK) averaged CO_2 data (TIR ave. minus CONTRAIL (AK) ave.), and a priori (NIES TM 05) and CONTRAIL (raw) averaged CO_2 data (a priori ave. minus CONTRAIL (raw) ave.) for each season for each latitude band (40°S–20°S, 20°S–0°, 0°–20°N, 20°N–40°N, 40°N–60°N, 60°N–70°N), shown by black, gray, and green lines, respectively. Left and right panels show the differences in the upper troposphere and lower stratosphere, respectively. The 1-σ standard deviations of the latitudinal averages of TANSO-FTS TIR CO_2 data are shown by vertical bars.

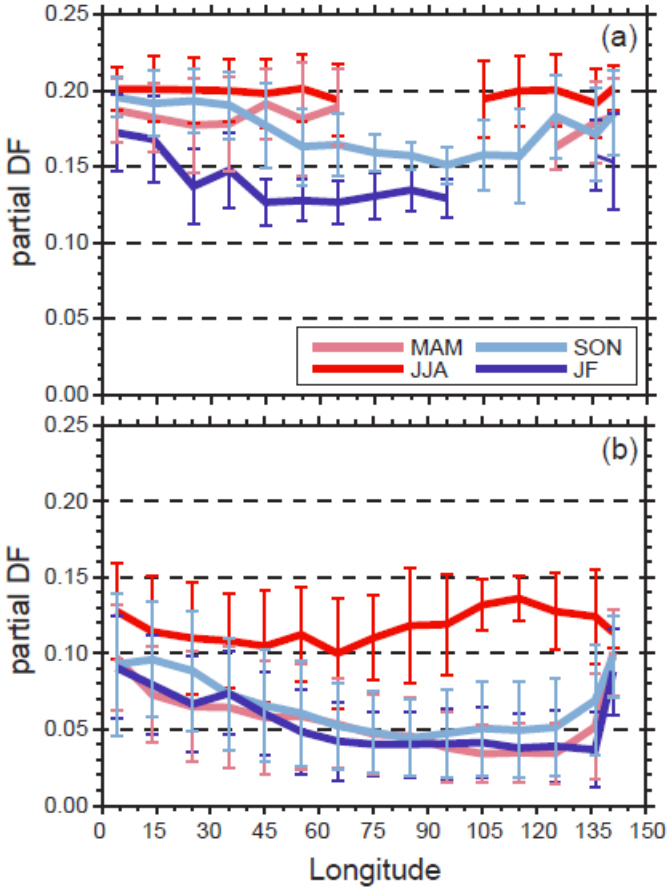

Figure 8. Partial degree of freedom (DF) for GOSAT/TANSO-FTS TIR CO_2 data in the upper troposphere (a) and the lower stratosphere (b) for each area of the flight between Tokyo and Europe (NRT_DME_AMS). The means and their 1-σ standard deviations of the partial DF data were calculated in spring (MAM), summer (JJA), fall (SON), and winter (JF), as shown by the pink, red, light blue, and blue lines, respectively.